Nano-Micro Letters

ISSN 2311-6706
e-ISSN 2150-5551
CN 31-2103/TB

REVIEW

https://doi.org/10.1007/s40820-020-00462-w

Cite as
Nano-Micro Lett.
(2020) 12:122

Received: 15 January 2020
Accepted: 28 February 2020

$NiCo_2O_4$ Nano-/Microstructures as High-Performance Biosensors: A Review

Rajesh Kumar[1] ✉

✉ Rajesh Kumar, rk.ash2k7@gmail.com

[1] Department of Chemistry, Jagdish Chandra DAV College, Dasuya, Distt. Hoshiarpur 144205, Punjab, India

HIGHLIGHTS

- Various synthetic methods for the synthesis of $NiCo_2O_4$ nano-/microstructures in bare, doped, and composite/hybrid forms are reviewed.
- Currents status and development prospects of $NiCo_2O_4$ nano-/microstructure-based electrochemical biosensors for bioanalytes such as glucose, urea, and H_2O_2, along with condition governing the electrochemical biosensor parameters, are summarized.
- Also provide an insight into the key challenges and future perspectives about point-of-care monitoring of bioanalytes using $NiCo_2O_4$ nano-/microstructure-based biosensors.

ABSTRACT Non-enzymatic biosensors based on mixed transition metal oxides are deemed as the most promising devices due to their high sensitivity, selectivity, wide concentration range, low detection limits, and excellent recyclability. Spinel $NiCo_2O_4$ mixed oxides have drawn considerable attention recently due to their outstanding advantages including large specific surface area, high permeability, short electron, and ion diffusion pathways. Because of the rapid development of non-enzyme biosensors, the current state of methods for synthesis of pure and composite/hybrid $NiCo_2O_4$ materials and their subsequent electrochemical biosensing applications are systematically and comprehensively reviewed herein. Comparative analysis reveals better electrochemical sensing of bioanalytes by one-dimensional and two-dimensional $NiCo_2O_4$ nano-/microstructures than other morphologies. Better biosensing efficiency of $NiCo_2O_4$ as compared to corresponding individual metal oxides, viz. NiO and Co_3O_4, is attributed to the close intrinsic-state redox couples of Ni^{3+}/Ni^{2+} (0.58 V/0.49 V) and Co^{3+}/Co^{2+} (0.53 V/0.51 V). Biosensing performance of $NiCo_2O_4$ is also significantly improved by making the composites of $NiCo_2O_4$ with conducting carbonaceous materials like graphene, reduced graphene oxide, carbon nanotubes (single and multi-walled), carbon nanofibers; conducting polymers like polypyrrole (PPy), polyaniline (PANI); metal oxides NiO, Co_3O_4, SnO_2, MnO_2; and metals like Au, Pd, etc. Various factors affecting the morphologies and biosensing parameters of the nano-/microstructured $NiCo_2O_4$ are also highlighted. Finally, some drawbacks and future perspectives related to this promising field are outlined.

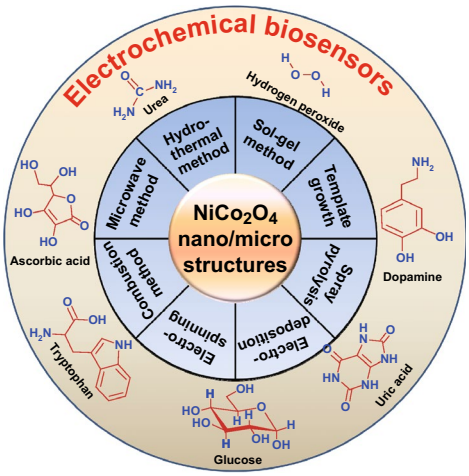

KEYWORDS Nano-/micro-structured; Spinel $NiCo_2O_4$; Synthetic methods; Modified electrodes; Electrochemical biosensors

Published online: 08 June 2020

1 Introduction

Recently, spinel single-phase binary metal oxides containing two metal cations such as manganese cobaltate ($MnCo_2O_4$) [1], zinc cobaltate ($ZnCo_2O_4$) [2, 3], nickel ferrite ($NiFe_2O_4$) [4], copper manganate ($CuMn_2O_4$) [5], copper cobaltate ($CuCo_2O_4$) [6], cobalt manganate ($CoMn_2O_4$) [7], nickel cobaltate ($NiCo_2O_4$) [8] have attracted widespread attention from researchers worldwide due to their invariably better electrochemical properties as compared to individual metal oxides or a mixture of metal oxides. The excellent electrochemical performances of these single-phase binary metal oxides are attributed to the synergetic effects of properties of the individual metal oxide components [9]. Among various such single-phase binary metal oxides, $NiCo_2O_4$ is considered to be the best one as it possesses at least two times higher electronic conductivity as compared to corresponding individual metal oxides, viz. NiO and Co_3O_4 along with intrinsic-state redox couples of Ni^{3+}/Ni^{2+} (0.58 V/0.49 V) and Co^{3+}/Co^{2+} (0.53 V/0.51 V) [10–12]. Other key features are the exhibition of variable but sufficiently stable oxidation states by Ni (Ni^{2+}, Ni^{3+}) and Co (Co^{2+}, Co^{3+}, Co^{4+}) and very high conductivity of 500 S cm^{-1} [13, 14].

Many transition metals, rare earth metals, non-metal-doped $NiCo_2O_4$, and conjugated polymer-modified $NiCo_2O_4$ materials have been reported in the literature with versatile applications. N- and P-doped $NiCo_2O_4$ with oxygen vacancies have been explored for electrochemical performance for supercapacitors, electro-catalyst for O_2 and H_2 evolution reaction [15–18], and anodic material for lithium-ion batteries [19]. Lin et al. [20] explored S-doped $NiCo_2O_4$ nanosheet arrays as the efficient and bifunctional electrode for overall water-splitting reactions. Compared with non-metal-doped $NiCo_2O_4$, transition metal and rare earth metal-doped $NiCo_2O_4$ are considered superior due to the latter's excellent electrical conductivity. Zn- and Fe-doped $NiCo_2O_4$ showed electrocatalytic properties for oxygen evolution reactions and remarkable capacitive properties in asymmetric supercapacitors [21–23]. Ma et al. [24] synthesized highly porous hierarchical spinel Mn-doped $NiCo_2O_4$ nanosheets for high-performance anodes in lithium-ion batteries. Xia et al. [25] used Au–$NiCo_2O_4$ nanomaterials supported on 3D hierarchical porous graphene-like material as electrocatalyst for oxygen evolution reaction. Among the rare earth metal oxides, CeO_2 is reported to be an excellent dopant for $NiCo_2O_4$ nanomaterials [26, 27]. Carbonaceous and polymer composite/hybrid $NiCo_2O_4$ nano-/microstructures are also found suitable for their potential applications in supercapacitors [28], fuel cells [29], Li-ion batteries [30], electrocatalyst for oxygen reduction reaction and oxygen evolution reaction [31], photo-detector [32], optoelectronic devices [33], perovskite solar cells [34], gas sensors [35–37] and biosensors [38, 39].

Facile, low-cost and eco-friendly synthetic methods lead to varieties of low dimensional nano-/micro-structured morphologies with excellent porosity and specifically large surface area, opportunities to synthesize composite/hybrid and ease of electrode fabrications for end-user applications. Spinel $NiCo_2O_4$ is a p-type semiconductor in which Ni occupies octahedral sites while Co is distributed in both octahedral and tetrahedral sites [13] (Fig. 1a, b). It shows a face-centered cubic arrangement and belongs to Fd3m space group with lattice constant $a_o = 8.269$ Å [40].

Electrochemical sensing through miniaturized sensors based on nano-/micro-structured materials has taken over the conventional, expensive, laborious sensing techniques like lateral flow immunoassay, liquid chromatography, capillary electrophoresis, enzyme-linked immunosorbent assay, chemiluminescence, sequential injection analysis, gas chromatography–mass spectrometry and fluorescent methods [43–48]. Electrochemical biosensors can be categorized into amperometric and potentiometric sensors [49]. The amperometric biosensing involves a change in current response due to electrochemical redox reactions of the analytes when a potential is applied between the working and reference electrodes while the potentiometric biosensing makes use of ion-selective electrodes to transduce the biological reactions into a measurable electrical signal [43, 50].

Among the main classes of biosensors, the non-enzymatic biosensor is considered to be better, faster, and more convenient as compared to an enzymatic biosensor that involves complicated and multi-step enzyme immobilization processes and high specificity of the enzymes. Also, due to pH and temperature sensitiveness, the enzyme-based biosensors are highly unstable as enzymes undergo denaturation leading to biological inactivity beyond physiological conditions [51–53]. Nanomaterials not only provide high-density catalytic sites for the electro-oxidation or electro-reduction in the biomarkers but also provide large surface area for adsorption of biomarkers and facilitate an appropriate path for electron transport for electrochemical activity [54–56]. Since the

https://doi.org/10.1007/s40820-020-00462-w

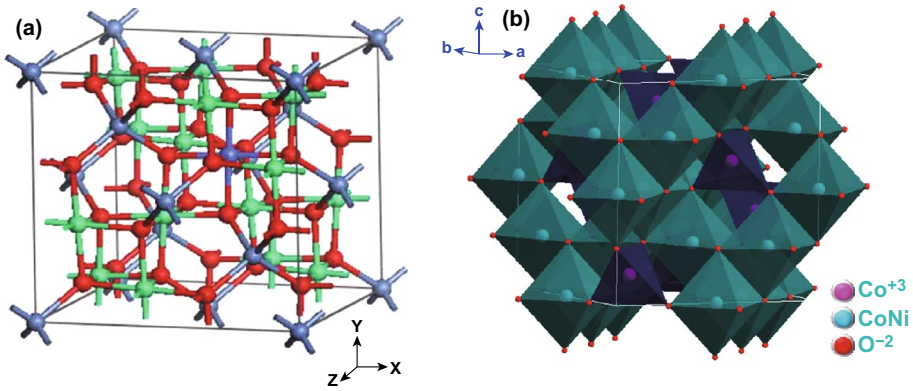

Fig. 1 **a** Crystal structure of $NiCo_2O_4$. Reproduced with permission from Ref. [41]. Copyright © 2014 Elsevier B.V. **b** $NiCo_2O_4$ cubic spinel. Reproduced with permission from Ref. [42]. Copyright © 2013 American Chemical Society

crucial part in electrochemical biosensors is the modified electrode, much attention has been devoted to modulate the electrocatalytic behavior of the $NiCo_2O_4$ as electron mediator by engineering its composition, structure, specific surface area, and redox properties.

To date, many reviews have been reported for the applications of $NiCo_2O_4$ nano-/micro-structured materials including Li-ion batteries [10], supercapacitors [11, 57], fuel cells [58], and electro-catalyst for oxygen reduction, oxygen and hydrogen evolution reactions [59, 60]. The applications of the $NiCo_2O_4$-based non-enzymatic biosensors are aimed not only at the extension of the spectrum of target bioanalytes but also at the improvement in the biosensor performance in terms of sensitivity, selectivity, detection limits, long-term stability as well as reusability. Many new synthetic strategies and techniques have been developed for the fabrication of $NiCo_2O_4$-based non-enzymatic biosensors, but they are rarely summarized. Hence, it is an appropriate time to go through the periodical progress of $NiCo_2O_4$-based non-enzymatic biosensors. This review covers the crystal structure of the spinel $NiCo_2O_4$, various synthetic strategies employed for the synthesis of nano-/micro-structured $NiCo_2O_4$, electrochemical biosensing toward biomarkers such as glucose, H_2O_2, and urea, through the fabrication of modified electrodes. Various factors affecting the morphologies and biosensing parameters of the nano-/micro-structured $NiCo_2O_4$ are also reviewed.

2 General Biosensing Mechanism

Two types of strategies are generally involved in the electrochemical biosensing of biomarkers, i.e., enzyme based and enzyme-free [61, 62]. An enzymatic biosensor operates on three main components which include sensitive recognition element, signal transducer element, and data evaluation component [63–66]. Enzymes, antibodies, and nucleic acid are generally used as recognition components. Glucose oxidase and glucose dehydrogenase for glucose [67, 68], horseradish peroxidase for H_2O_2 [69], urease for urea [70], laccase and polyphenol oxidase for rutin [71], tryptophan oxidase for tryptophan [72], etc. act as sensitive recognition elements. The function of the signal transducer is to convert chemical changes into detectable and readable electronic signals which are finally transferred to the data evaluation component. Recent developments in the field of nanotechnology and nanoscience reveal the excellent efficiencies of the nanostructured materials as signal transducers. Biosensors based on nanostructured materials as artificial bioreceptors are used for early detection and diagnosis of diseases through the estimation of the levels of biomarkers [73–75]. The signal transducer behavior of the nanomaterials mainly depends upon the electrochemical redox properties, surface-to-volume ratio, crystal structure and phase, morphology, and the presence of some other conducting matrices along with the nanostructured materials [76–78]. In contrast,

in enzyme-free biosensors, nanostructured materials are used as signal transducers as well as sensitive recognition elements.

Electrochemical biosensors are mainly based on the output electrical signals changes incurred from either the oxidation or the reduction of the target bioanalyte on the surface of the transducer (Fig. 2) [79–81]. These redox reactions are catalyzed by signal transducer enzymes and nanostructured materials in enzyme-based and enzyme-free biosensors, respectively. The strength of the electrical signals is significantly affected by the concentrations of target bioanalytes, temperature, pH, and the presence of the interfering species [82–85].

3 Synthesis of Nano-/Micro-Structured $NiCo_2O_4$

3.1 Hydrothermal/Solvothermal Method

Hydrothermal synthesis involves heterogeneous reactions in an aqueous medium within a temperature range of 100–200 °C and high pressure. To achieve these conditions, the reaction is usually carried out in Teflon-lined sealed steel autoclaves. Alkali metal hydroxide or NH_3 is added to convert the precursor metal salts into their respective hydroxides at basic pH conditions [86, 87]. An initial nucleation phase is followed by the directed crystal growth along appropriate crystal planes. The morphology, surface, and the structural features of the materials synthesized through hydrothermal method depend upon the conditions like temperature, pH of the solution, concentration of the precursor, nature of the solvent, and the presence of the templates [88]. $NiCo_2O_4$ nano-/microstructures of various shapes and morphologies have been prepared hydrothermally. Nano-/micro-structured $NiCo_2O_4$ of morphologies such as urchin shaped [89], coral-like [90], core–ring-structured nanoplatelets [91], porous coral-like nanospheres [36], hollow nanospheres [92], nanospheres [93], urchin-like spheres [94], mesoporous nanoparticles [95], mesoporous nanoneedles [96, 97], 3D network-like mesoporous nanostructures [98], 3D hierarchical tremella-like, flower-like, urchin-like and pine needle-like [99], nanoflakes [100], nanowalls [101], etc. are reported.

Ni and Co precursor salt solutions with molar atomic ratio of 1:2 are taken during hydrothermal growth since Ni and

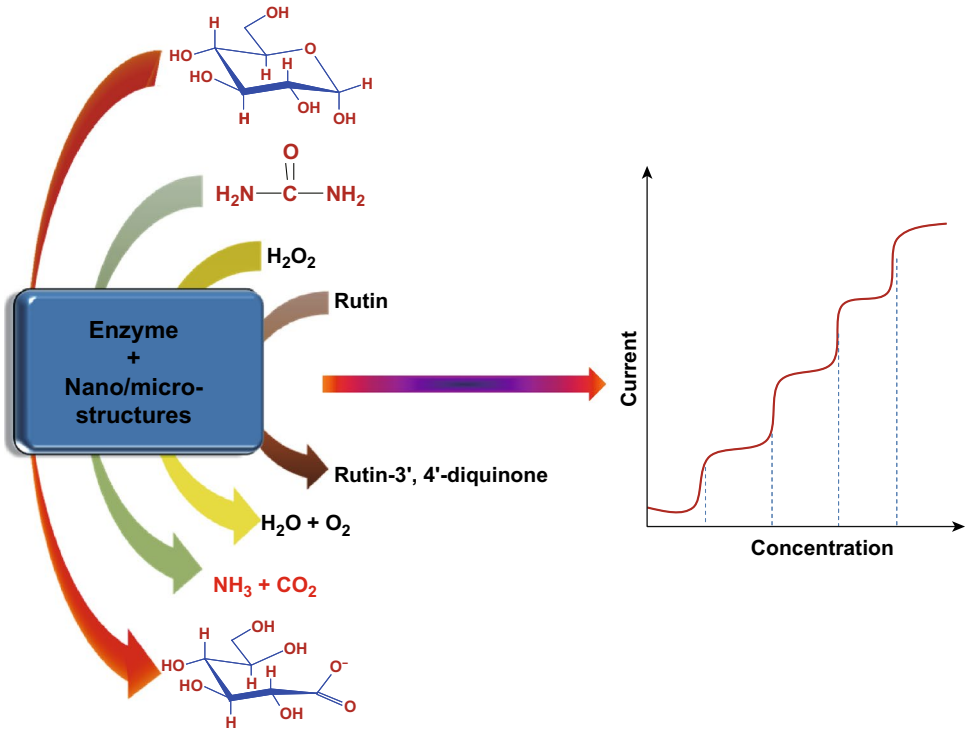

Fig. 2 Proposed biosensing mechanism of nano-/microstructures

https://doi.org/10.1007/s40820-020-00462-w

Co atoms are present in the 1:2 atomic ratio. Liu et al. [94] used 1 mmol $Ni(NO_3)_2{\cdot}6H_2O$ and 2 mmol $Co(NO_3)_2{\cdot}6H_2O$ solution to prepare urchin-like $NiCo_2O_4$ spheres. Yang et al. [102] mixed 1 mmol of $Ni(CH_3COO)_2{\cdot}4H_2O$ and 2 mmol of $Co(CH_3COO)_2{\cdot}4H_2O$ for the preparation of $NiCo_2O_4$ nanospheres. Yu et al. [96] used 0.5 mmol $Ni(NO_3)_2{\cdot}6H_2O$, 1 mmol $Co(NO_3)_2{\cdot}6H_2O$ for the synthesis of $NiCo_2O_4$ mesoporous nanoneedles. Zhu et al. [98] mixed 0.225 mmol of $Ni(CH_3COO)_2{\cdot}4H_2O$ and 0.45 mmol of $Co(CH_3COO)_2{\cdot}4H_2O$ for the synthesis of 3-D network-like mesoporous nanostructures. For the initial formation of binary metal hydroxides or metal carbonate hydroxides, reagents like NH_3, urea, NaOH, NH_4HCO_3, NH_4F, hexamethylenetetramine (HMTA) [103], diethylene glycol (DEG), cetyltrimethylammonium bromide (CTAB) [104], sodium dodecyl sulfate (SDS) [105], poly(diallyldimethylammonium chloride) (PDDA) [106], glycine [107], methyl glycerate [108], and ethylene glycol are added in the reaction mixture. The combination of some polar solvents such as ethanol, ethanol, propanol, ethylene glycol, and acetone along with water has also been found to facilitate the morphological characteristics [109]. Water:polar solvent ratio also significantly affects the growth mechanism. In Fig. 3a–d, different morphologies for the $NiCo_2O_4$ nanostructures are shown for water:ethanol ratios 1:0, 3:1, 1:1, and 1:3. More porous, denser, and thinner sheets were formed for the synthesized 3D flower-like $NiCo_2O_4$ nanostructures as the composition of ethanol was increased.

In the hydrothermal growth, the temperature is also a key factor in controlling the morphology of the nanostructures. Urchin- and sheaf-like $NiCo_2O_4$ nanostructures were synthesized by Umeshbabu et al. [104] using CTAB as a surfactant under hydrothermal conditions at 120 °C and 200 °C temperatures, respectively. Different morphologies were attributed to different degrees of crystal splitting and anisotropic crystal growth at different growth temperatures [110]. Further, the temperature also affects the magnitude of the van der Waals forces, hydrogen bonding, hydrophobic attraction, crystal field attraction, and intrinsic crystal contraction which subsequently control the Ostwald ripening process [111, 112].

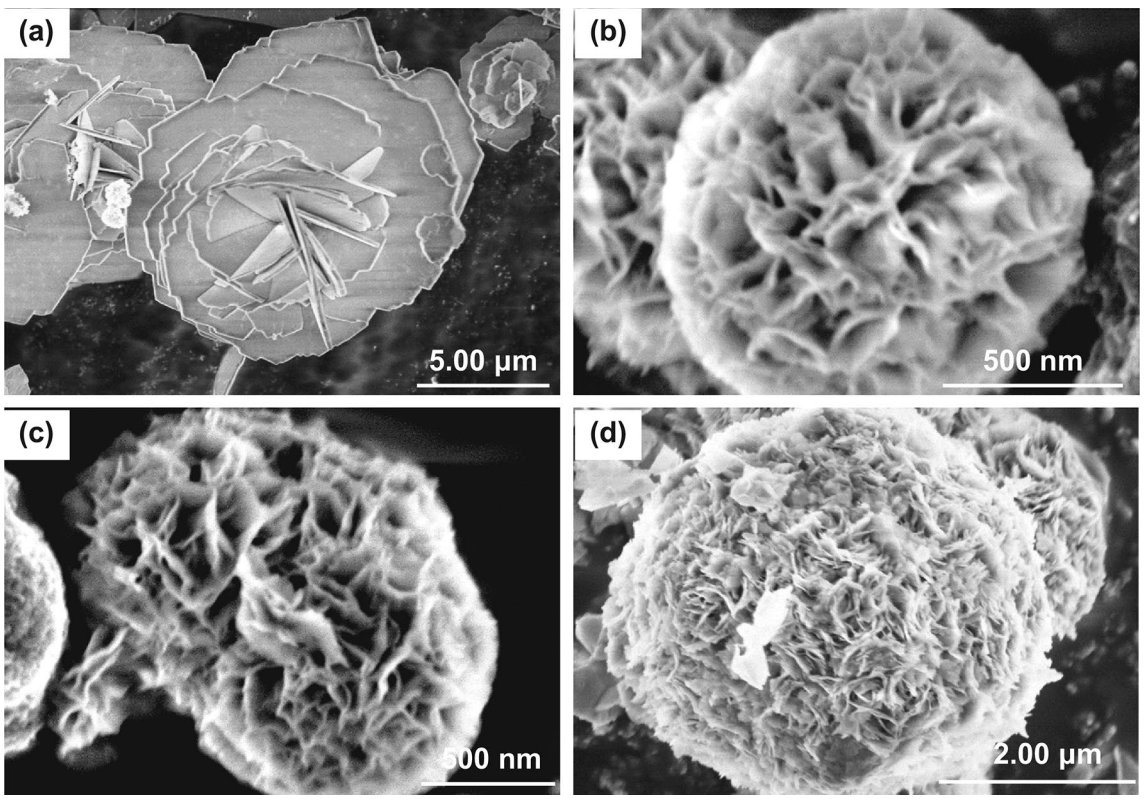

Fig. 3 FESEM image of $NiCo_2O_4$ samples using water: ethanol ratios **a** 1:0, **b** 3:1, **c** 1:1, and **d** 1:3. Reproduced with permission from Ref. [109]. Copyright © 2017 Elsevier B.V.

Nayak et al. [89] mixed $Ni(NO_3)_2{\cdot}6H_2O$ and $Co(NO_3)_2{\cdot}6H_2O$ salts in a 1:2 atomic ratio along with urea which produced OH^- ions in the reaction mixture according to Eqs. 1–3.

$$CO(NH_2)_2 + H_2O \rightarrow 2NH_3 + CO_2 \quad (1)$$

$$NH_3 + H_2O \rightarrow NH_4OH \quad (2)$$

$$NH_4OH \rightarrow NH_4^+ + OH^- \quad (3)$$

Ni^{2+} and Co^{2+} on reaction with these OH^- ions formed Ni–Co bimetallic hydroxide $[NiCo_2(OH)_6]$ which were finally converted into $NiCo_2O_4$ nanoneedles after crystal growth and calcinations. However, according to some reports, in the presence of urea, metal carbonate hydroxides are initially formed instead of bimetallic hydroxides (Eqs. 4–7) [113].

$$CO_2 + OH^- \rightarrow HCO_3^- \rightarrow H^+ + CO_3^{2-} \quad (4)$$

$$2Ni^{2+} + CO_3^{2-} + 2OH^- \rightarrow Ni_2(CO_3)(OH)_2 \quad (5)$$

$$2Co^{2+} + CO_3^{2-} + 2OH^- \rightarrow Co_2(CO_3)(OH)_2 \quad (6)$$

$$Ni_2(CO_3)(OH)_2 + 2Co_2(CO_3)(OH)_2 + O_2 \rightarrow 2NiCo_2O_4 + 3CO_2 + 3H_2O \quad (7)$$

Even ethanol as the solvent can also initiate the formation of metal carbonate hydroxides. Two-dimensional porous $NiCo_2O_4$ nanodisks were synthesized by a low-temperature hydrothermal method by Jain et al. [114] (Eqs. 8, 9). Figure 4 proposes the initial formation of $Ni_2(CO_3)(OH)_2$ and $Co_2(CO_3)(OH)_2$. Subsequent hydrothermal treatment in basic medium followed by calcination at 500 °C formed two-dimensional porous $NiCo_2O_4$ nanodisks.

$$C_2H_5OH + 3H_2O \rightarrow 2CO_2 + 6H_2 \quad (8)$$

$$CO_2 + H_2O \rightarrow H_2CO_3 \rightarrow 2H^+ + CO_3^{2-} \quad (9)$$

The nature of alkali source, capping agent, and other additives significantly affects the morphology of the $NiCo_2O_4$ nanostructures. Wang et al. [99] reported tremella-like $NiCo_2O_4$ nanostructures in the presence of HMTA, which transformed into flower-like nanostructures when NH_4F was also added along with HMTA. However, when HMTA was replaced with urea, urchin-like and pine needle-like $NiCo_2O_4$ nanostructures were formed, respectively, in the absence and presence of NH_4F additive [99]. HMTA is hydrolyzed to produce NH_3 which finally produces OH^- ions as stated earlier in this section (Eq. 10).

$$(CH_2)_6N_4 + 6H_2O \rightarrow 4NH_3 + 6HCHO \quad (10)$$

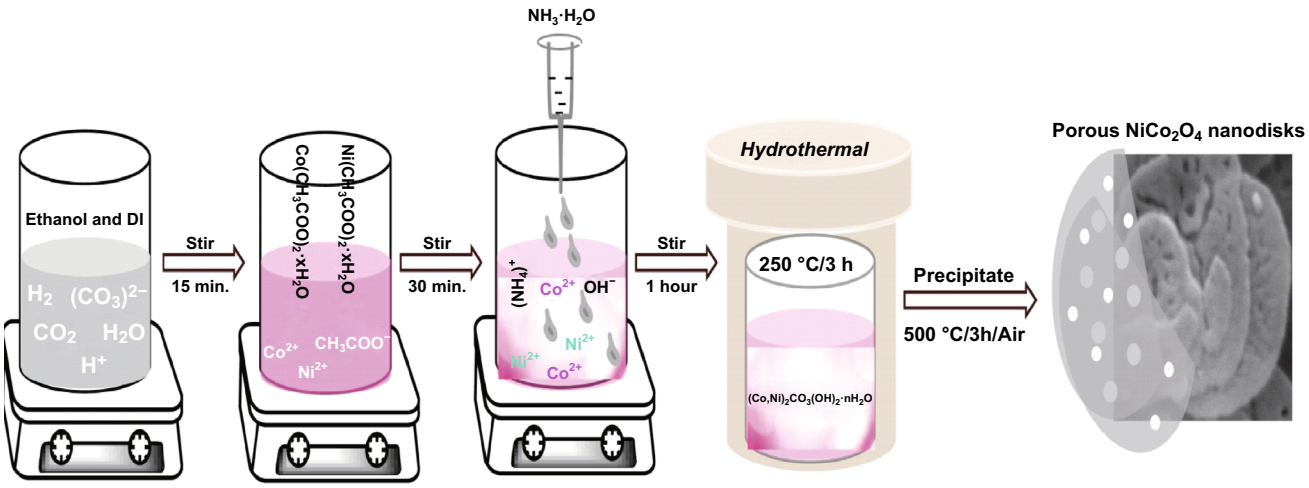

Fig. 4 Schematic diagram for the synthesis of two-dimensional porous nanodisks of $NiCo_2O_4$. Reproduced with permission from Ref. [114], Copyright © 2018 Elsevier B.V.

https://doi.org/10.1007/s40820-020-00462-w

It was suggested that the F^- ions released from NH_4F stimulate the initially formed nanosheets and nanoneedles to produce more active sites to further activate nucleation, more mass loading of active material per unit area, firm binding between the active material, and hence more crystal growth [115–117]. The possible set of reactions elaborating the role of F^- ions released from NH_4F is shown as follows [118] (Eqs. 11–13).

$$Co^{2+} + Ni^{2+} + 2F^- \rightarrow CoF^+ + NiF^+ \quad (11)$$

$$CoF^+ + NiF^+ + OH^- \rightarrow CoF(OH) + NiF(OH) \quad (12)$$

$$4CoF(OH) + 2NiF(OH) + O_2 \xrightarrow{\text{Annealing}} 2NiCo_2O_4 + 6HF \quad (13)$$

Further, different concentrations of the NH_4F also stimulated the initially formed nanostructures to acquire more versatile morphologies. For 3, 9, and 12 mmol concentrations of NH_4F, various morphologies of the $NiCo_2O_4$ nanostructures are shown in Fig. 5. With an increase in concentration from 3 to 9 mmol, aggregation of the neighboring nanosheets occured. Further increase in concentration to 12 mmol, rhombus-shaped architectures were formed [117].

Deng et al. [119] prepared novel urchin-like peapoded $NiCo_2O_4$@C nanostructures as a bifunctional catalyst for the water-splitting reaction. A three-phase process was proposed which included the initial hydrothermal synthesis of nanoneedles self-assembled microsphere followed by coating with polymerized glucose as green carbon source onto $NiCo_2O_4$ microsphere. The final stage was the calcination

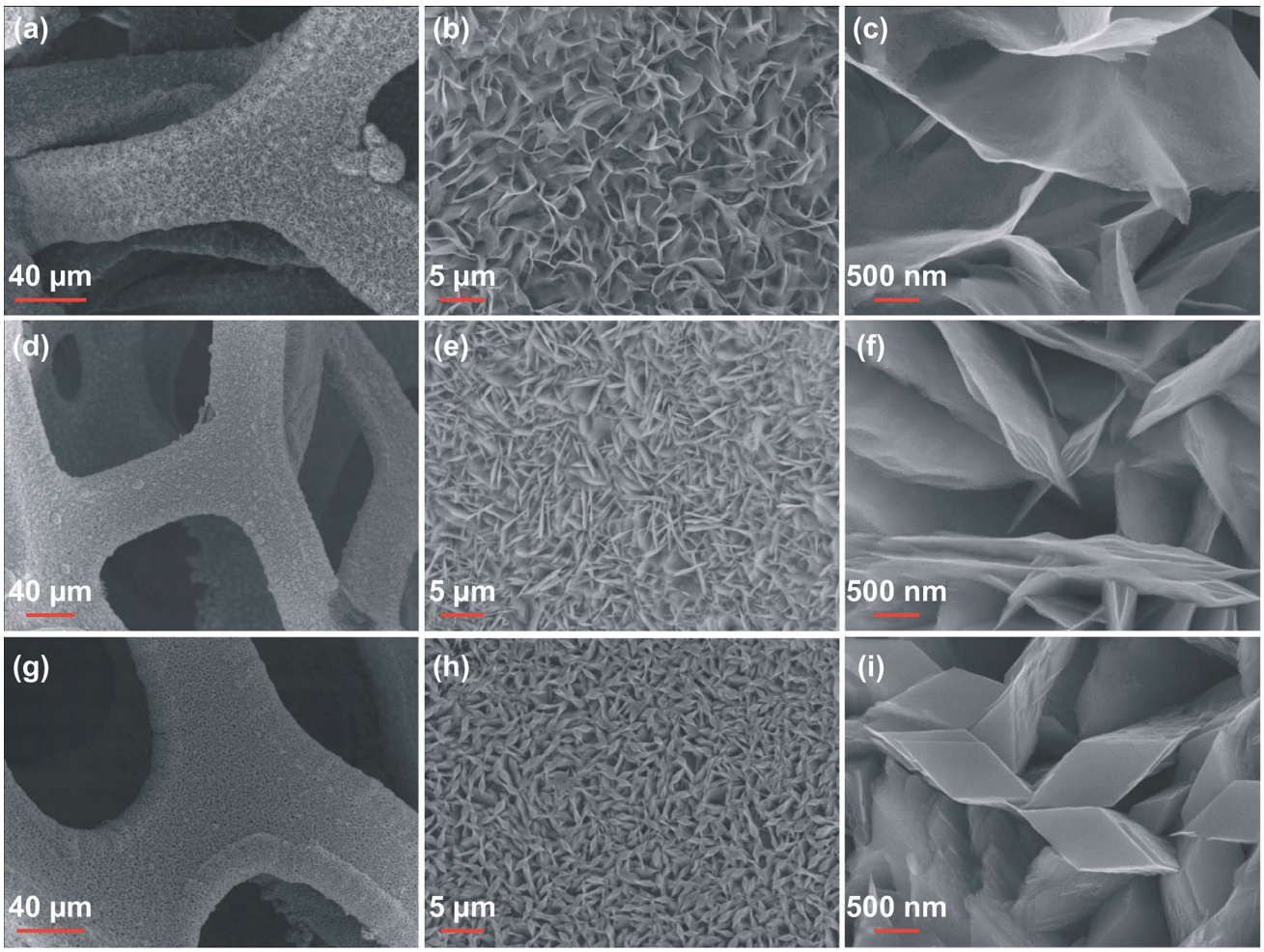

Fig. 5 FESEM images representing the effect of concentration of NH_4F on the morphologies of $NiCo_2O_4$ nanostructures: **a–c** 3 mmol NH_4F; **d–f** 9 mmol NH_4F; **g–i** 12 mmol NH_4F. Reproduced with permission from Ref. [117]. Copyright © 2014 Elsevier Ltd.

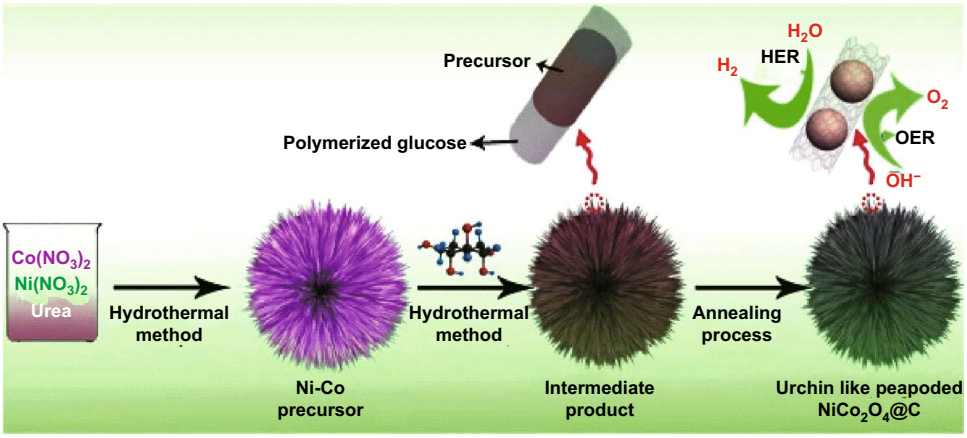

Fig. 6 Schematic diagram of the process of urchin-like peapoded $NiCo_2O_4$@C. Reproduced with permission from Ref. [119], Copyright © 2017 Elsevier B.V.

of the coated $NiCo_2O_4$ microsphere under N_2 atmosphere to give urchin-like peapoded $NiCo_2O_4$@C. The fabrication process of urchin-like peapoded $NiCo_2O_4$@C is pictorially demonstrated in Fig. 6.

Still another way of engineering the morphology, porosity, and growth of the crystals along the particular oriented crystal planes of the nanomaterials, is the use of non-aqueous solvents. The modified method is named as solvothermal instead of hydrothermal. Solvents with different solubilities and polarities can significantly affect the degree of supersaturation, the diffusion rates of the chemical species to the surface of the growing crystals, the interfacial surface energy, etc. [120, 121]. Fu et al. [122] synthesized 1D porous $NiCo_2O_4$ microrods (using metal acetate salts) (Fig. 7a) and microspheres (using metal nitrate salts) (Fig. 7b) in aqueous and isopropanol media, respectively, under similar conditions of temperature and reaction time. In 1:1 ethanol:water medium, spindle-like hierarchical architectures composed

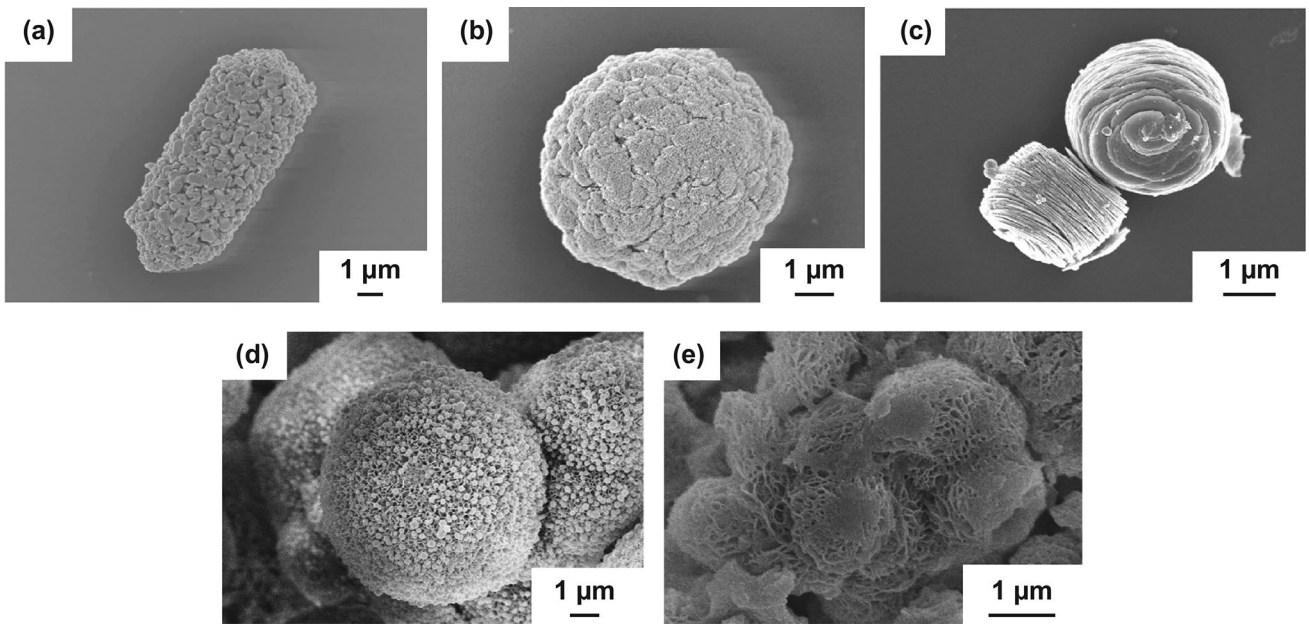

Fig. 7 FESEM images of $NiCo_2O_4$ architectures prepared solvothermally using different solvents **a** water, **b** isopropanol, **c** 1:1 ethanol: water, **d** pure ethanol, and **e** diethylene glycol. Reproduced with permission from Ref. [122]. Copyright © 2017 American Chemical Society

 https://doi.org/10.1007/s40820-020-00462-w

of closely packed microplates aligned along one direction with sizes of 3–5 μm were formed (Fig. 7c). In pure ethanol microspheres composed of nanosheets, interweave together with an average diameter of 8 μm were formed (Fig. 7d). However, in diethylene glycol, irregular aggregates with sheet-like structures were synthesized (Fig. 7e).

Wang et al. [123] in an interesting stepwise hydrothermal growth synthesized layers of $NiCo_2O_4$ nanosheets on the surface of $NiCo_2O_4$ nanocones precursor to give highly ordered 3D hierarchical $NiCo_2O_4$@$NiCo_2O_4$ core–shell nanocone arrays on nickel foams (Fig. 8). Different morphologies were engineered by controlling the reaction time and the temperature during stepwise hydrothermal growth. Further, $NiCo_2O_4$ nanocones arrays on Ni foam were synthesized in the absence of HMTA while the $NiCo_2O_4$ nanosheets growth on $NiCo_2O_4$ nanocones was guided by the presence of HMTA.

3.2 Templated Solution Growth Method

The morphology, size, shape, and surface area of nanostructures can be designed through template-based synthesis to produce nanostructures with controlled physical, chemical, electrical, and electronic properties essential in notable applications and are also quite different from those of the bulk materials. Generally, three stages, viz., template preparation, directed synthesis of the desired material using the template, and the template removal, are described in the overall growth process of nanostructures [124]. The chemical nature, structure, concentration, and growth temperature are some of the important environmental factors affecting the growth of nanomaterials. Template-based methodologies are reported in the literature which govern the synthesis of $NiCo_2O_4$ nanomaterials with versatile morphologies including nanospheres, hollow spheres, nanocages, hollow submicron spheres, hollow irregular octahedra-like cages, flower-like nanostructure, microspheres with highly ordered mesoporous structures, nanowires, etc. With the development of new methods for synthesizing mesoporous binary $NiCo_2O_4$ metal oxides, the combination of template method with other methods such as hydrothermal/solvothermal, sol–gel has been widely used. In one such study, Ren et al. [125] prepared mesoporous $NiCo_2O_4$ microspheres using a mesoporous silica (KIT-6) template. The KIT-6 template was added into the metal nitrate precursor solution prepared in ethanol. The schematic illustration of the formation of mesoporous $NiCo_2O_4$ microspheres is shown in Fig. 9a. The high porosity of the synthesized mesospheres was ascertained by FESEM and TEM images (Fig. 9b, c). The template was finally removed by etching with 2 M NaOH solution [125].

Yuan et al. [126] utilized silica spheres as hard templates prepared by the modified Stöber method [127], for

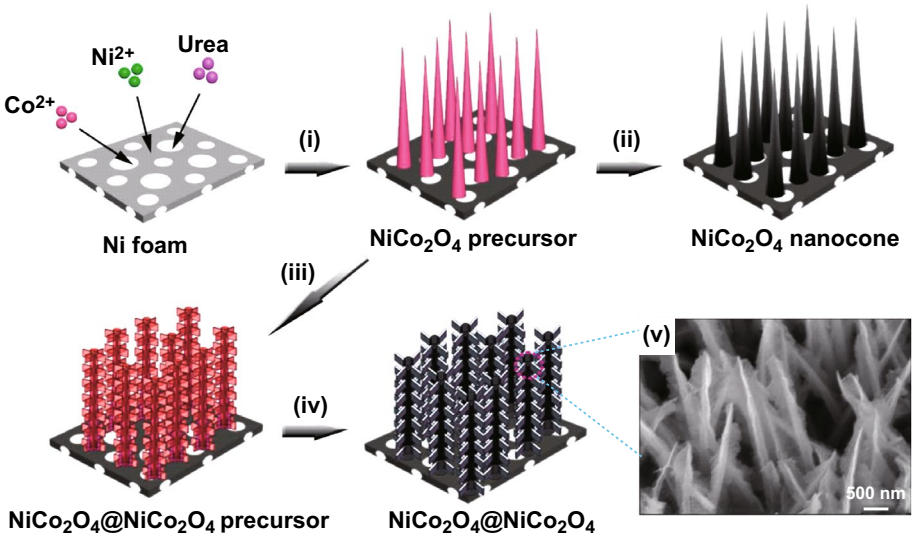

Fig. 8 Schematic illustration for the formation of highly ordered 3D hierarchical $NiCo_2O_4$@$NiCo_2O_4$ core–shell nanocones arrays on nickel foams. Reproduced with permission from Ref. [123], Copyright © 2018 Elsevier B.V.

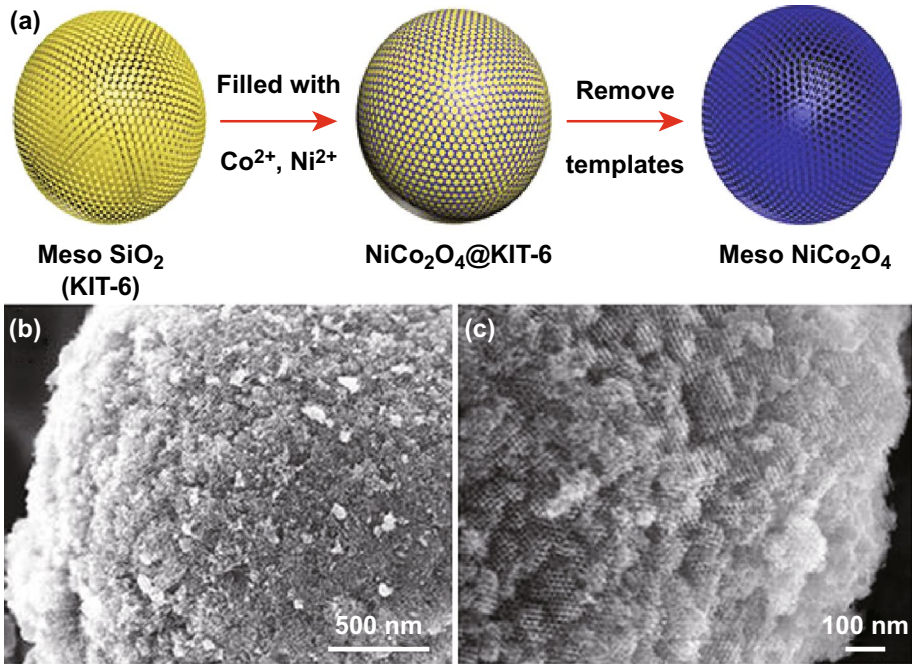

Fig. 9 **a** Schematic illustration of the formation of mesoporous $NiCo_2O_4$ microspheres, **b** high-magnification FESEM image, and **c** TEM image of the mesoporous $NiCo_2O_4$ microspheres. Reproduced with permission from Ref. [125]. Copyright © Authors

the synthesis of hierarchical mesoporous hollow $NiCo_2O_4$ submicron spheres with uniform size and mesoporous textual property. These submicron spheres were composed of ultrathin nanosheets with a thickness of a few nanometers. The NaOH solution was used for the in situ removal of silica spheres. Dopamine—a biomolecule containing amine functional groups is capable of self-polymerize under alkaline conditions. It forms a layer of the polydopamine which attracts various metal ions including Co^{2+} and Ni^{2+} cations due to strong electrostatic interactions.

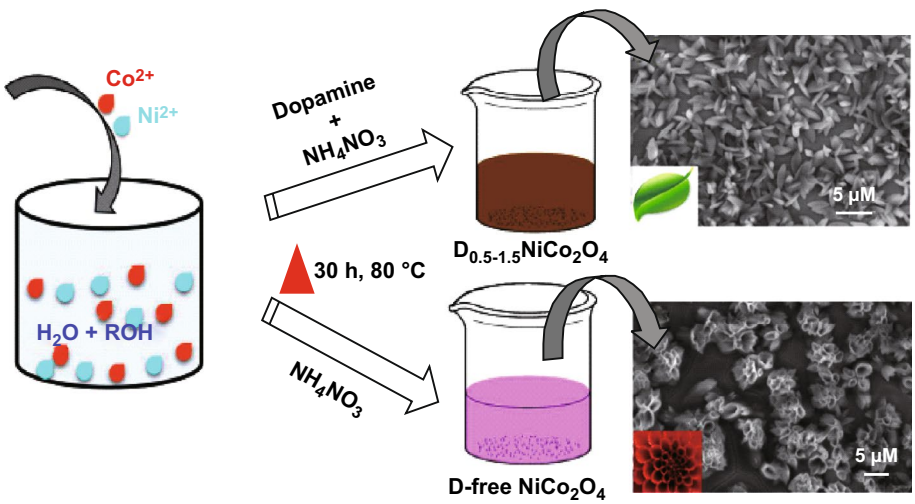

Fig. 10 Schematic illustration of the synthesis of dopamine-free and dopamine-$NiCo_2O_4$ nanostructures. Reproduced with permission from Ref. [128], Copyright © 2016 American Chemical Society

https://doi.org/10.1007/s40820-020-00462-w

Further, the alkalinity of the medium results in the formation of –OH–Ni–OH–Co–OH– complex networks. This property has been explored for the synthesis of $NiCo_2O_4$ nanostructures by Veeramani et al. [128]. FESEM images shown in Fig. 10 are demonstrating the effect of dopamine on the morphology of the $NiCo_2O_4$ nanostructures. Flower-like dopamine derived $NiCo_2O_4$ nanostructures were formed.

In another significant strategy, Xiong et al. [129] used mollusk shell-based macroporous carbon material (MSBPC), as a template to grow $NiCo_2O_4$ nanowires hydrothermally (Fig. 11a, b). The MSBPC was obtained from mollusc shells

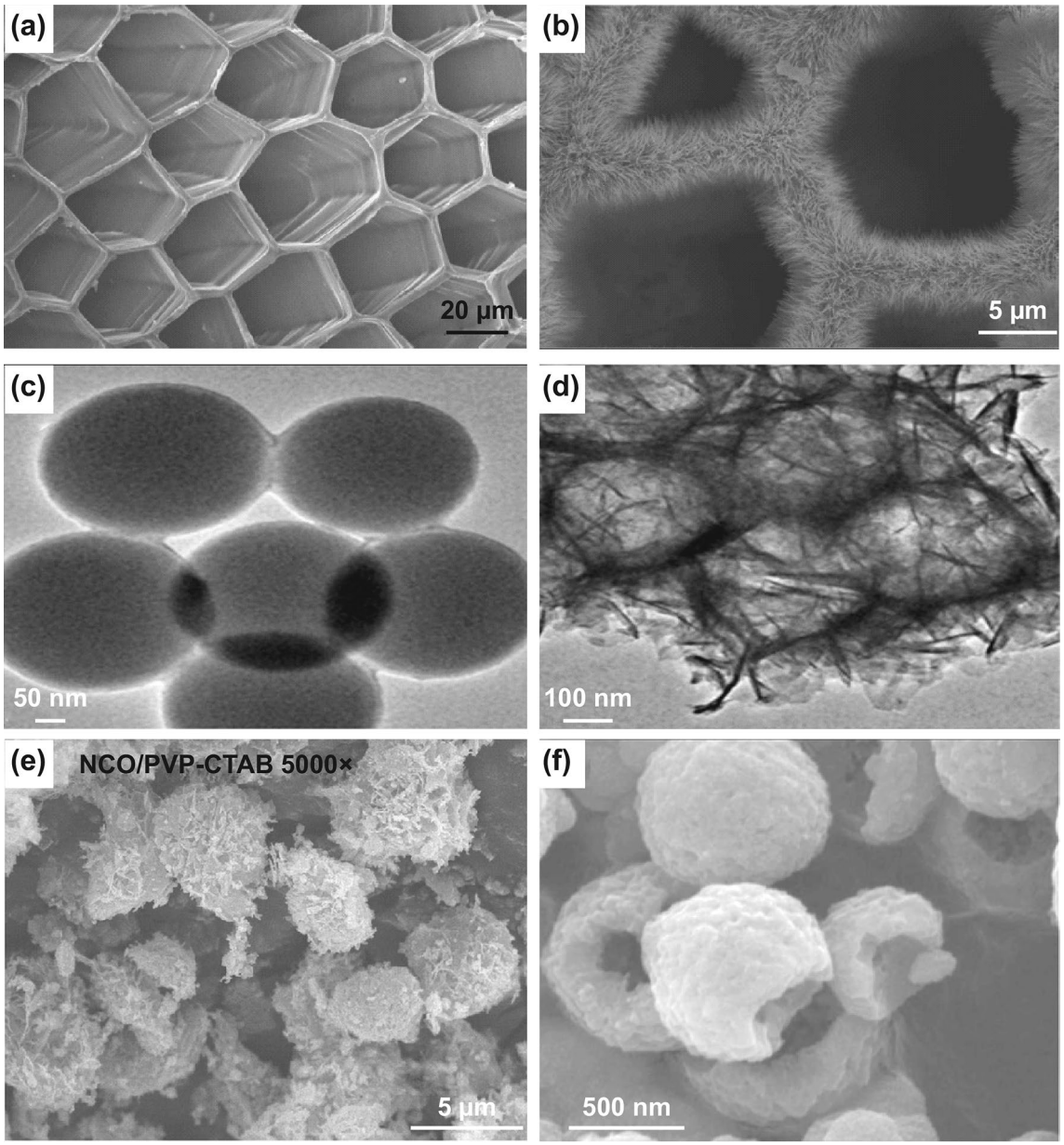

Fig. 11 FESEM images of **a** MSBPC, **b** $NiCo_2O_4$ nanowires grown on MSBPC. Reproduced with permission from Ref. [129]. Copyright © 2014 American Chemical Society. **c** TEM image of SiO_2@RF spheres, **d** TEM image of $NiCo_2O_4$ nanoflakes grown on SiO_2@RF spheres. Reproduced with permission from Ref. [130]. Copyright © 2018 Elsevier B.V. **e** FESEM image of micron-sized $NiCo_2O_4$ pompon. Reproduced with permission from Ref. [132]. Copyright © 2019 Elsevier B.V. **f** FESEM image of $NiCo_2O_4$ hollow submicron spheres. Reproduced with permission from Ref. [133]. Copyright © 2015 Elsevier B.V.

by removing calcium carbonate crystal and other biomacromolecules by acid treatment and carbonization. It was observed that there was uniform and dense growth of the $NiCo_2O_4$ nanowires on the inner walls of MSBPC channels. The average length of the $NiCo_2O_4$ nanowires was about 1.5 μm. Li et al. [130] reported the synthesis of composite C@$NiCo_2O_4$ hollow microspheres via a two-step strategy of hard template-induced hydrothermal synthesis followed by calcination. SiO_2@RF (resorcinol–formaldehyde resin, RF) sphere was used as a hard template, whereas HMTA was used as precipitant. The template SiO_2@RF was synthesized via a one-pot sol–gel process under alkaline condition using an alcohol–water mixed solvent [131]. The SiO_2 core was removed by treating the prepared material with 2 M NaOH at room temperature for 12 h. The SiO_2@RF template was having a core–shell structure with an average diameter of 350 nm (Fig. 11c). The $NiCo_2O_4$ nanoflakes were grown and assembled on the carbon surface of the SiO_2@RF spheres (Fig. 11d). Recently, novel micron-sized $NiCo_2O_4$ pompon was prepared by templated growth using polyvinylpyrrolidone (PVP) non-ionic polymer and cationic surfactant CTAB as co-template [132]. Columbic and coordinative forces between template, co-template, and the metal ions help to form a stable "hairball" structure which finally was converted into a micron-sized pompon-like product on annealing (Fig. 11e). In contrast, in the absence of co-template CTAB, mesoporous $NiCo_2O_4$ hollow submicron spheres with a uniform diameter of 400–500 nm were obtained through a soft template method assisted by PVP (Fig. 11f). Further, in the absence of even PVP, solid submicron spheres were obtained [133].

Qi et al. [131] also used RF microspheres as templates for the synthesis of $NiCo_2O_4$ hollow microspheres with tunable shell numbers and shell thickness. The shell numbers were controlled by adjusting the solvent ratio (DI water: ethylene glycol) and heating ramp rate, whereas the shell thickness and porosity were controlled by adjusting the metal ion concentrations (Fig. 12). For total molar concentrations of Ni^{2+} and Co^{2+} of 0.05 and 0.1 M, thin and thick shells, respectively, were formed. $NiCo_2O_4$ hollow microspheres with double and triple shells were formed at a heating ramp rate of 2 and 5 °C min^{-1}, respectively, in EG as a solvent. With the increase in the ramp rate, the increased temperature gradient of the infused RF microspheres along the radial direction favors the separation of adjacent $NiCo_2O_4$ layers and the infused RF cores, thereby transforming double shell to triple shells [134]. Furthermore, EG prevents the formation of the metal aqua ions, and thus, the penetration of the metal ions into RF microspheres is accelerated which is essential for the formation of multi-shell $NiCo_2O_4$ hollow microspheres [135, 136]. Additionally, the final calcination process also results in some adhesion force in the outward direction and the contraction force by decomposition of the inner core which segregates the outer $NiCo_2O_4$ shell and the inner infused RF [131].

In addition to templates of organic origin, inorganic metal oxides have also been reported as template materials for the synthesis of $NiCo_2O_4$ nano-/microarchitectures [137]. Lv

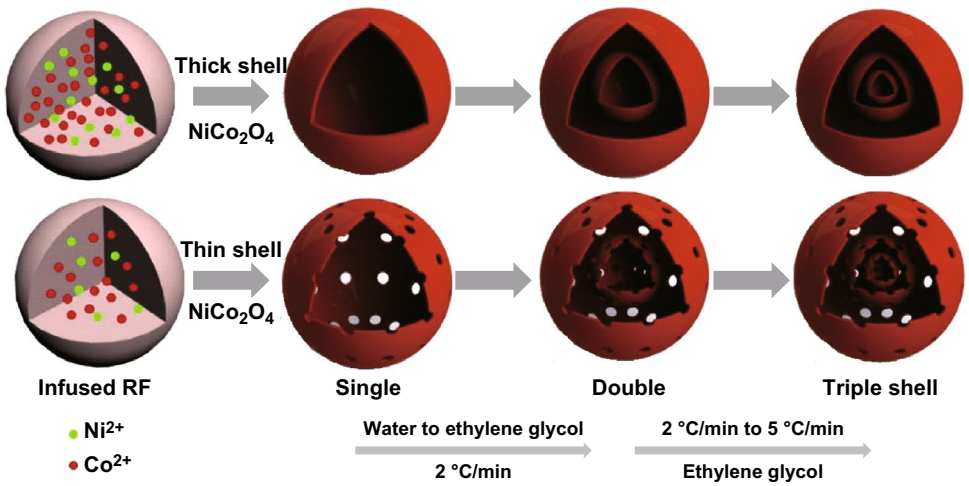

Fig. 12 Pictorial representation for the formation of $NiCo_2O_4$ hollow microspheres with tunable numbers and shell thickness. Reproduced with permission from Ref. [131]. Copyright © 2016 Elsevier B.V.

 https://doi.org/10.1007/s40820-020-00462-w

et al. [138] synthesized hollow $NiCo_2O_4$ octahedral nanocages via a Cu_2O-templated strategy in combination with a coordination reaction. Uniform Cu_2O octahedral crystals were prepared by reducing a copper-citrate complex solution with ascorbic acid in the presence of PVP. Initially, amorphous (NiCox)O(OH) was deposited onto the Cu_2O octahedral crystals through a precipitation method. Cu_2O octahedral crystals were etched according to a "coordinating etching and precipitating" (CEP) using $Na_2S_2O_3$ as coordinating etchant [139] (Eqs. 14, 15). After that, the product was annealed at 400 °C for 2 h to get the hollow $NiCo_2O_4$ nanocages. In a similar study, Huang et al. [140] reported the synthesis of highly porous $NiCo_2O_4$ hollow nanospheres through a polycrystalline Cu_2O-templated route based on "coordinating etching and precipitating" process. The excellent electron transfer capability, large specific surface area, and intrinsic redox couples of Ni^{2+}/Ni^{3+} and Co^{2+}/Co^{3+} ions, and superior electrocatalytic activity of $NiCo_2O_4$ hollow nanospheres were explored for glucose sensing by cyclic voltammetry and electrochemical impedance spectroscopy. $NiCo_2O_4$ hollow nanosphere-modified glassy carbon electrode (GCE) exhibited a high sensitivity of 1917 μA mM^{-1} cm^{-2}, linear dynamic ranges of 0.01–0.30 mM and 0.30–2.24 mM, and very low detection limit of 0.6 μM (S/N = 3). Solid CuO octahedral is also reported as template materials for the synthesis of hollow octahedra-like $NiCo_2O_4$ cages. However, CuO templates can be simply removed by dissolving with a diluted NH_4OH solution [141].

$$Cu_2O + S_2O_3^{2-} + H_2O \rightarrow Cu_2(S_2O_3) + 2OH^- \quad (14)$$

$$S_2O_3^{2-} + H_2O \leftrightarrow HS_2O_3^- + OH^- \quad (15)$$

Yang et al. [142] reported $NiCo_2O_4$ hollow nanorods prepared by the sacrificial template-accelerated acid hydrolysis of ZnO (Eq. 16).

$$ZnO + 2H^+ \rightarrow Zn^{2+} + H_2O. \quad (16)$$

3.3 Sol–gel Method

The sol–gel process represents the chemical conversion of the liquid "sol" to the network "gel" phase, subsequently post-treatment into solid metal oxides with microcrystalline ultrafine particles. It is superior to other methods because it can better control the texture and surface properties of synthesized nanomaterials. The sol–gel method for the synthesis of nanomaterials is affected by numerous factors including pH, temperature, nature of solvent, growth time, agitations time, presence of capping agents, template, etc. With the consideration of these factors and potential applications, many protocols have been used to design materials of different sizes and features, including nano-, micro-, meso-, and macro-materials. To get excellent porosity and conductivity for potential electrochemical applications, the addition of polymers stuffs such as PVP [143], organic solvents/additives like propionic acid [144], citric acid [145, 146], *N*,*N*-dimethylformamide (DMF) [147], and epoxides like propylene oxide [148, 149], during the post-annealing process is suggested. Significantly the additive/metal ion molar ratio is very important in controlling the pore size and pore volume. Traditional use of SiO_2 is avoided as its addition decreases the conductivity and limits the connection of the film with conducting substrate in thin film forms of $NiCo_2O_4$ [143]. In a typical sol–gel method, the $NiCo_2O_4$ spinel oxide was prepared by mixing appropriate amounts of metal salt precursors along with citric acid. The resulting solution was magnetically stirred at 80 °C for 2 h to get a gelatinous matrix. Finally, the matrix was calcined at 550 °C for 5 h to get the desired product [146]. Citric acid was also used as a chelating ligand for the synthesis of highly porous coral-like crystalline $NiCo_2O_4$ nanoparticles with submicron sizes via a facile sol–gel method in H_2O-DMF mixture as solvent [147]. Liu et al. prepared nanoporous $NiCo_2O_4$ thin films deposited on ITO glass. The precursor solutions for $NiCo_2O_4$ nanospheres were prepared via a sol–gel method in glacial acetic acid and ethanol as solvents, and ethylene glycol and CTAB were used as a viscosity modifier template, respectively [150]. Thus, the sol–gel process is a proven and important method for preparing $NiCo_2O_4$ nanoparticles.

3.4 Co-precipitation Method

Better stoichiometric control and high purity of the metal oxide nanomaterials can be easily achieved through the coprecipitation method which involves simultaneous precipitation from a homogeneous solution of two or more cations. Simultaneous occurrence of nucleation, growth, coarsening, Ostwald ripening, and aggregation dramatically affect the size, morphology, and properties of the metal oxide

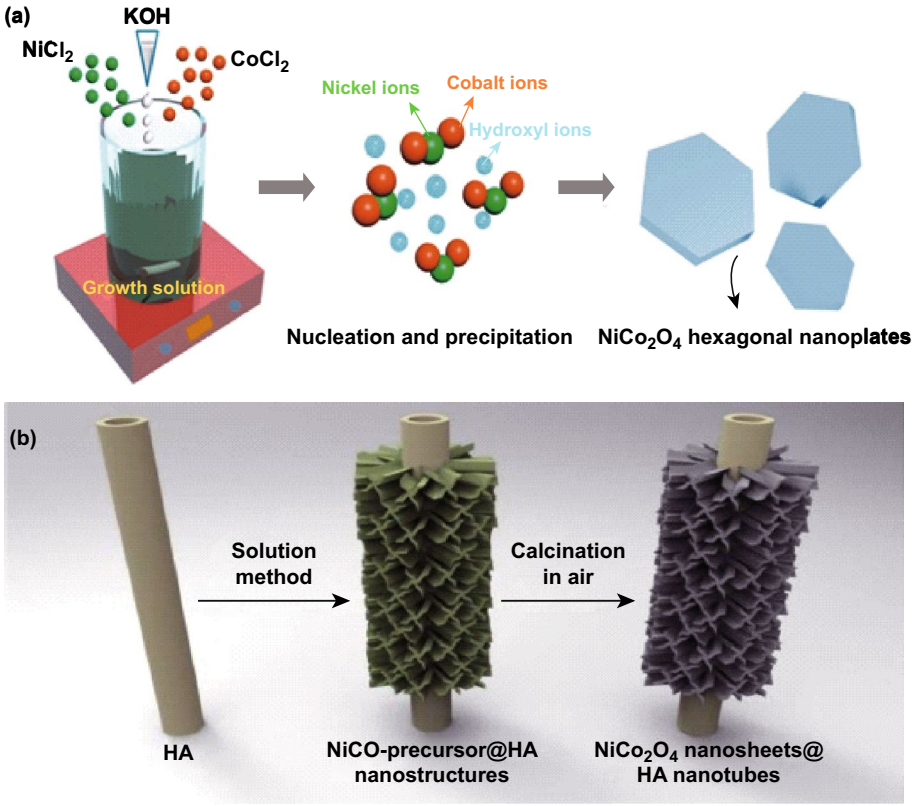

Fig. 13 **a** Schematic representation for the synthesis of hexagonal $NiCo_2O_4$ nanosheets, Reproduced with permission from Ref. [151]. Copyright © 2019 Elsevier Ltd. and **b** hierarchical $NiCo_2O_4$ nanosheets@halloysite nanotubes via co-precipitation method. Reproduced with permission from Ref. [152]. Copyright © 2014 American Chemical Society

nanoparticles. The technique has been applied for the synthesis of $NiCo_2O_4$ nanomaterials. $NiCo_2O_4$ hexagonal nanostructures were prepared by Bhagwan et al. [151] using Ni and Co chlorides and 6 M KOH as the precipitating agent. The schematic illustration for the formation of $NiCo_2O_4$ hexagonal is shown in Fig. 13a. It was suggested that the strong alkaline environment in the growth solution caused nickel and cobalt ions to precipitate and nucleate together, forming nickel–cobalt hydroxide which was subsequently converted into $NiCo_2O_4$ hexagonal after calcination at 300 °C. Liang et al. [152] reported hierarchical $NiCo_2O_4$ nanosheets@halloysite nanotubes (Fig. 13b). The initial formation of NiCo precursor@halloysite nanotubes was assisted by HMTA and dehydrated citric acid trisodium salt.

A stepwise co-precipitation template free method was designed by Chen et al. [153] for the synthesis of hierarchical urchin-like $NiCo_2O_4$ hollow nanospheres. Urea-assisted mesoporous urchin-like $NiCo_2O_4$ nanostructures were prepared by Jadhav et al. [154] by an easy, viable, and cost-effective co-precipitation method. Yu et al. [155] explored the structure-stabilizing properties of PVP, which can bind the metal ions through electrostatic interaction with the –N and/or C=O functional groups, for the formation of Ni–Co precursor particles with tetragonal prism-like shapes by a modified coprecipitation method. The yolk–shell Ni–Co oxide nanoprisms with a highly porous interior core structure consisting of numerous polycrystalline primary particles were obtained finally after annealing. Other stabilizing and precipitating agents like ethylene glycol (EG) [156], urea [157], NaOH, NH_4OH, NH_4HCO_3, $H_2C_2O_4$ [158, 159] and $NaHCO_3$ [153] are reported in the literature. Organic stabilizers such as EG are supposed to form a protective layer around the particle surface through interactions with hydroxyl groups preventing the aggregation. Moreover, EG also acts as a bidentate chelating ligand for solvated metal ions [160]. Another important factor that controls the morphology, shape, and size of the nanoparticles is the pH of the reaction medium during

 https://doi.org/10.1007/s40820-020-00462-w

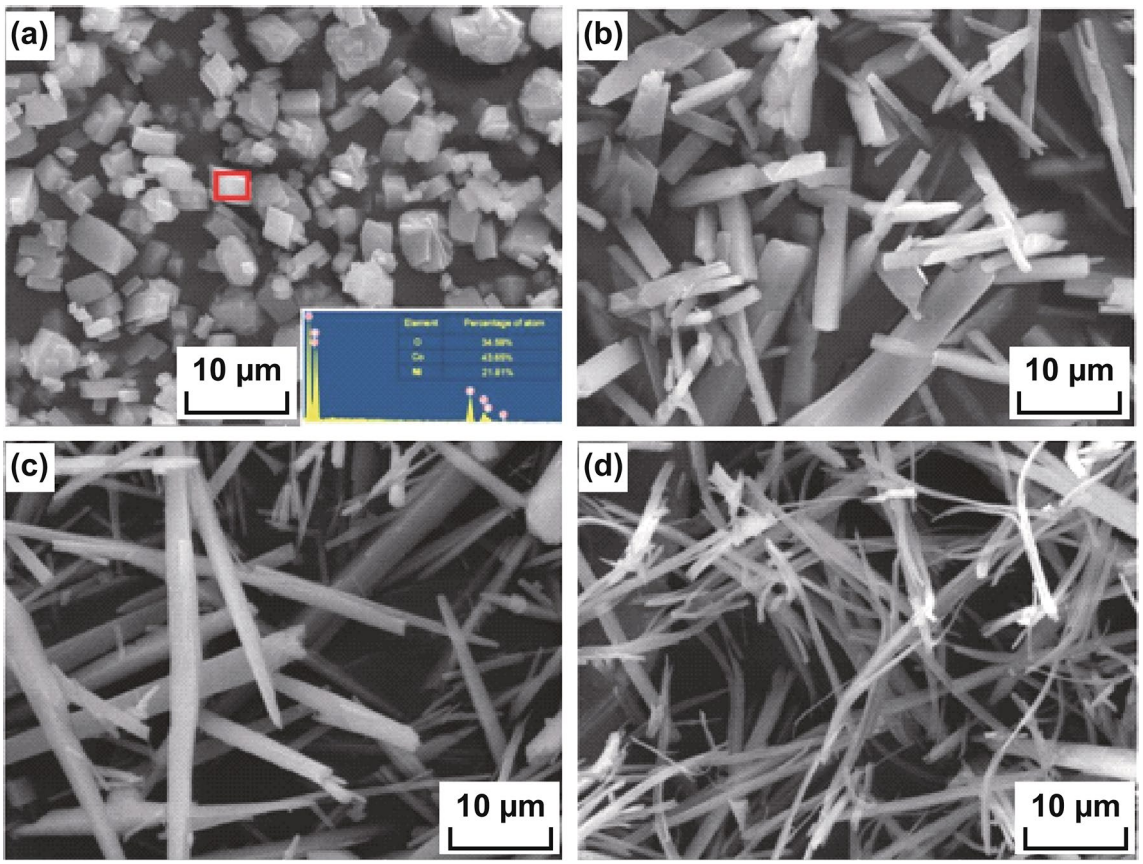

Fig. 14 FESEM images $NiCo_2O_4$ precursor powders prepared at **a** pH = 3, **b** pH = 7, **c** pH = 8 and **d** pH = 8.4. Reproduced with permission from Ref. [159]. Copyright © 2018 Elsevier Ltd.

coprecipitation. Wan et al. [159] observed the change in morphology of the $NiCo_2O_4$ precursors from the cubic to the fibrous along the axial direction. The fibrous morphology was maintained at a still higher pH value of 8.4; however, the aspect ratio was increased (Fig. 14a–d). A dynamic equilibrium was suggested to exist between metal ammoniated complexes and the coprecipitation of Ni^{2+} and Co^{2+} as their oxalates.

The post-annealing temperature is also an important factor for controlling the morphology of the $NiCo_2O_4$ spinel structures. The homogeneous dark blue-colored suspension which was obtained by mixing the metal nitrates and NaOH solution was initially evaporated under rotation and reduced pressure conditions by a cost-effective rotary evaporation method. Hexagonal column-like mesoporous loose architectures and hexagonal dense blocks were obtained at 200 and 400 °C calcination temperatures, respectively (Fig. 15) [161].

3.5 Electro-Deposition

Electro-deposition is considered a very useful, versatile, and flexible tool for the deposition of dendritic hierarchical structures, thin and thick films, nanosheet, nanofoil, nanotubes, nanowires, and many well-ordered transition metal oxides on conducting surfaces. Potentiostatic, galvanostatic, and pulse plating are the three main techniques employed for electro-deposition [162, 163]. The basic principle of electro-deposition involves three steps, viz. preparation of a metal ions precursor solution, co-electro-deposition, and final thermal decomposition [164]. Recently, this technique has also been used for the preparation of $NiCo_2O_4$ spinel structures for various applications, including supercapacitors, anode materials for Li-ion batteries, gas sensors, biosensors, etc. Wu et al. [165] deposited nanostructured cauliflower-like $NiCo_2O_4$ film through galvanostatic electro-deposition combined with annealing treatment (Fig. 16). Galvanostatic

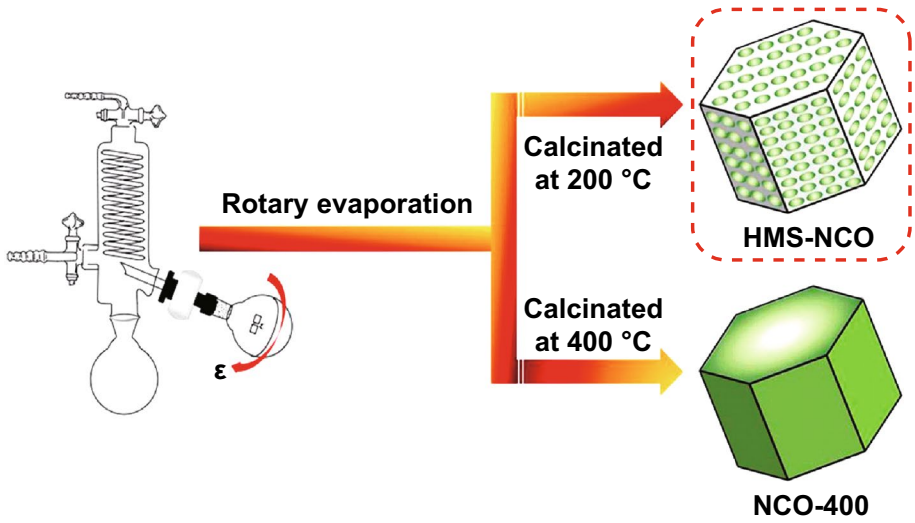

Fig. 15 Schematic illustration of the synthesis of hexagonal mesoporous structured $NiCo_2O_4$ (HMS-NCO) and $NiCo_2O_4$ calcined at 400 °C (NCO-400). Reproduced with permission from Ref. [161]. Copyright © 2018 Elsevier Ltd and Techna Group S.r.l.

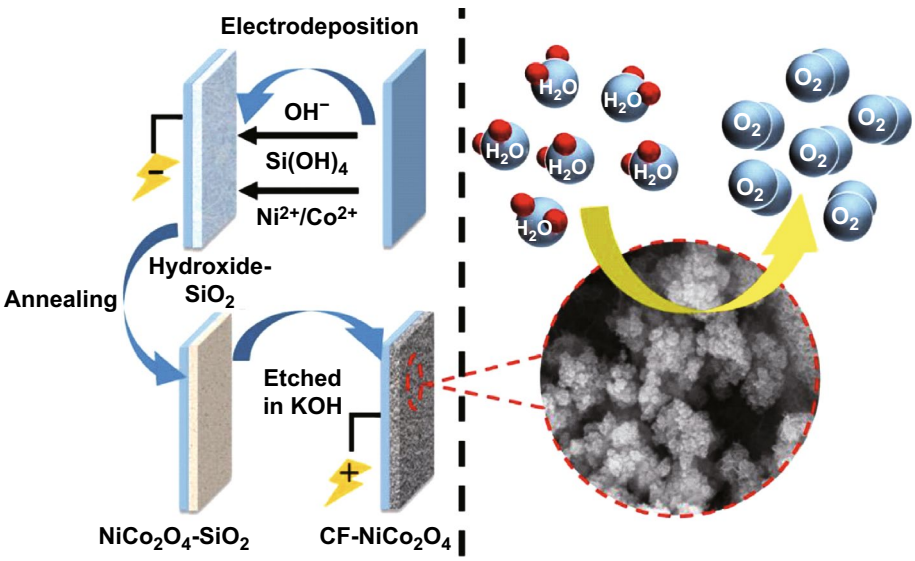

Fig. 16 Schematic illustration of the formation of cauliflower-like $NiCo_2O_4$ film. Reproduced with permission from Ref. [165]. Copyright © 2017 Hydrogen Energy Publications LLC. Published by Elsevier Ltd

electro-deposition was performed using a three-electrode compartment comprising a stainless steel disk as a working electrode. An Ag/AgCl saturated with KCl and a platinum plate were used as the reference and counter electrodes, respectively. Hydroxide-SiO_2 template transformed nanoflakes to cauliflower-like $NiCo_2O_4$ nanoparticles. Under cathodic potential, the generated OH^- ions catalyzed the sol–gel process for the formation of SiO_2. The generated OH^- ions facilitated the formation of $Ni(OH)_2$ and $Co(OH)_2$. Heat treatment of the deposited at 250 °C in air for 2 h converts the metal hydroxides into $NiCo_2O_4$ films.

Wang et al. [166] reported the electro-deposition of the nickel/cobalt/zinc ternary alloy layer on ultrafine nickel wire. Removal of the zinc by dealloying with NaOH solution followed by oxidation at the atmospheric environment resulted in mesoporous $NiCo_2O_4$ film on the surface of ultrafine nickel wire. Zhao et al. [167] grew $NiCo_2O_4$ nanosheet networks on carbon cloth through a simple cathodic

 https://doi.org/10.1007/s40820-020-00462-w

electro-deposition process followed by post-annealing at 300 °C in an air atmosphere for 120 min. The average mass loadings for $NiCo_2O_4$ nanosheet networks grown on carbon cloth at different electro-deposition times 200, 400, and 600 s were 0.4, 0.6, and 0.9 mg cm^{-2}, respectively. The NO_3^- ions from the metal salts were reduced to NO_2^- and NH_4^+ ions at the cathode. This reduction also resulted in the formation of OH^- ions which combined with the Ni^{2+} and Co^{2+} to form amorphous binary metal hydroxide $NiCo_2(OH)_6$ nanosheet networks [168]. Post-annealing transforms the $NiCo_2(OH)_6$ into $NiCo_2O_4$ nanosheet networks [57, 169] (Eqs. 17–20).

$$NO_3^- + H_2O + 2e^- \rightarrow NO_2^- + 2OH^- \quad (17)$$

$$NO_2^- + 6H_2O + 6e^- \rightarrow NH_4^+ + 8OH^- \quad (18)$$

$$Ni^{2+} + 2Co^{2+} + 6OH^- \rightarrow NiCo_2(OH)_6 \quad (19)$$

$$NiCo_2(OH)_6 + \frac{1}{2}O_2 \rightarrow NiCo_2O_4 + 3H_2O \quad (20)$$

The dissolution of the ions decreases near the electrode due to the formation of the OH^- ions and an increase in pH near the electrode is observed. Since the solubility constants of $Ni(OH)_2$ (8.2×10^{-16}) and $Co(OH)_{2/3}$ (2.5×10^{-16}) are very low and comparable, their simultaneous precipitations occur which finally gives $NiCO_2(OH)_6$ [170, 171]. Ramadoss et al. [169] electrodeposited highly porous and binder-free 3D flower-like $NiCo_2O_4$/Ni nanostructures on Ni wire and explored their supercapacitor applications (Fig. 17a). The high porosity of the nanostructures was attributed to the presence of H_2 bubbles produced by hydrogen evolution reaction during electro-deposition. Furthermore, H_2 bubbles also acted as a template for the construction of a 3D flower-like $NiCo_2O_4$/Ni with dendritic walls on the Ni wire. Nanoforest hierarchical composites Co_3O_4@$NiCo_2O_4$ nanowire arrays were synthesized by Zhang et al. [172]. Co_3O_4 nanowires were initially grown on Ni foam through a facile hydrothermal method. After that, $NiCo_2O_4$ was electrochemically deposited in the Co_3O_4 nanowires to avoid the conventional aggregation (Fig. 17b). Mirzaee et al. [173] proposed a two-step method involving initial electrodeposition followed by thermal treatment at 300 °C with a ramping rate of 1 °C min^{-1} to form flower-like arrays of $NiCo_2O_4$ on electrochemically reduced graphene oxide

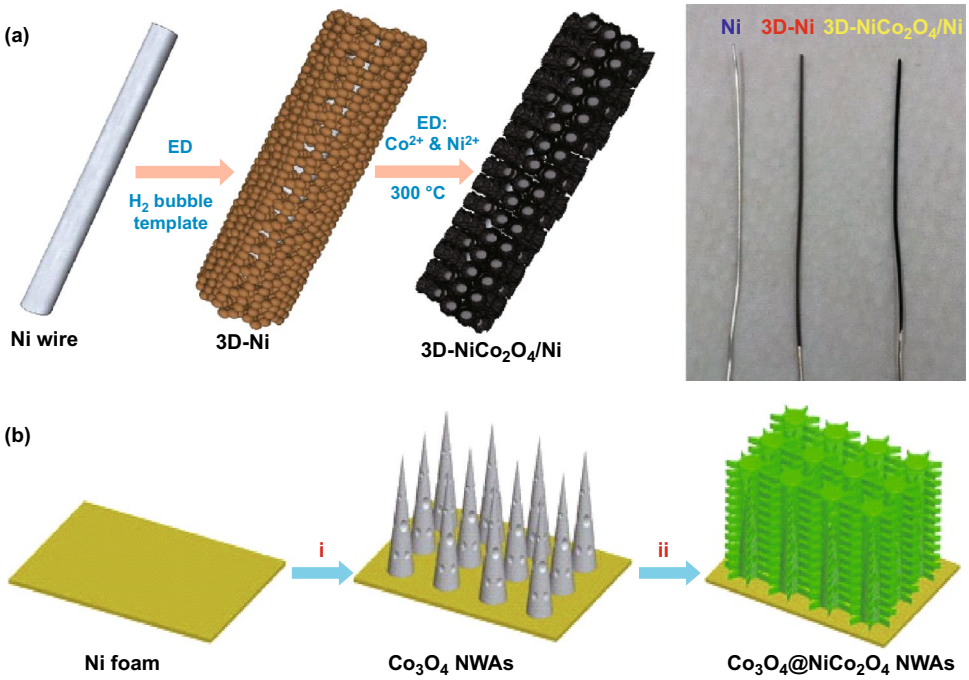

Fig. 17 **a** Electrodeposited 3D flower-like $NiCo_2O_4$/Ni nanostructures on Ni-wire. Reproduced with permission from Ref. [169], Copyright © 2016 The Royal Society of Chemistry. **b** Schematic representation of the formation of nanoforest hierarchical composites Co_3O_4@$NiCo_2O_4$ nanowire arrays. Reproduced with permission from Ref. [172]. Copyright © 2013 Elsevier Ltd.

(ERGO) which itself was deposited on nickel–nickel oxide foam.

In addition to these, $NiCo_2O_4$ architectures of versatile morphologies have been electrochemically deposited on a variety of conducting surfaces. Some of these include honeycomb-shaped $NiCo_2O_4$ on carbon cloth [174], ultrathin $NiCo_2O_4$ nanosheets on three-dimensional interwoven nitrogen-doped carbon nanotubes [175], ultrathin porous $NiCo_2O_4$ nanosheet arrays on flexible carbon fabric, 3D vertically aligned carbon nanotubes/$NiCo_2O_4$ core/shell structures [176], hybrid composite $Ni(OH)_2$@$NiCo_2O_4$ on carbon fiber paper [177], 3D hierarchical $NiCo_2O_4$@MnO_2 hybrid nanomaterial on stainless steel mesh [178], free-standing bowl-like $NiCo_2O_4$ on carbon fiber paper [179], network-like holey $NiCo_2O_4$ nanosheet arrays on Ni foam [180], $NiCo_2O_4$@ carbon nanofibers [181], and many more.

3.6 Combustion Method

Combustion synthesis, also referred to as self-propagating high-temperature synthesis is one of the most versatile, convinced, convenient, cost-effective, and fast method for the synthesis of nanomaterials. It involves a thermally induced redox reaction between precursor salt as oxidizers and an organic fuel [182–184]. Glucose, fructose, tartaric acid, sucrose, glycine, citric acid, hydrazine, urea, and oxalic acid are generally used as organic fuels. However, if metal oxalate or acetate salts are used, the combustion process can be directly conducted in the absence of fuel [185]. Byproduct gases like CO_2, H_2O, N_2, oxides of N (NO_x) and S (SO_x), etc. are evolved during the combustion process [186]. The release of these gases promotes the expansion of the product and rapid fall in temperature after the reaction ceases. This provides a solid product with a high degree of porosity and good dispersibility [187]. As compared to solid-state combustion, liquid phase combustion synthesis has proved to be the most suitable one as oxidizers and fuel are well dissolved in aqueous or alcoholic solutions [188]. $Ni(NO_3)_2{\cdot}6H_2O$, $Co(NO_3)_2{\cdot}6H_2O$ (in 1:2 molar ratio) as oxidizers and tartaric acid as fuel were dissolved in acidified 2-methoxy ethanol solution. The resulting solution was combusted at 250 °C for 1 h to prepare $NiCo_2O_4$ nanoparticles [189]. Sucrose assisted combustion of the Ni and Co nitrates also resulted in $NiCo_2O_4$ nanoparticles when the combustion process was carried out at 350 °C for 6 h [190]. The oxalate precursors were directly decomposed into $NiCo_2O_4$ powders by heating in an air ambient atmosphere at 320 °C for 10 h [185]. Citric acid assisted combustion at 400 °C for 4 h resulted in highly porous $NiCo_2O_4$ nanomaterials [191]. Urea-assisted combustion was processed at 400 °C for 2 h in ethyl acetate as a solvent [192]. In each case, a viscous gel is obtained initially by heating the reaction solution at low temperature followed by auto-ignition resulting in the formation of highly fluffy mass which is finally calcined at high temperature. Direct calcination of the metal nitrate salts in the presence of alkalis without any fuel has also been reported for the synthesis of the $NiCo_2O_4$ nanorods [41].

Though it is a fast and low-cost method for the synthesis of $NiCo_2O_4$ powders, it suffers from some major drawbacks including less control over morphological uniformity and particle size, the simultaneous formation of a variety of crystal phases, the formation of highly agglomerated structures, complex and uncertain growth mechanism, and critically very low possibilities of formation of a versatile and wide range of morphological structures as those of in hydrothermal and other solution methods.

3.7 Electro-Spinning Method

Many electrospun carbonaceous materials such as carbon nanofibers, single-walled carbon nanotubes, multi-walled carbon nanotubes, etc. prepared from oxidation and carbonization of polymers like PVP, PAN, PVA have been used as templates for the growth and deposition of $NiCo_2O_4$ nanostructures with versatile morphologies. In one synthetic way, there is simultaneous growth of $NiCo_2O_4$ nanostructures and electro-spinning of template material [193, 194]. In another strategy, $NiCo_2O_4$ nanostructures are grown through other synthetic methods like hydrothermal, sol–gel, coprecipitation, etc. on pre-electrospun carbonaceous templates [39]. Electro-spinning setup comprises a high-voltage system, spinneret, and collector which results in the formation of continuous nanofibers with diameters ranging from nanometer to micrometer [195–197]. The deposition of $NiCo_2O_4$ nanostructures on these carbonaceous materials not only improves the electrical and electronic properties but also enhances the thermal, mechanical and chemical stabilities which are the important prerequisite characteristics for the biosensing and other applications. The composition of the precursor solution, presence of additives like templates and

https://doi.org/10.1007/s40820-020-00462-w

capping agents, modification in the electro-spinning setup, post-annealing, electrospun voltage are some of the major factors which control the thickness, porosity, and morphology of the deposited $NiCo_2O_4$ films. Lai et al. [198] through electro-spinning, co-deposition, redox deposition fabricated $NiCo_2O_4$-doped carbon nanofiber@MnO_2 nanosheet and nanorod hybrid membranes. Busacca et al. [199] prepared $NiCo_2O_4$/carbon nanofibers composites and investigated their oxygen evolution reaction in alkaline electrolyte. Metal acetate salt precursor in a molar ratio 1:2 was mixed in PAN (as carbon source) and DMF. The electrospun layer was thermally oxidized at 270 °C in air for 30 min followed by subsequent carbonization at 900 °C for 1 h under a helium gas flow. Li et al. [193] fabricated porous one-dimensional $NiCo_2O_4$ nanostructures via a single-spinneret electro-spinning method. Stoichiometric amounts of Ni and Co nitrates were homogeneously mixed in a solution prepared by dissolving PVP in ethanol and *N*,*N*-dimethylformamide. Metallic precursor concentration: PVP (M: PVP) ratio was significant in determining the morphologies of the electrospun one-dimensional $NiCo_2O_4$ nanostructures. For 0.44:1, 0.61:1, and 0.87:1 M: PVP ratios, $NiCo_2O_4$ nanofibers, nanotubes, and nanobelts were formed. The versatility in morphologies was attributed to the fast water evaporation and burning off of PVP during annealing. Guan et al. [194] synthesized spinel $NiCo_2O_4$ nanofibers with diameters of 50–100 nm through electro-spinning of the PVA/cobalt acetate/nickel acetate composite precursor followed by annealing at high temperatures ranging from 400 to 800 °C. Liu et al. [39] demonstrated the surfactant-assisted hydrothermal uniform growth $NiCo_2O_4$ nanoneedle on electrospun carbon nanofiber (ECF) and explored their glucose sensing properties non-enzymatically. ECF film was prepared through initial electro-spinning and subsequent oxidation and carbonization of PAN (Fig. 18a–c). Xu et al. [200] instead of PAN used PVP as a carbon source to produce $NiCo_2O_4$ nanotubes. These nanotubes were used as scaffolds for hydrothermal growth of MnO_2 nanosheets for the additional improvement in electronic conductivity and electrochemical activity for supercapacitor applications (Fig. 18d–f). Copolymers like poly (acrylonitrile-co-methylhydrogen itaconate) [201] and biobased polymer composites such as PAN/lignin [202] are also reported in the literature for the formation of flexible carbon nanofibers. The hollow carbon nanofibers were used as a template for the hydrothermal growth of $NiCo_2O_4$ with uniform dandelion-like morphology consisting of densely grown nanoneedle (Fig. 18g, h) [203]. The above discussion thus reveals that the proper combination and the composition of the polymers can result in the formation of carbonaceous materials with versatile structural features with high surface area necessary for potential applications.

3.8 Microwave-Assisted Method

Microwaves are the electromagnetic radiations having a frequency range between 300 MHz and 300 GHz and a wavelength range of 1 m–1 mm. Microwave-assisted synthesis of nano-/microstructures is superior to the conventional methods described above because it requires a very short reaction duration, is energy efficiency, cost-effectiveness, and gives an excellent yield of highly porous materials. Microwaves result in volumetric heating as they can penetrate throughout the volume of reactants [204]. This volumetric heating is caused by various types of polarization in the medium, including electron polarization, atomic polarization, directional polarization, and space charge polarization [205]. To obtain better morphological results, microwave-assisted synthesis of nanomaterials is usually combined with other synthetic methods such as sol–gel, co-precipitation, and hydro/solvothermal, etc. Recently, the improvement in the hydrothermal method in harmony with microwave assistance has been studied to synthesize $NiCo_2O_4$ nano-/microstructures. Other ways of engineering the structural aspects of the $NiCo_2O_4$ are the use of a template, capping agents, organic solvents, ionic solvents, and addition of other growth additives. The microwave-assisted hydrothermal method was applied by Zhang et al. [206] to prepare $NiCo_2O_4$ double-shelled hollow spheres with an outer and inner shell thickness of ~ 20 and ~ 70 nm, respectively. A mixture of isopropanol and glycerol was used to prepare a reaction solution (Fig. 19a). Glycerol molecules were supposed to form a self-assembled quasi-emulsions in isopropanol that serve as a soft template for the growth of Ni–Co double hydroxides. In the absence of glycerol, solid microspheres with diameters of ~ 1 μm were formed, demonstrating the templated role of glycerol in the synthesis of a double-shelled hollow nanostructure (Fig. 19b–d). In the presence of microwaves, the reaction mixture is heated due to dielectric loss, which significantly accelerates the reaction kinetics. Additionally, the presence of microwaves improves uniformity in terms of dispersion and size distributions.

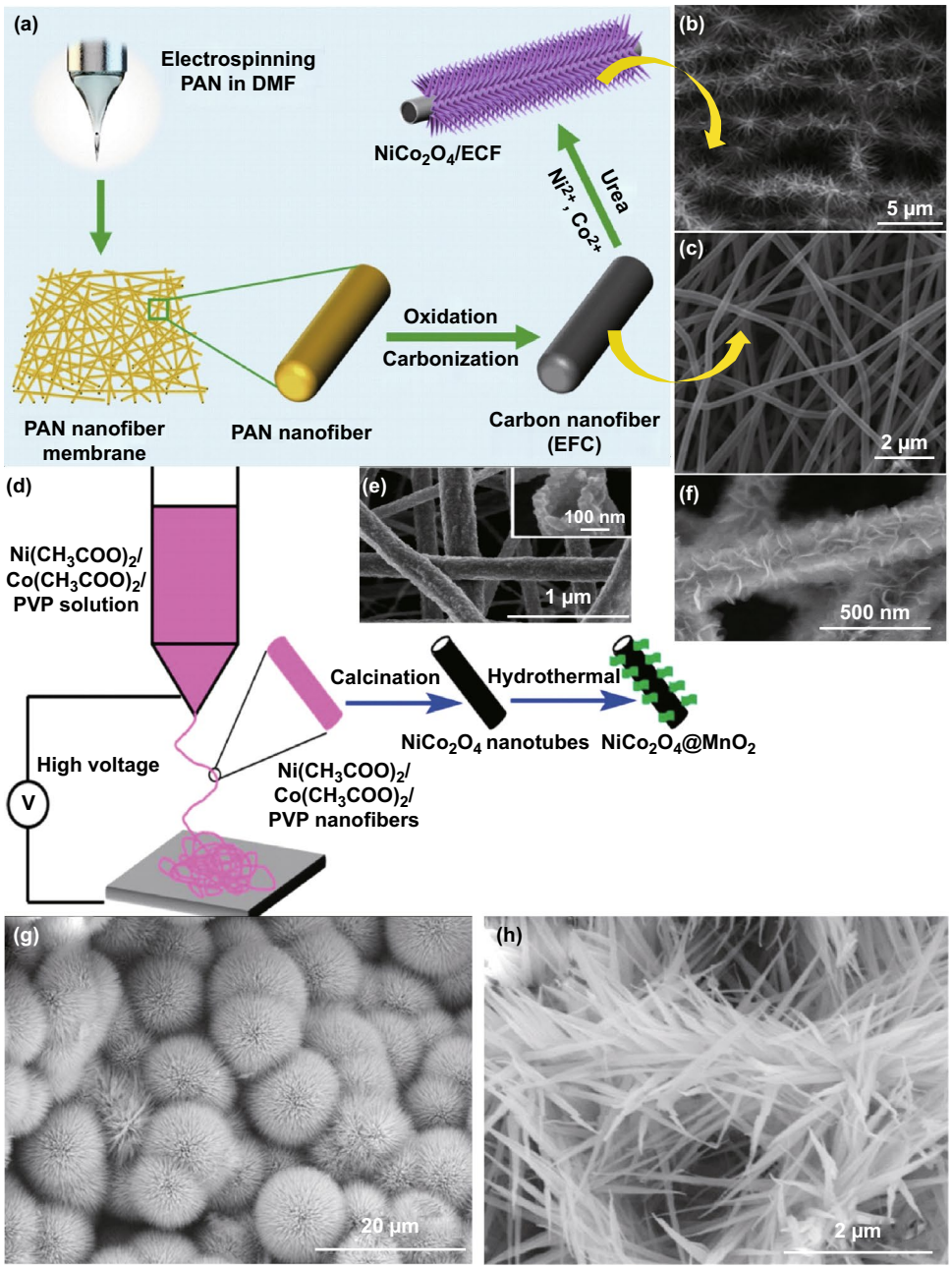

Fig. 18 **a** Fabrication procedure of $NiCo_2O_4$/ECF nanohybrids, **b** FESEM image of ECF and **c** FESEM image of $NiCo_2O_4$ nanoneedles grown on ECF. Reproduced with permission from Ref. [39]. Copyright © 2017 Elsevier B.V. **d** The fabrication procedure for $NiCo_2O_4$@MnO_2 composites, **e** FESEM image of $NiCo_2O_4$ nanotubes and **f** FESEM image of MnO_2 nanosheets grown of $NiCo_2O_4$ nanotubes. Reproduced with permission from Ref. [200]. Copyright © 2016 Elsevier B.V. **g, h** Low- and high-magnification FESEM images, respectively, of $NiCo_2O_4$ with uniform dandelion-like morphologies. Reproduced with permission from Ref. [203]. Copyright © 2019 Elsevier Ltd.

Shanmugavani et al. [207] analyzed the effect of reaction times on the morphology of the $NiCo_2O_4$/NiO nanocomposites. The reaction was carried out in the presence of oxalic acid at an operating frequency of 2.45 GHz and 800 W output power. It was proposed that the initially formed nanoparticles are converted into bundled-like structures as the reaction time was increased. Recently, Sun et al. [103] reported novel porous nanoscale NiO/$NiCo_2O_4$ heterostructure through two-stage calcination of nickel–cobalt bimetallic hydroxide precursors (NiCo precursors) which were

 https://doi.org/10.1007/s40820-020-00462-w

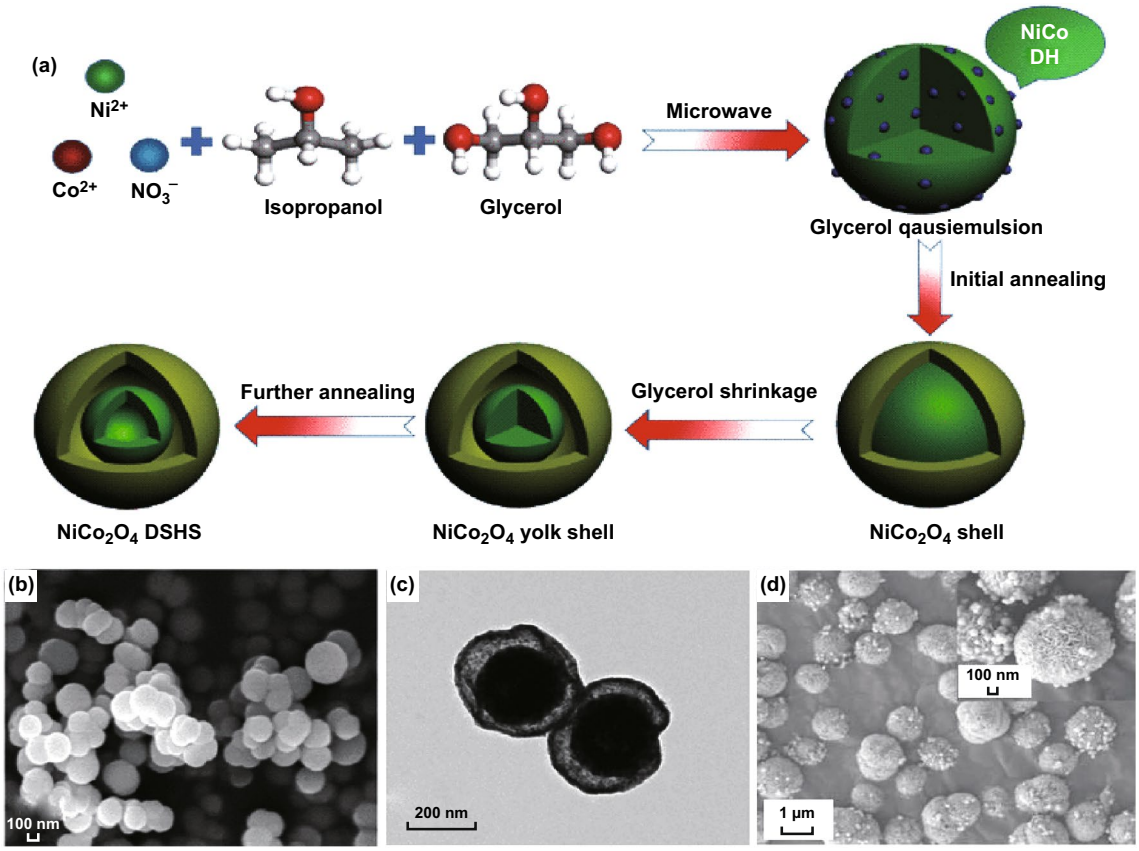

Fig. 19 **a** Pictorial representation of the microwave-assisted hydrothermal synthesis of $NiCo_2O_4$ double-shelled hollow spheres. **b** FESEM and **c** TEM images of $NiCo_2O_4$ hollow spheres prepared in the presence of glycerol and d FESEM image of the $NiCo_2O_4$ structures prepared in the absence of glycerol. Reproduced with permission from Ref. [206]. Copyright © 2017 Springer Nature

initially synthesized using a microwave-assisted hydrothermal method in the presence of HMTA and NH_4F. Notably, F^- ions were supposed to act as functional template agents. Prolonged irradiation significantly affects the morphology of $NiCo_2O_4$ materials. When the irradiation time was increased from 5 to 40 min, the incompletely self-assembled and non-uniform 2D nanosheets are converted into more optimized and thickened 3D frameworks with large open spaces (Fig. 20a–i).

Nakate et al. [208] prepared nanocrystalline $NiCo_2O_4$ nanoplates in the surfactant-free environment using metal chloride salts precursors through microwave irradiation. Gu et al. [209] reported 3D nanosphere-like $NiCo_2O_4$ nanostructure composed of intertwined 2D ultrathin mesoporous nanosheets having large specific surface area 146.5 $m^2\ g^{-1}$. The reaction solution was exposed to microwaves (power 560 W) for 6 min. Su et al. [210] reported highly crystalline $NiCo_2O_4$ supported on carbon black via a simple, one step intermittent microwave heating method avoiding the calcination process. However, in a contrary study, Tao et al. [211] analyzed the effect of post-annealing temperature on the morphologies of the $NiCo_2O_4$. Ni–Co double hydroxide was initially prepared through a microwave-assisted method using a tertbutanol solution (98%). Flower-shaped morphology of the Ni–Co double hydroxide was completely converted into unique coral-like morphology on calcination. As the post-annealing temperature was increased from 400 to 700 °C, individual ultrathin nanosheets shrink to smaller nano-sized crystal grains which finally self-assembled to form coral-like $NiCo_2O_4$ architectures.

For greener perspectives, ionic solvents like [1-butyl-3-methylimidazolium][BF_4] {[Bmim][BF_4]}, [Bmim]$FeCl_4$, [Bmim]Cl [212], and non-ionic glucose-based polymeric surfactant, β-C_{10}Alkyl Poly Glucoside [213] are also reported in the literature for the synthesis of $NiCo_2O_4$ architectures with versatile morphologies.

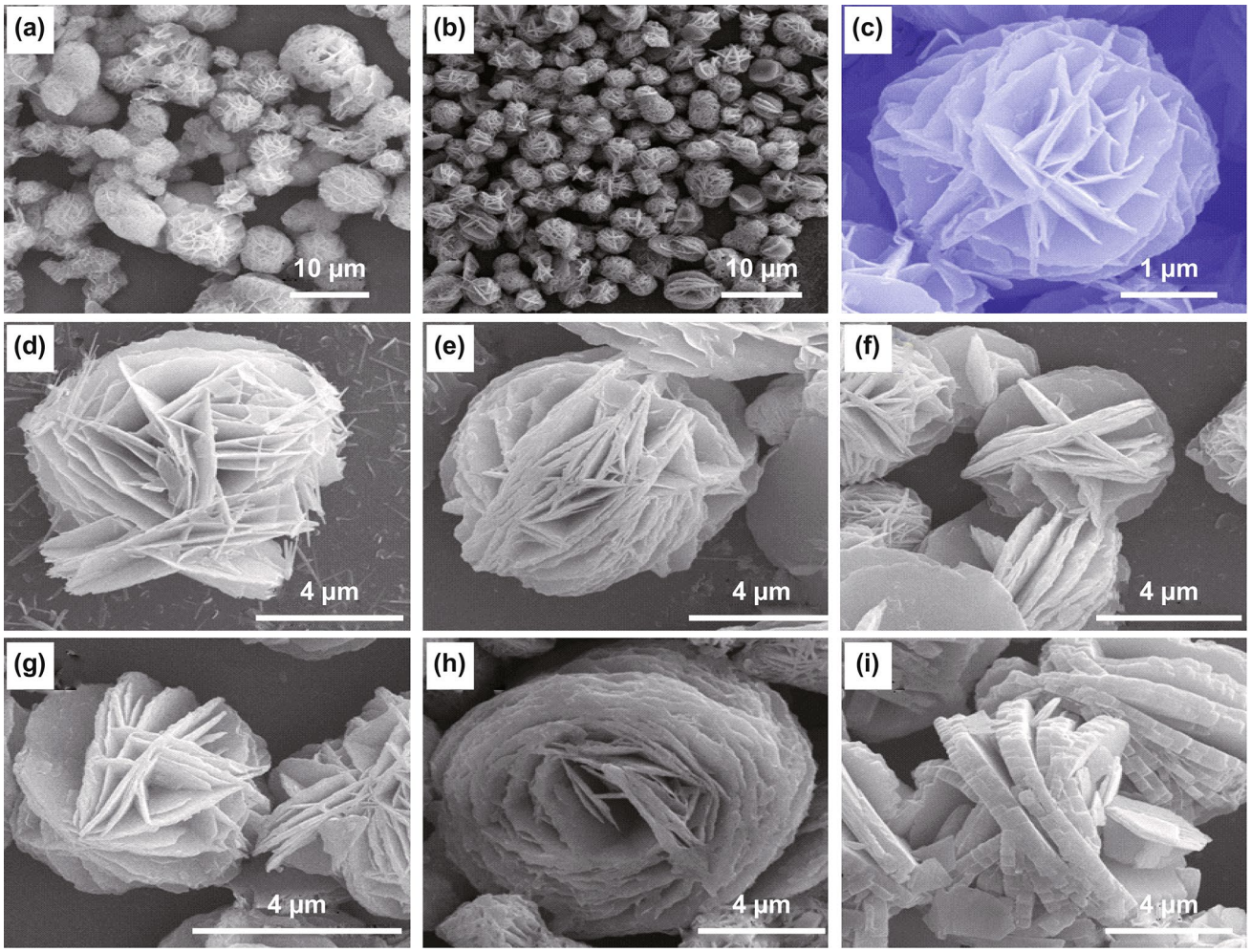

Fig. 20 FESEM images of bimetal Ni-Co-precursors obtained under various microwave-assisted hydrothermal reaction times. **a** 5 min, **b, c** 10 min, **d** 15 min, **e** 20 min, **f** 25 min, **g** 30 min, **h** 35 min, and **i** 40 min. Reproduced with permission from Ref. [103]. Copyright © 2019 Elsevier Inc.

3.9 Spray Pyrolysis Method

In spray pyrolysis technique, an aerosol of various precursor components is prepared in suitable solvent and is sprayed on the substrate. After that, sequential evaporation of the solvent from the surface of the substrate, heating to precipitate out the solute, high-temperature annealing, formation of microporous particles, and finally, sintering of solid particles is carried out [214]. $NiCo_2O_4$ nanostructures with morphologies hollow nanosphere [215], hollow microspheres [216], dried plum-like particles [217], yolk–shell microspheres [218], nanoaggregates [219], thin films with uniform particle distribution size 20–30 nm [220], etc. are reported (Fig. 21a–e).

Similar to the electro-spinning method, carbonaceous materials such as reduced graphene oxide, carbon nanotubes, carbon nanofibers are also mixed in the precursor solution to improve the electrochemical properties of $NiCo_2O_4$. Park et al. [221] synthesized three-dimensional macroporous multi-walled carbon nanotubes microspheres densely loaded with $NiCo_2O_4$ hollow nanospheres via spray pyrolysis process. The schematic illustration depicting the formation mechanism is shown in Fig. 22a. The polystyrene nanobeads added in the solution improved the structural uniformity and the dispersion of CNT microspheres. The similarity in the atomic radii of the Ni and Co ions resulted in the Kirkendall diffusion into the outer surface of the where they were oxidized to form $NiCo_2O_4$ (Fig. 22b).

 https://doi.org/10.1007/s40820-020-00462-w

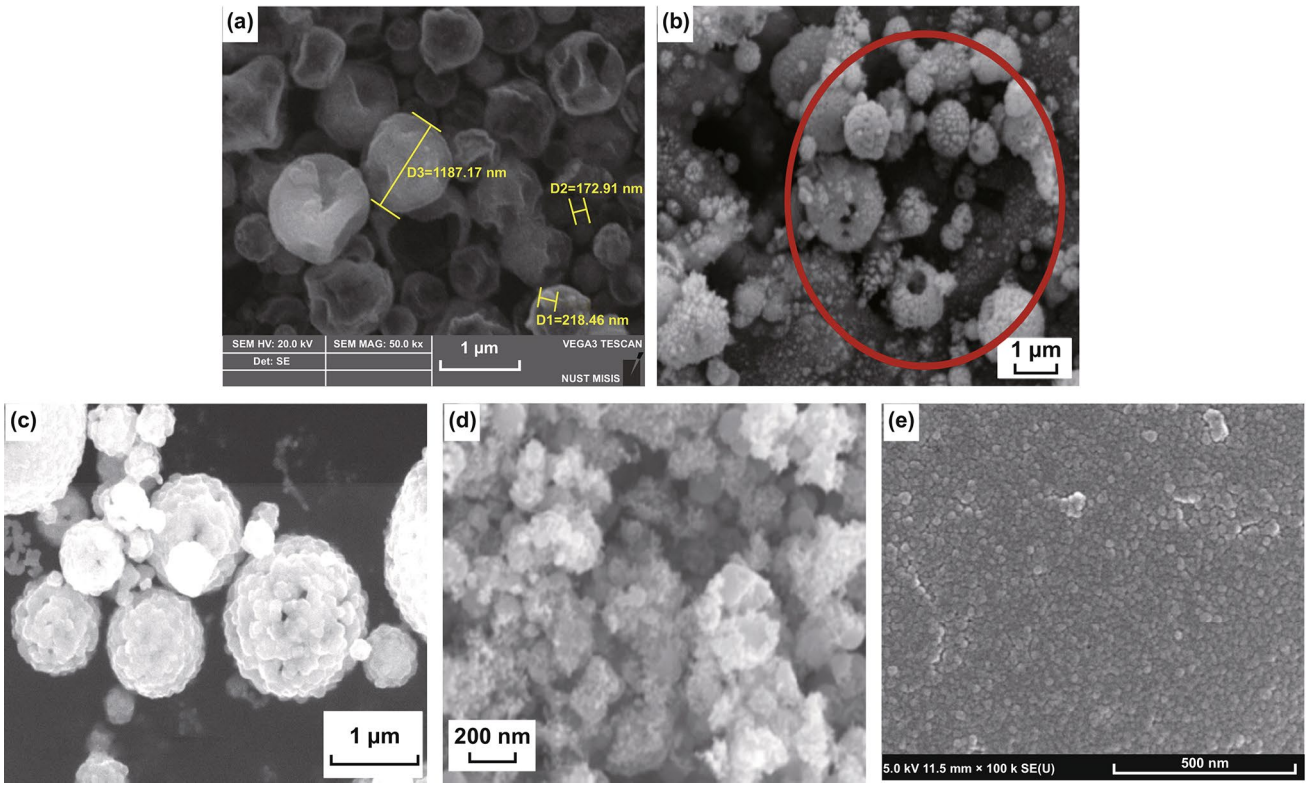

Fig. 21 Morphologies of various $NiCo_2O_4$ nanostructures **a** hollow nanosphere. Reproduced with permission from Ref. [215]. Copyright © 2017 The Korean Society of Industrial and Engineering Chemistry, Published by Elsevier B.V. **b** hollow microspheres. Reproduced with permission from Ref. [216]. Copyright © 2019 Elsevier Ltd and Techna Group S.r.l. **c** yolk–shell microspheres. Reproduced with permission from Ref. [218]. Copyright © 2017 Elsevier Ltd. **d** nanoaggregates. Reproduced with permission from Ref. [219]. Copyright © 2015 Elsevier Inc. and **e** thin films with uniform particle distribution size 20–30 nm. Reproduced with permission from Ref. [220]. Copyright © 2016 Elsevier Ltd.

4 Biosensor Applications of Nano-/Micro-structured $NiCo_2O_4$

4.1 Glucose Biosensors

Non-enzymatic glucose sensing is considered to be a better, fast, and convenient way as compared to the enzymatic method since the later is a complicated and multi-step process involving immobilization of enzyme bioreceptor such as glucose oxidase, glucose dehydrogenase, and quinoprotein glucose dehydrogenase onto the electrode surface [51, 52]. Furthermore, maintaining the enzyme stability under non-physiological conditions of observations is another major issue related to enzymatic glucose biosensing. Most of the biosensing measurements are based on cyclic voltammetry (CV) and amperometric analysis. Better biosensing behavior and electrochemical activity using $NiCo_2O_4$ nano-/microstructure-modified electrodes are adjudged by broader redox peaks with larger area coverage in the CV curves. Since the spinel $NiCo_2O_4$ comprises binary intrinsic-state redox couples of Ni^{3+}/Ni^{2+} (0.58 V/0.49 V) and Co^{3+}/Co^{2+} (0.53 V/0.51 V), only a pair of redox peaks in the CV curves is generally observed due to almost similar redox potential values for NiO and Co_3O_4 [142, 222, 223]. In alkaline medium, $NiCo_2O_4$ is oxidized to Ni and Co perhydroxides which finally convert glucose into gluconolactone (Eqs. 21–26) [224].

$$NiCO_2O_4 + OH^- + H_2O \leftrightarrow NiOOH + 2CoOOH + e^- \quad (21)$$

$$CoOOH + OH^- \rightarrow Co_2O_3 + H_2O + e^- \quad (22)$$

$$NiOOH + \text{Glucose} \rightarrow Ni(OH)_2 + \text{Gluconolactone} \quad (23)$$

$$CoOOH + \text{Glucose} \rightarrow Co(OH)_2 + \text{Gluconolactone} \quad (24)$$

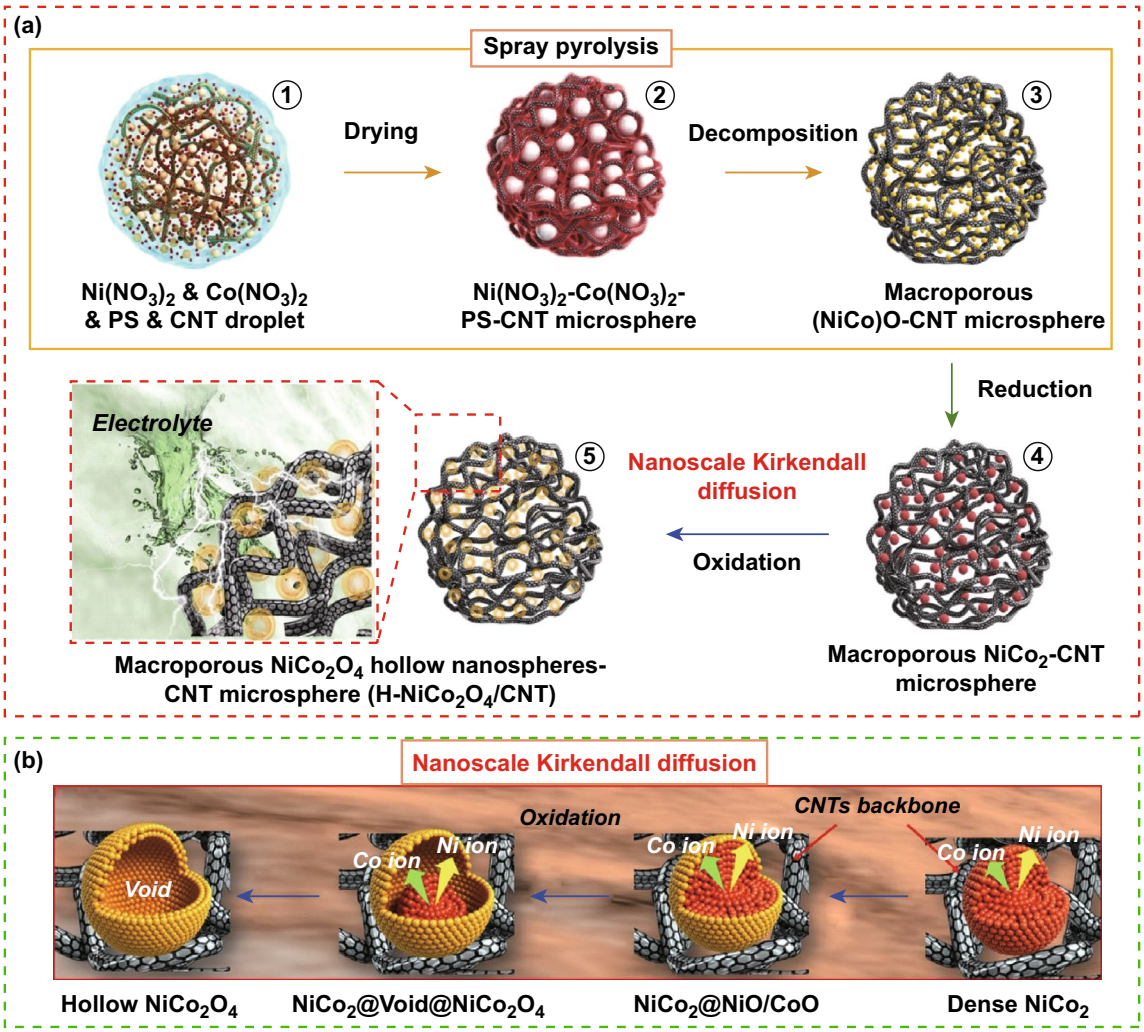

Fig. 22 Formation mechanism of 3D macroporous multi-walled carbon nanotubes microspheres densely loaded with $NiCo_2O_4$ hollow nanospheres. Reproduced with permission from Ref. [221]. Copyright © 2017 Elsevier Ltd.

$$Ni^{2+} + Co^{2+} \rightarrow Ni^{3+} + Co^{3+} + 2e^- \quad (25)$$

$$\text{Glucose}\left(C_6H_{12}O_6\right) \rightarrow \text{Gluconolactone}\left(C_6H_{10}O_6\right) + 2H^+ + 2e^- \quad (26)$$

Since the rates of oxidation of Ni^{2+} and Co^{2+} ions on the electrode surface during anodic scan determine the rate of sensing of glucose, $NiCo_2O_4$ nano-/microstructures with versatile morphologies having large specific surface area, permeability, and most importantly short electron and ion diffusion pathways are synthesized. Ni^{3+} and Co^{3+} ions are reduced back to Ni^{2+} and Co^{2+} ions by the electrons lost by the oxidation of glucose to gluconolactone. According to Hussain et al. [225], H_2O_2 is formed as one of the products along with gluconolactone if the electrochemical sensing is performed in the presence of oxygen. Glucose undergoes a spontaneous reaction with water and O_2 to form gluconolactone which is further oxidized into gluconic acid (Eqs. 27, 28). In a slightly basic medium (pH = 7.4), gluconic acid ionizes to gluconate ions which act as mobile charge carriers on the surface of the $NiCo_2O_4$ nanostructures producing a strong electrical signal (Eq. 29). Elakkiya et al. [226] reported highly porous flower-like $NiCo_2O_4$ nanostructures synthesized via a facile hydrothermal method for excellent electrocatalytic activity in alkaline electrolyte for the oxidation of glucose and lactic acid.

https://doi.org/10.1007/s40820-020-00462-w

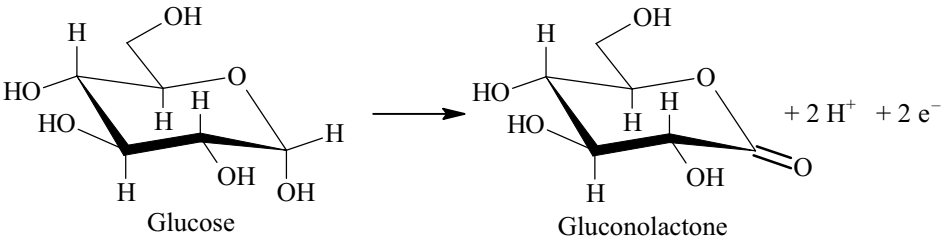

(27)

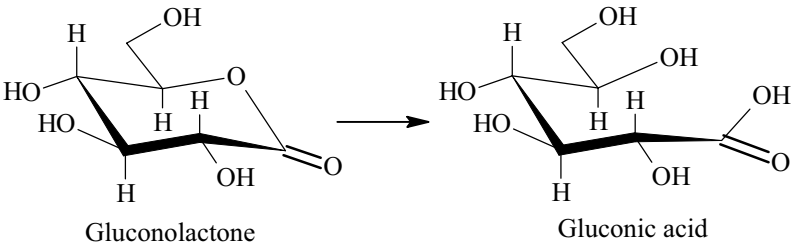

(28)

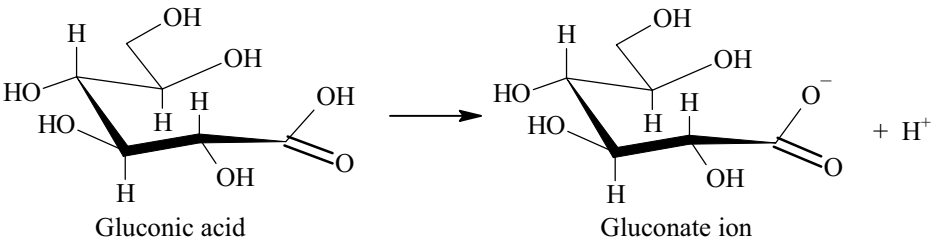

(29)

The binary spinel $NiCo_2O_4$ architecture exhibits better intrinsic electronic conductivity as compared to pure NiO and Co_3O_4 which is attributed to the doping of Ni^{3+} ions in the octahedral sites of the Co_3O_4 crystal lattice which accelerates the electron hopping process [227]. Huang et al. [140] compared the electron transfer resistance (R_{et}) through electrochemical impedance spectroscopy for GCE modified with $NiCo_2O_4$, NiO, and Co_3O_4. Nyquist plots for all the modified GCE consisted of two portions; an inclined line at low frequencies and a semicircular portion at high frequencies. However, the lowest R_{et} of $NiCo_2O_4$/GCE was an indication of the enhanced conductivity for $NiCo_2O_4$ (Fig. 23a). Broader redox peaks $NiCo_2O_4$/GCE as compared to NiO/GCE and Co_3O_4/GCE confirmed the better biosensing behavior of the $NiCo_2O_4$ as compared to Co_3O_4 and NiO (Fig. 23b).

Spinel $NiCo_2O_4$ hollow nanocages were prepared by using Co-based zeolite imidazole frameworks (ZIF-67) as a template and precursor by Feng et al. [228]. Morphological characterization revealed that the thickness of the cage shell was about 30 nm. The outer surface of the nanocages was covered with small nanosheets. A wide linear dynamic range 0.18 μM–5.1 mM, high sensitivity 1306 μA mM^{-1} cm^{-2}, a fast response time of 1 s, and limit of detection 27 nM were observed for $NiCo_2O_4$ hollow nanocage-based modified GCE.

$NiCo_2O_4$ nanoplates interconnected through MoS_2 nanosheets performed excellent electrocatalytic behavior toward glucose. $NiCo_2O_4$ nanoplates and MoS_2 nanosheets illustrated a significance synergic effect. Though not an active catalyst for the oxidation of glucose, the highly active edge of vein-like MoS_2 nanosheets inhibited the agglomeration of $NiCo_2O_4$ nanoplates and formed long conducting chains which provide an alternative pathway with lower electrical resistance [229] (Fig. 24a, b). The fabricated glucose biosensor exhibited a high sensitivity of 1748.58 μA mM^{-1} cm^{-2} and a very low detection limit of 0.152 μM. MoS_2 nanosheets have also been reported

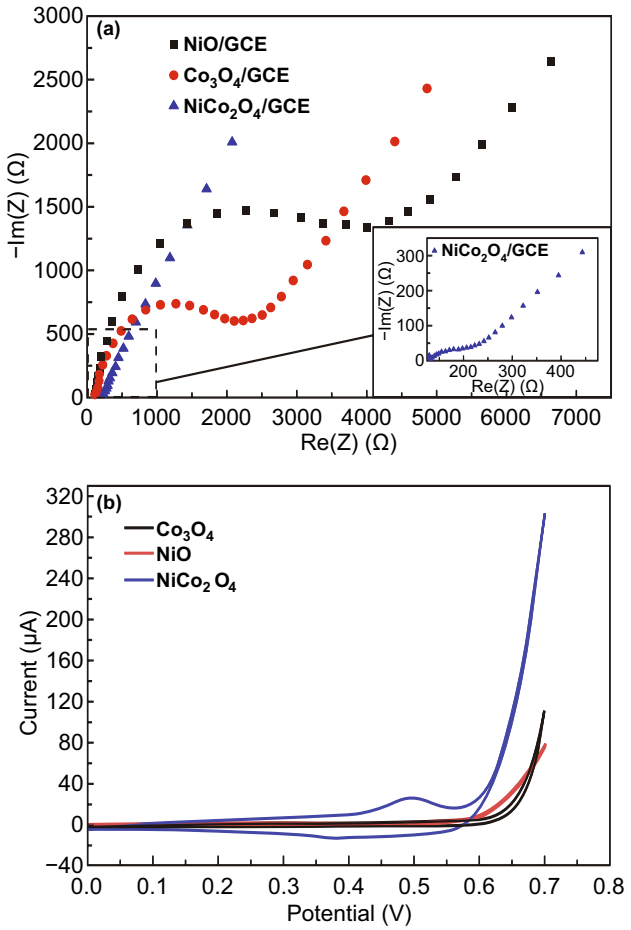

Fig. 23 **a** Nyquist plots of $NiCo_2O_4$, Co_3O_4, and NiO-modified GCE in 0.1 M NaOH. **b** CV curves for $NiCo_2O_4$, Co_3O_4, and NiO-modified GCE in 0.2 M NaOH without glucose. Reproduced with permission from Ref. [140]. Copyright © 2016 Elsevier B.V.

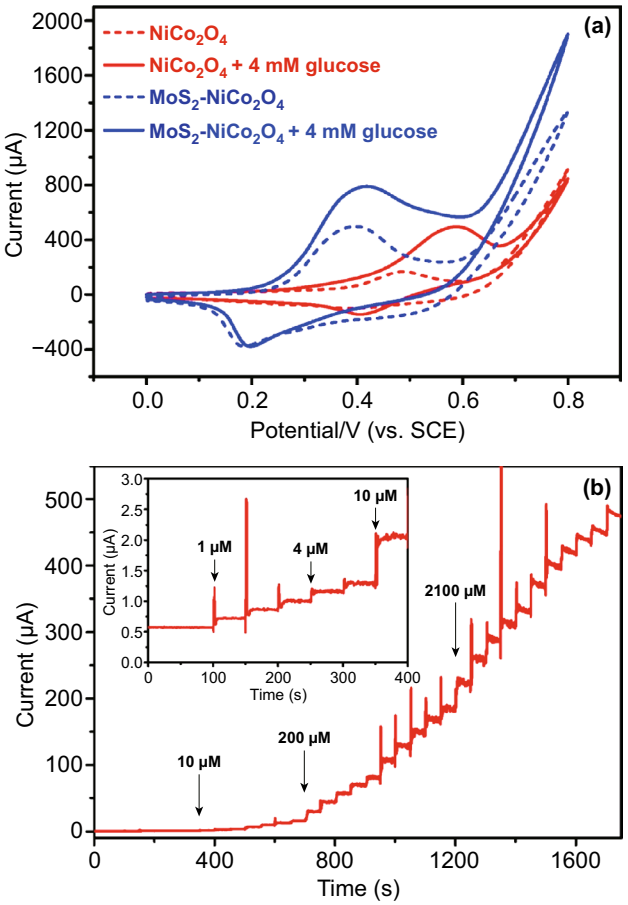

Fig. 24 **a** Electrocatalytic activities of MoS_2-$NiCo_2O_4$/GCE in 0.1 M NaOH at a scan rate of 50 mV s^{-1}. **b** Amperometric response curves for MoS_2-$NiCo_2O_4$/GCE. Reproduced with permission from Ref. [229]. Copyright © 2017 Elsevier B.V.

as support material for the fabrication of $NiCo_2O_4/MoS_2$ nanocomposites through a simple ionothermal method in deep eutectic solvent (choline chloride (ChCl)-urea mixture) [230]. Deep eutectic solvents consist of simple eutectic-based ionic liquids prepared by eutectic mixing of ChCl and some hydrogen bond donors like acids, amides, alcohols, etc. [231]. These solvents have excellent thermal stability, high surface tensions, negligible vapor pressure, and most importantly biodegradability [232–236]. The $NiCo_2O_4$-MoS_2/chitosan/GCE-modified electrode was used as an electrochemical sensor for glucose in red wine and honey [230].

Analysis of non-enzymatic glucose sensing properties of $NiCo_2O_4$ nanosheets showed linear response with respect to the change in glucose concentration varying from 5 to 65 μM. The high sensitivity of 6.69 μA μM^{-1} cm^{-2} with a LOD value of 0.38 μM and liquid of quantification of 1.27 μM was observed. During CV measurements, scan rates increased the oxidation and reduction peak currents as well as peak-to-peak separations [224]. The electrochemical kinetics of the $NiCo_2O_4$ hollow nanorods grown on stainless steel via a sacrificial template showed similar trends during glucose sensing in 0.1 M NaOH solution with scan rates ranging from 5 to 100 mV s^{-1} (Fig. 25a). Amperometric studies revealed a steady-state current optimization within 2 s of glucose addition. Calculated sensitivity, linear detection range, and detection limit were 1685.1 μA mM^{-1} cm^{-2}, 0.0003–1.0 mM, and 0.16 μM (S/N = 3), respectively (Fig. 25b) [142]. Cui et al. [237] prepared rectangular flake-like mesoporous $NiCo_2O_4$ via a facile hydrothermal method and observed glucose

https://doi.org/10.1007/s40820-020-00462-w

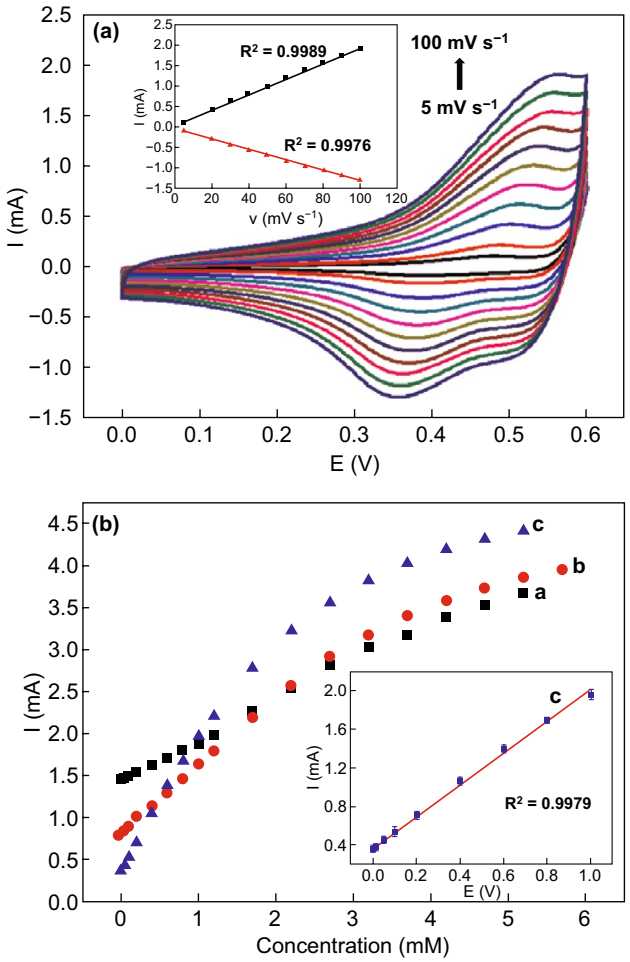

Fig. 25 **a** CV curves of $NiCo_2O_4$ hollow nanorods with various scan rates. Inset: redox peak currents as a function of the scan rates, **b** variation in response current for NiO (curve a), Co_3O_4 (curve b), and $NiCo_2O_4$ hollow nanorods (curve c) as a function of glucose concentrations. Inset: calibration curve of $NiCo_2O_4$ hollow nanorods. Reproduced with permission from Ref. [142]. Copyright © 2015 Elsevier B.V.

biosensing sensitivity of 662.31 μA mM^{-1} cm^{-2} and very low detection limit of 0.3 nM at S/N = 3. The other optimized operational parameters were: 0.2 M KOH, +0.5 V applied potential and 1.0 mg mL^{-1} loading of meso-$NiCo_2O_4$ in the suspensions. Dry rod-like $NiCo_2O_4$ synthesized through a facile hydrothermal reaction followed by subsequently microwave treatment. The non-enzymatic glucose sensor fabricated using these rod-like features showed a high sensitivity of 431.29 μA mM^{-1} cm^{-2} [238]. The microwave treatment completely removed the water and made the material highly porous for exhibiting excellent biosensing applications. One-dimensional porous $NiCo_2O_4$ nanowires array grown on nickel foam ($NiCo_2O_4$ NWs/NF) via a facile hydrothermal method exhibit highly efficient glucose sensitivity of 5916 μA mM^{-1} cm^{-2}, a detection limit of 1 μM–3.987 mM and LOD of 0.94 μM (S/N = 3) [239]. As conducting substrate, nickel foam not only provides the large electrochemically active surface area due to three-dimensional interconnected features, but also directs the growth of one-dimensional $NiCo_2O_4$ porous nanowires [240]. Besides, the one-dimensional porous $NiCo_2O_4$ nanowires array provided sufficient transport channels for ions and abundant active sites for redox reactions. Carbon cloth has also been used as a potential conducting surface for the growth of porous $NiCo_2O_4$ nanowires. As fabricated enzyme-free $NiCo_2O_4$ porous nanowire arrays supported on carbon cloth-based electrode for glucose sensing exhibited a linear dynamic range of 1 μM–0.63 mM, the sensitivity of 4.12 mA mM^{-1} cm^{-2}, and low detection limit of 0.5 μM [241].

One of the main disadvantages of using bare $NiCo_2O_4$ is its poor electrical conductivity. However, this limitation can be overcome by forming its composite/hybrid materials. It has been reported that the electrical conductivity and hence the electrochemical biosensing performance of $NiCo_2O_4$ can be improved by making its composites with conducting carbonaceous materials like graphene, reduced graphene oxide, carbon nanotubes (single and multi-walled), carbon nanofibers; conducting polymers like polypyrrole (PPy), polyaniline (PANI); metal oxides NiO, Co_3O_4, SnO_2, MnO_2; and metals like Au, Pd, etc. Among these, the carbonaceous materials are considered to be potential candidates as compared to others due to their excellent electrical conductivities, good mechanical strength, thermal and chemical stabilities, and resistance to oxidation–reduction reactions. Besides, these carbonaceous materials provide a large specific surface area for better adsorption of analytes, which ultimately results in very high sensitivity and very low detection limits.

The two-dimensional one-atom-thick layered structure of graphene has been extensively used for making composites with $NiCo_2O_4$ due to its high specific surface area of 2670 m^2 g^{-1} and excellent conductivity [242, 243]. Studies have revealed a higher specific surface area for the $NiCo_2O_4$/reduced graphene oxide composites as compared to bare $NiCo_2O_4$ nanoparticles (Fig. 26a) [244]. Even the pore width was less in the case of $NiCo_2O_4$/reduced graphene oxide composites. Various glucose-sensing scans are given in Fig. 26b–d. The enhanced redox peak current density for $NiCo_2O_4$/reduced graphene oxide composites as

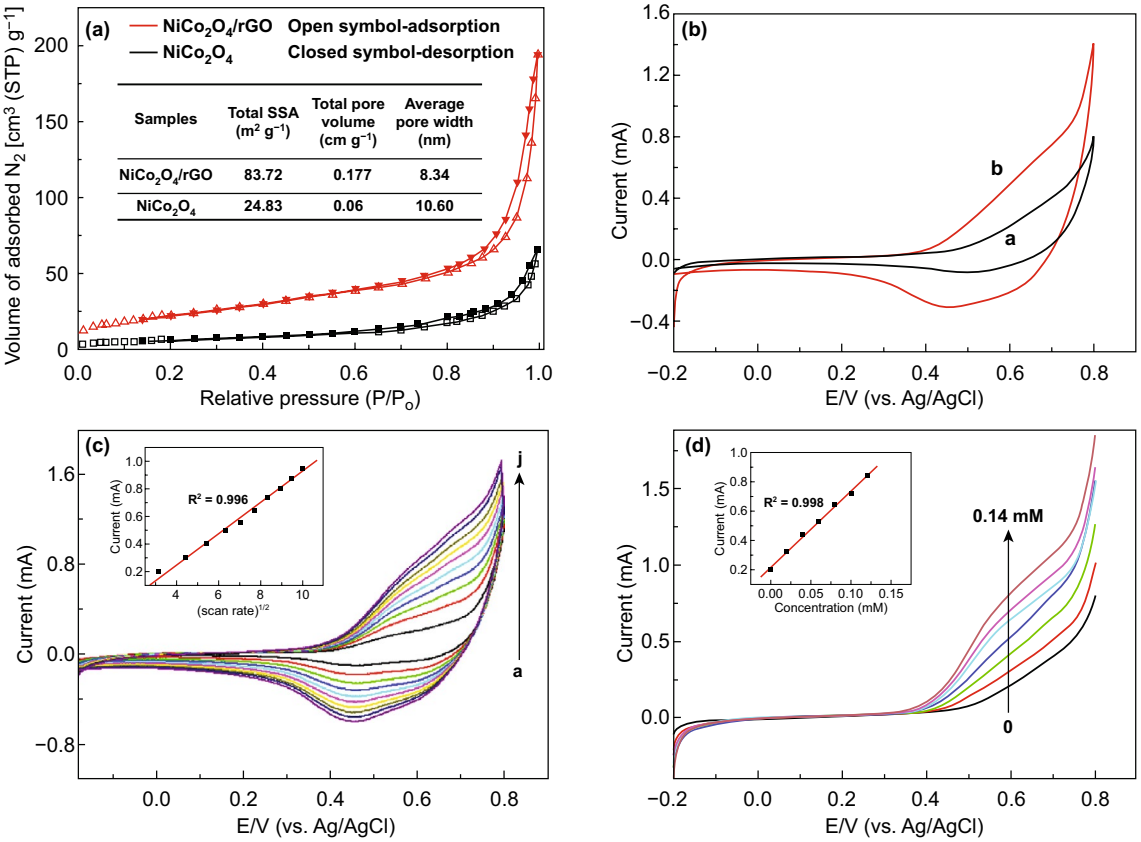

Fig. 26 **a** Adsorption–desorption hysteresis loop, specific surface area (SSA), average pore width, and total pore volume of the synthesized pure $NiCo_2O_4$ and $NiCo_2O_4$/graphene nanohybrids. **b** CV for $NiCo_2O_4$/graphene hybrid-modified electrode. **c** Effect of scan rates scan rate for the solution with 0.1 mM glucose in 0.1 M NaOH. **d** Linear sweep voltammetric curves for glucose in the concentration of 0–0.14 mM and calibration plot (Inset). Reproduced with permission from Ref. [244]. Copyright © 2016 Elsevier B.V.

compared to pure $NiCo_2O_4$ was attributed to the lesser extent of aggregation of graphene sheets due to the interception of the $NiCo_2O_4$ nanoparticles on graphene surface causing weakening of π–π interaction between individual graphene sheets, faster diffusion rates and electron transfer between the glucose molecules and the electrode surface [245].

Ma et al. [246] developed $NiCo_2O_4$ nanowrinkles/reduced graphene oxide hybrid-based modified GCE for non-enzymatic glucose detection at the physiological level. As far as the concentration of the glucose is concerned, the oxidation potential of glucose decreased while oxidation peak current increased proportionally to a greater extent for $NiCo_2O_4$ nanowrinkles/reduced graphene oxide hybrid-based modified GCE as compared to single component Co_3O_4, NiO and bare $NiCo_2O_4$ at a scan rate of 100 mV s^{-1} in 0.1 M NaOH (Fig. 27a–d). The results confirmed the crucial role of reduced graphene oxide in improving the electrocatalytic biosensing performance of the $NiCo_2O_4$ spinel for different concentrations of glucose.

In addition to two-dimensional graphene, Wu et al. [245] reported the synthesis of three-dimensional graphene foam (3DGF) through a chemical vapor deposition technique. The 3DGF provides additional stability and large porous surface as well as high conductivity to the hierarchical $NiCo_2O_4$ composites. $NiCo_2O_4$ hierarchical nanoneedles were deposited onto the surface of 3DGF via a hydrothermal method. The synergism between hierarchical $NiCo_2O_4$ nanoneedles and 3DGF exhibited a high sensitivity of 2524 μA mM^{-1} cm^{-2} and a limit of detection 0.38 μM (S/N = 3). Further, as fabricated electrode showed excellent selectivity for glucose even in the presence of interfering compounds like dopamine, ascorbic acid, lactose, D-Fructose, and urea as negligible current responses were observed on their additions as compared to glucose. $NiCo_2O_4$

https://doi.org/10.1007/s40820-020-00462-w

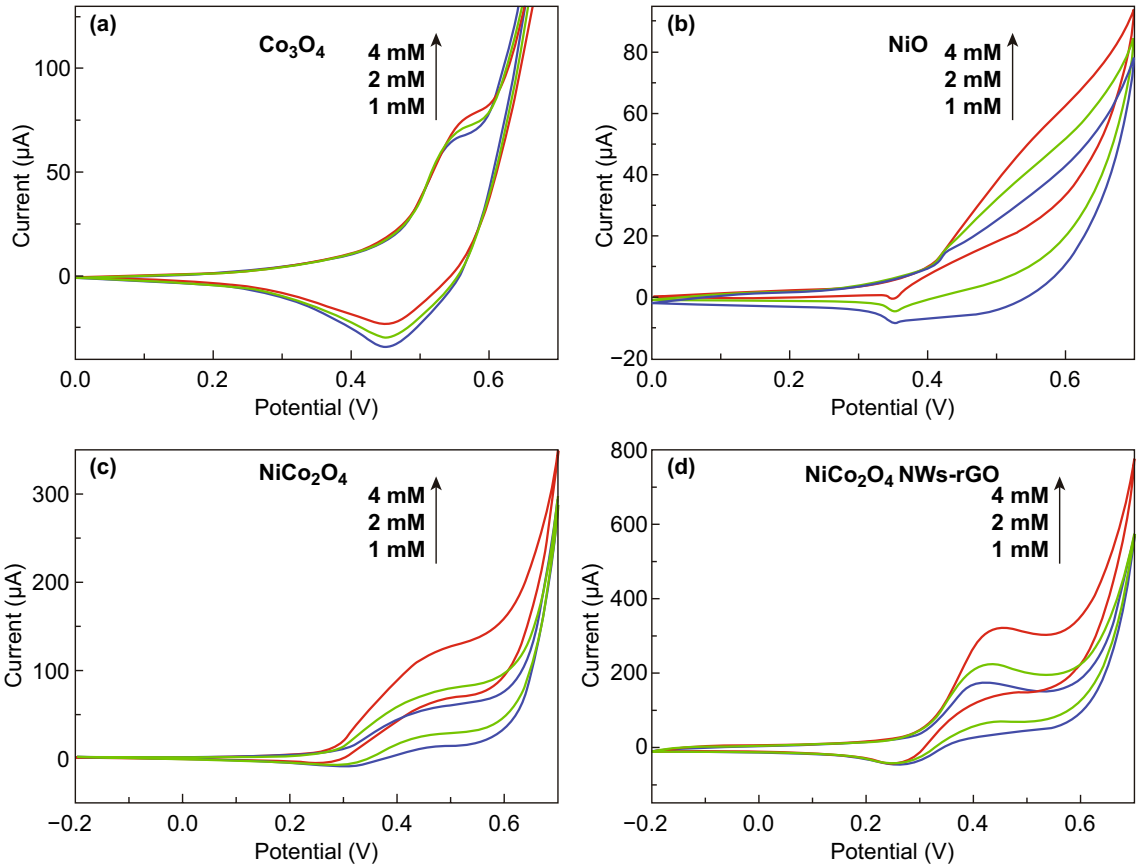

Fig. 27 CV plots for different glucose concentrations (1–4 mM) in 0.1 M NaOH **a** Co_3O_4, **b** NiO, **c** $NiCo_2O_4$, and **d** $NiCo_2O_4$ nanowrinkles/reduced graphene oxide-modified GCE. Reproduced with permission from Ref. [246]. Copyright © 2016 Elsevier Ltd.

nanospheres/reduced graphene oxide composite prepared by a template-based method using the Cu_2O/GO template achieved a high sensitivity of 2082.57 μA mM^{-1} cm^{-2}, the detection range of 0.04–1.28 mM, and low detection limit of 0.7 μM [137]. Ni et al. [247] reported a reduced graphene oxide supported $NiCo_2O_4$ nanorods composite prepared via an ionothermal method using deep eutectic solvents. The modified GCE exhibited superior electrocatalytic biosensing of glucose with a wide double-linear range from 1 μM to 25 mM and a very low detection limit of 0.35 μM (S/N = 3). The presence of a large number of small interconnected nanoparticles on the surface of the $NiCo_2O_4$ nanorods provided the dense electrocatalytic active site in coordination with reduced graphene oxide which provided large surface area and excellent electrical conductivity (Fig. 28a).

Another way of preventing the aggregation of graphene sheets, which reduces the specific surface area and inhibits the fast mass transfer, is the nitrogen doping. This nitrogen doping is not only supposed to facilitates the charge transfers between adjacent carbon atoms but also suppresses the electrons and holes recombination necessary for better electrical conductivity and electrocatalytic oxidation of glucose [248, 249]. Detailed characterization revealed that in the course of hydrothermal reactions, the graphene was reduced to nitrogen-doped reduced graphene oxide when glycine acted as a source of nitrogen. Further, the nitrogen-doped reduced graphene was self-assembled into hydrogels with interconnected 3D porous network structure resulted from an increased extent of π–π stacking interactions. This 3D form provides a sufficiently large surface area and active sites for the better adsorption of the analyte species. To ascertain this, Lu et al. [38] explored the interactions of flower-like $NiCo_2O_4$ and 3D nitrogen-doped holey graphene hydrogel (NHGH)-modified GCE for electrochemical biosensing of glucose (Fig. 28b).

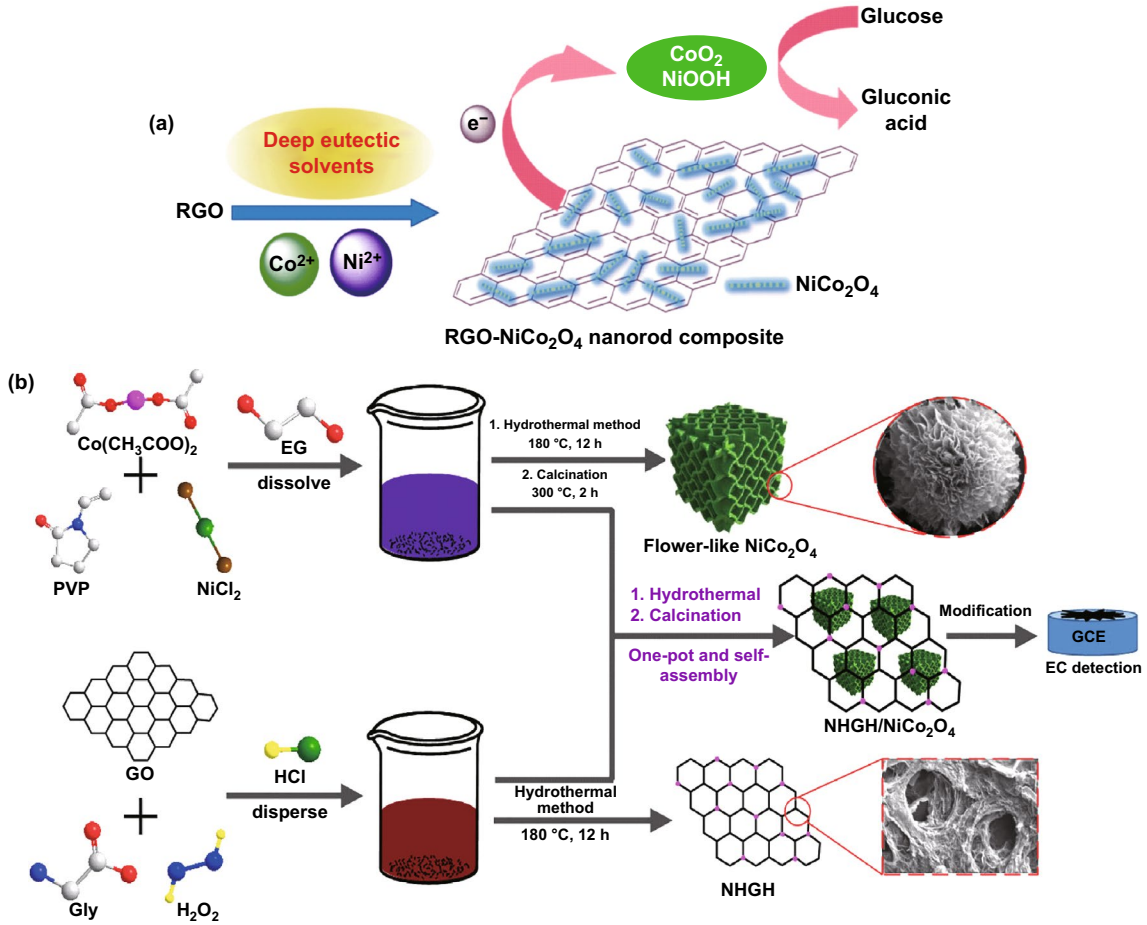

Fig. 28 **a** Proposed mechanism of glucose sensing using $NiCo_2O_4$ nanorods/rGO/Nafion composite-modified GCE. Reproduced with permission from Ref. [247]. Copyright © 2018 Elsevier Ltd. **b** Schematic presentation of the synthesis of the NHGH/$NiCo_2O_4$ electro-catalyst for non-enzymatic glucose sensing, Reproduced with permission from Ref. [38]. Copyright © 2019 Elsevier B.V.

Similar to graphene, carbon nanofibers also possess excellent dimensional, thermal and chemical stability as well as good electrical conductivity. Recently, these fibers have attracted wide attention and have been widely explored in fields such as electrochemical cells, catalysis, adsorption, structure enhancement, biosensors, gas sensors, and nanodevices [250, 251]. Among various synthetic methods, electro-spinning is considered to be the most suitable low-cost and simple method for synthesizing carbon nanofibers [252, 253]. Liu et al. [39] explored the glucose-sensing behavior of $NiCo_2O_4$ nanoneedle-decorated electrospun carbon nanofiber nanohybrids. Faster electrocatalytic oxidation of glucose was reported for nanohybrids as compared to bare $NiCo_2O_4$ nanoneedle and electrospun carbon nanofiber-modified GCEs. The fact was supported by a large increase in the anode peak current and a positive shift in the anode peak potential.

Novel metals such as Au, Ag, and Pd, have also been used to prepare $NiCo_2O_4$ composites to improve the biosensing capabilities. Recently, dealloying has been used as a convenient method for preparing nanoporous metals with a 3D bicontinuous structure, which is characterized by open nanopores with adjustable sizes [254–256]. These 3D nanoporous metals act as conductive surfaces for the deposition of biosensors electrocatalytic materials such as $NiCo_2O_4$ since they provide high conductivity and large surface area. Disposable needle-type hybrid electrode comprising a stainless steel core modified with a 3D nanoporous Au/$NiCo_2O_4$ nanowall hybrid structure-modified electrochemical non-enzymatic glucose sensor showed a linear response of 0.01–21 mM glucose, high

 https://doi.org/10.1007/s40820-020-00462-w

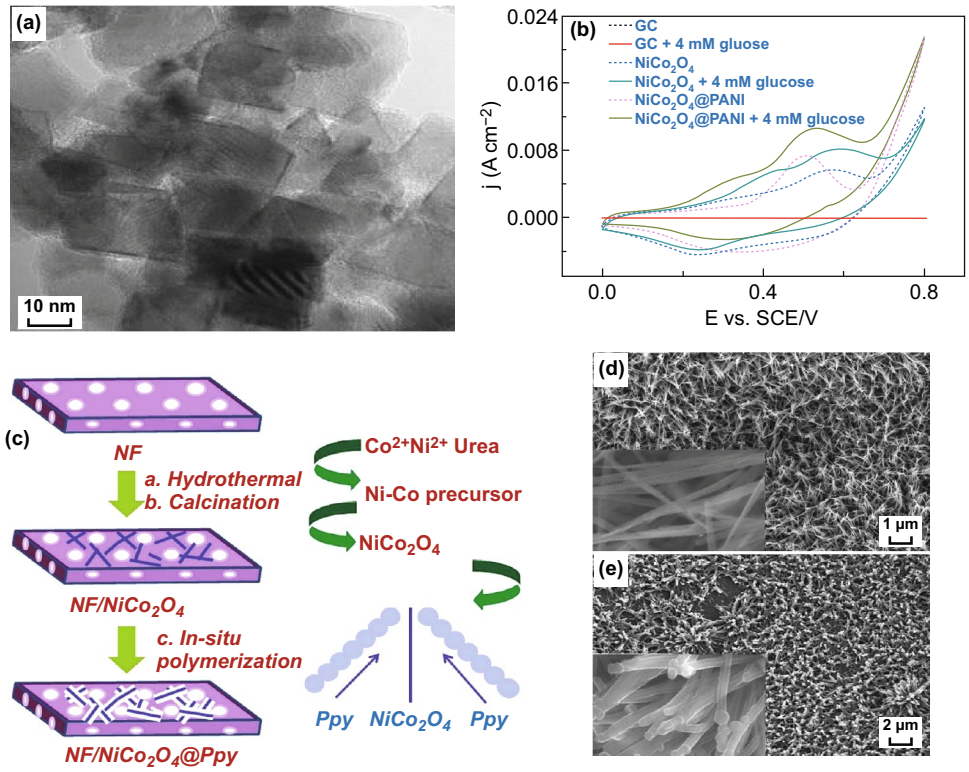

Fig. 29 **a** HRTEM image of $NiCo_2O_4$@PANI nanocomposite and **b** CV plots for different GCE electrodes in the absence and presence of 4 mM glucose in 0.1 M NaOH solution at scan rate = 50 mV s^{-1}. Reproduced with permission from Ref. [263]. Copyright © 2015 Elsevier B.V. **c** Schematic illustration of the preparation of core–shell $NiCo_2O_4$@Ppy on Ni foam substrate. **d** FESEM image of bare $NiCo_2O_4$. **e** FESEM image of $NiCo_2O_4$@Ppy composite, Reproduced with permission from Ref. [264]. Copyright © 2019 Elsevier B.V.

sensitivity of 0.3871 μA μM^{-1} cm^{-2}, detection limit of 1 μM within a response time of < 1 s [257]. Naik et al. [258] compared the bare $NiCo_2O_4$/Ni foam, $NiCo_2O_4$–Ag/Ni foam and $NiCo_2O_4$–Au/Ni foam nanosheets electrodes. The calculated sensitivity for pure $NiCo_2O_4$, $NiCo_2O_4$–Ag, and $NiCo_2O_4$–Au nanosheets electrodes in the linear range 5–45 μM and 45–465 μM were 20.8, 29.86, and 44.86 μA μM^{-1} cm^{-2} and 6.2, 11.5, and 13.96 μA μM^{-1} cm^{-2}, respectively. The respective limits of detection were 9.33, 5.82, and 2.64 μM. DFT studies confirmed strong binding between Au and $NiCo_2O_4$ as compared to Ag. Further, the binding energy of glucose was more for the $NiCo_2O_4$–Au surface compared to the $NiCo_2O_4$–Ag surface. The enhanced density of states near the Fermi level improved the conductivity of the $NiCo_2O_4$–Au nanosheet than $NiCo_2O_4$–Ag that caused superior glucose sensing performance. In a similar type of report, the sensitivities for pure $NiCo_2O_4$ and $NiCo_2O_4$–Pd nanosheets electrodes in the linear range 5–90 μM and 70–450 μM were 27.5 and 40.03 μA μM^{-1} cm^{-2} and 8.53 and 8.23 μA μM^{-1} cm^{-2}, respectively [259].

Similar to metals, conducting polymers also possess the electronic, electrical, and optical properties, easy synthesis, excellent mechanical stabilities and most importantly the low toxicity and biodegradability, the issues which are generally associated with metals. Moreover, the noble metals are easily poisoned by some intermediates produced during the oxidation of glucose. Among various conducting polymers, polyaniline and polypyrrole have gained much attention due to their superior thermal and oxidative stabilities [260, 261]. Constructing a core–shell nanostructure comprising conductive polymer coating as the outer walls of metal oxides is the most important strategy for enhancing the conductivities [262]. $NiCo_2O_4$@PANI nanoparticles with an average particle size 25 nm shortened the ion transport pathway and the modified GCE exhibited a sensitivity of 4.55 mA mM^{-1} cm^{-2}, a detection limit of 0.3833 μM and linear dynamic range of 0.0150–4.7350 mM (Fig. 29a, b)

[263]. The PANI core–shell provided more effective electrical contact between redox-active centers and the electrolyte resulting in good contact and small diffusion distances for electron transports which subsequently improved the sensor activity. $NiCo_2O_4$@Ppy nanowires grown on Ni foam were synthesized via hydrothermal growth and oxidant-induced polymerization process (Fig. 29c–e). The fabricated glucose sensor showed high sensitivity 3059 μA mM^{-1} cm^{-2}, low detection limit 0.22 μM, and wide linear dynamic range 0.001–20 mM. The excellent electrocatalytic behavior was attributed to the synergism due to bimetallic oxide, the significant role of Ppy in transmitting charges among electrode material due to its excellent conductivity, non-collapsing and non-agglomeration of the $NiCo_2O_4$ due to Ppy coating, and absence of any adhesive or conductive agent during electrode fabrication [264].

$NiCo_2O_4$ nano-/microstructures combined with smarter nano-architectured metal oxides (Co_3O_4, SnO_2, NiO, and MnO_2, etc.) have many synergistic multifunctional properties of nanostructured components including dense and easily accessible electroactive sites, altered bandgap energies, faster charge transfer processes, and reduced internal resistance. The p-type semiconductor nanostructured $NiCo_2O_4$ [32], Co_3O_4 [265], and n-type materials SnO_2 [266] and MnO_2 [267] have the bandgap energies of 2.1, 2.2, 3.6, and 1.3 eV, respectively. Due to slightly different bandgap energies, the semiconductor metal oxides introduce in situ impurity bands in $NiCo_2O_4$ which increase the electron conductivity to extract excellent electrocatalytic efficiencies [268]. Chen et al. [269] reported porous Co_3O_4 nanosheets synthesized via a simple hydrothermal method. The Co_3O_4 nanosheets provided the growth sites for the hydrothermal synthesis of $NiCo_2O_4$ nanorods. At the optimized conditions, porous Co_3O_4–$NiCo_2O_4$ nanosheet-modified GCE exhibited a preeminent sensitivity of 1463.13 μA mM^{-1} cm^{-2}, a low detection limit of 0.112 μM and linear dynamic range 0.001–2.1 mM with excellent selectivity and reproducibility. The amperometric current–time plot showed a successive increase in current with the concentration of glucose (1 μM–6.1 mM) at an applied voltage of + 0.55 V using porous Co_3O_4–$NiCo_2O_4$ nanosheet-modified GCE. The current–concentration calibration plot displayed two linear portions with concentration ranges 1 μM–2.1 mM and 2.1–6.1 mM. Further, the incorporation of graphene into Co_3O_4/$NiCo_2O_4$ double-shelled nanocages was explored by Xue et al. [270]. The Co_3O_4/$NiCo_2O_4$ double-shelled nanocages were prepared by using zeolite imidazole frameworks-67 as a template. The amperometric studies revealed a sensitivity of 0.196 mA mM^{-1} cm^{-2} with detection limit 0.744 μM in linearized concentration range 0.01–3.52 mM, whereas, in linearized concentrations range of 0.01–3.52 mM, the sensitivity was 0.304 mA mM^{-1} cm^{-2} with detection limit 0.384 μM.

The introduction of n-type semiconductors stuffs like SnO_2 in p-type $NiCo_2O_4$ semiconductors results in the formations of n–p junctions that facilitate the photo-induced electrochemical changes by altering the bandgap energies. Cai et al. [118] observed a prompt photocurrent reduction with the addition of the 100 μL–20 mM glucose solutions into the electrolyte solution. It was proposed that under sunlight stimulation, electron–hole (e^-–h^+) pairs are generated by the excitation of the electrons from the valence band of the n-type SnO_2 semiconductor after the absorption of light of suitable energy (more than bandgap energy). The OH^- of the solid electrolyte trap these h^+ holes and form $OH^{\cdot}$ radicals (Eq. 30). The $OH^{\cdot}$ radicals are then transferred to the counter electrode to oxidize $NiCo_2O_4$ to NiOOH and CoOOH (Eq. 31). However, in the presence of glucose, positively charged h^+ causes oxidation of glucose to gluconolactone. The electrons released during the oxidation process are transferred back to the valence band, so the photocurrent is decreased.

$$OH^- + h^+ \rightarrow OH^{\cdot} \quad (30)$$

$$NiCo_2O_4 + OH^{\cdot} + H_2O \rightarrow NiOOH + CoOOH \quad (31)$$

Chen et al. [271] synthesized bionics-inspired streptococcus-like mixed oxide $NiCo_2O_4$ coated on needle-like MnO_2 architectures. Initially, MnO_2 nanowires were synthesized via a quick precipitation method, while $NiCo_2O_4$ were grown on pre-synthesized MnO_2 nanowires via a facile hydrothermal method. MnO_2 nanowires prevented the agglomeration of $NiCo_2O_4$ by acting as nucleation sites and electrocatalytic centers for the uniform growth of $NiCo_2O_4$. The synergism between $NiCo_2O_4$ and MnO_2 was explored for the non-enzymatic electrochemical sensing of glucose. $NiCo_2O_4$–MnO_2/GCE exhibited high sensitivity, wide concentration ranges, very low detection limit, and long-term stability as compared to $NiCo_2O_4$/GCE and MnO_2/GCE.

Numerous studies have been conducted to verify the selectivity of the $NiCo_2O_4$-based modified sensors as ascorbic acid, dopamine, and uric acid coexist along with

 https://doi.org/10.1007/s40820-020-00462-w

Table 1 Electrochemical sensing parameters for various $NiCo_2O_4$-based modified electrodes toward glucose

Sensor material	Sensitivity ($\mu A\ mM^{-1}\ cm^{-2}$)	LDR (mM)	LOD (μM)	Refs.
3D nitrogen-doped holey graphene/$NiCo_2O_4$ nanoflowers	2072.0	0.005–10.95	0.39	[38]
$NiCo_2O_4$/ECF	1947.2	0.005–19.175	1.5	[39]
$NiCo_2O_4$/rGO	2082.6	0.04–1.28	0.7	[137]
Porous $NiCo_2O_4$ hollow nanospheres	1917.0	0.01–2.24	0.6	[140]
Hollow $NiCo_2O_4$ nanorod	1685.0	0.0003–1.0	0.16	[142]
$NiCo_2O_4$ nanosheet	6690.0	0.005–0.065	0.38	[224]
$NiCo_2O_4$ hollow nanocages	1306.0	0.00018–5.1	27[b]	[228]
MoS_2–$NiCo_2O_4$ architecture	1748.6	1.6–11.1	0.152	[229]
Mesoporous $NiCo_2O_4$	662.3	–	0.3[b]	[237]
Rod-like $NiCo_2O_4$	431.3	–	–	[238]
$NiCo_2O_4$ NWs/NF	5916.0	0.001–3.987	0.94	[239]
$NiCo_2O_4$ NWAs/CC	4.12[a]	0.001–0.63	0.5	[241]
$NiCo_2O_4$ 3DGF	2524.0	0.0005–0.59	0.38	[245]
$NiCo_2O_4$ NWs-rGO	548.9	5–8.6	2.0	[246]
RGO-$NiCo_2O_4$/Nafion/GCE	960.4	0.001–6.3	0.35	[247]
	216.7	6.3–25		
$NiCo_2O_4$ nanowalls/3D nanoporous gold/SS needle	387.1	0.01–21	1.0	[257]
$NiCo_2O_4$@PANI	4550.0	0.015–4.735	0.38	[263]
Co_3O_4–$NiCo_2O_4$ nanosheets	1463.13	0.001–2.1	0.112	[269]
Graphene/Co_3O_4/$NiCo_2O_4$ DS nanocages	304.0	0.01–3.52	0.384	[270]
$NiCo_2O_4$–MnO_2 nanosheets	2887.6	0.001–2600	0.036	[271]
Mesoporous $NiCo_2O_4$ nanowires	72.4	0.37–2.0	0.37	[273]
$NiCo_2O_4$ nanorods	4710.0	0.001–0.88	0.063	[276]
Dandelion-like $NiCo_2O_4$ hierarchical microspheres	430.86	10–10480	–	[277]

[a]$mA\ mM^{-1}\ cm^{-2}$ units

[b]nM units

glucose in human blood serum [272]. Therefore, for practical applications, these components should not affect the amperometric parameters and the positive results have been reported [230, 237, 238, 241, 247, 272, 273]. Additionally, reproducibility and stability of the modified $NiCo_2O_4$-based electrodes have been analyzed. The results have shown acceptable reproducibility with a very low relative standard deviations in many studies [123, 142, 161, 193, 199, 200, 227, 274]. The electrochemical sensing parameters such as sensitivity, linear dynamic range, and detection limits for various $NiCo_2O_4$-based modified electrodes toward glucose are compared in Table 1.

In addition to electrochemical sensing of glucose using $NiCo_2O_4$ nano-/microstructure-modified electrodes, colorimetric sensing has also been reported by Huang et al. [274]. They explored the peroxidase-like activity of the hierarchical $NiCo_2O_4$ hollow sphere which was directly dependent on the concentration of H_2O_2 produced by the oxidation of glucose to gluconic acid in the presence of glucose oxidase (Go_x). Hence, a colorimetric method for the detection of glucose can be designed using $NiCo_2O_4$. The higher the concentration of the glucose, the more was the production of H_2O_2 and hence the greater was the oxidation of the 3,3,5,5-tetramethylbenzidine (TMB) to oxidized TMB. Absorbance at $\lambda_{max} = 652$ nm for oxidized TMB was increased linearly with the concentration of glucose. The linear range was observed between 0.1 and 4.5 mM with a low detection limit of 5.31 μM (Fig. 30a, b). The corresponding reaction mechanism is shown in Fig. 30c. Intrinsic peroxidase and oxidase-like activities of the $NiCo_2O_4$ architectures were also confirmed by Su et al. [275] by analyzing the electron spin resonance spectra for the oxidation of TMB by $NiCo_2O_4$ mesoporous spheres. The oxidation was accompanied without the production of $^1O_2$ and $OH^·$ radicals. Additionally,

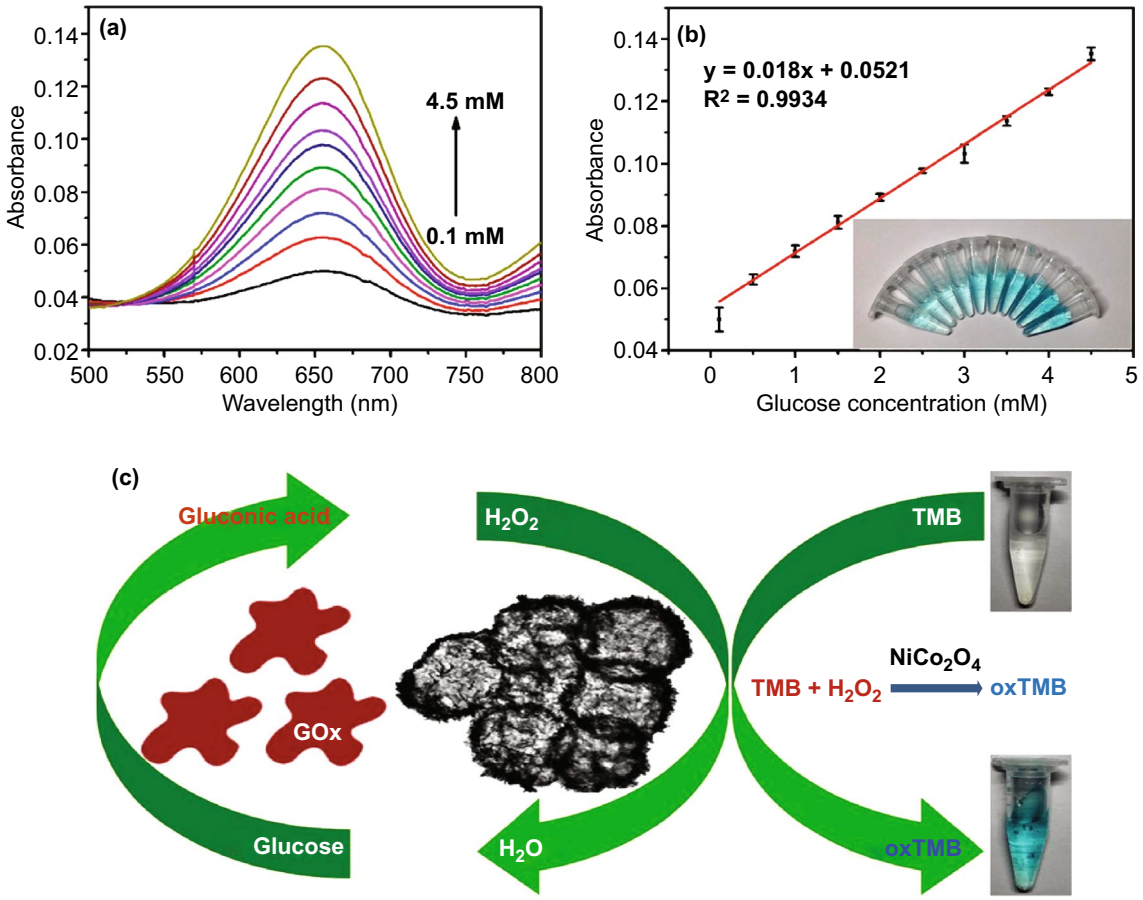

Fig. 30 **a** Effect of glucose concentrations on absorption. **b** Linearized calibration curve. **c** Proposed mechanism for colorimetric detection of glucose using the hierarchical $NiCo_2O_4$ hollow sphere. Reproduced with permission from Ref. [274], Copyright © 2017 by the authors; licensee MDPI, Basel, Switzerland

these peroxidase-like activities were feasible even over a broad temperature range.

4.2 H_2O_2 Biosensors

H_2O_2 is the most important byproduct produced from some enzyme-catalyzed biochemical reactions. In addition to its importance as a regulator of immune cell activation, vascular remodeling, and stomatal closure during metabolic processes, it also has pharmaceutical, clinical, environmental, textile, and food manufacturing applications [278]. Further, the concentration of H_2O_2 in urine is a direct indicator of the whole-body oxidative stress which is the common cause of renal failure, arteriosclerosis, myalgic, encephalomyelitis, Parkinson's disease, diabetes mellitus, cancer and cardiovascular diseases [279]. Similar to glucose, the literature reports enzymatic as well as non-enzymatic biosensors for the detection of H_2O_2. Horseradish peroxidase and heme protein-based enzymatic biosensor are the most researched H_2O_2 biosensor due to their high sensitivity, selectivity, and biodegradability. In recent years, non-enzymatic/enzymeless H_2O_2 biosensors based on metal oxides have become a new class of biosensors due to fast, low-cost, and easy-to-fabrication processes [280].

In this section of the review, some non-enzymatic H_2O_2 biosensors based on $NiCo_2O_4$ spinel nano-/microstructures are discussed. The current–time amperometric H_2O_2 biosensing using modified $Co_3O_4/NiCo_2O_4$ nanosheets/GCE at an applied potential of −0.35 V exhibited high sensitivity and low limit of detection of 303.42 μA mM^{-1} cm^{-2} and 0.596 μM, respectively [269]. The Co^{3+} ions of Co_3O_4 were supposed to play an important role in the sensing of H_2O_2.

https://doi.org/10.1007/s40820-020-00462-w

In alkaline medium, Co^{3+} ions reduce H_2O_2 to H_2O (Eq. 32) [281].

$$2Co^{3+} + H_2O_2 + 2OH^- \rightarrow 2H_2O + O_2 + 2Co^{2+} \quad (32)$$

The electro-reduction in H_2O_2 by $NiCo_2O_4$ spinel-based electrodes occurs according to Eqs. 33–36 [95, 282, 283].

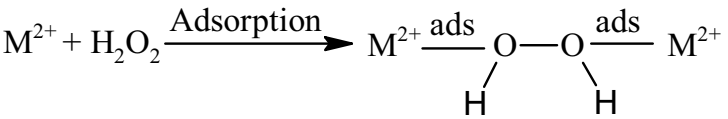

(33)

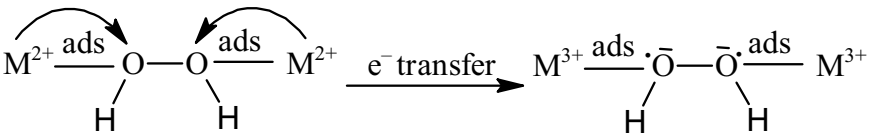

(34)

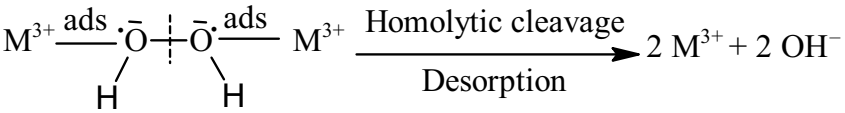

(35)

$$2M^{3+} + 2e^- \rightarrow 2M^{2+} \quad (36)$$

Since H_2O_2 is reduced to H_2O (O^{2-} ions) or OH^- ions as opposed to oxidation of glucose to gluconolactone, it was found that the current response during electrochemical sensing of H_2O_2 was reduced. Similar trends have been reported by other sensor materials such as $ZnFe_2O_4$/reduced graphene oxide [284], nickel phosphide (Ni_2P) nanosheets array on titanium mesh [285], cobalt nitride (Co_3N) nanowire array on Ti mesh [286], nanoporous carbon nanofibers/Pt nanoparticles [287], Ag decorated hierarchical Sn_3O_4 [288] and many more for the electrochemical sensing of H_2O_2 amperometrically.

Xiao et al. [289] reported that $NiCo_2O_4$ mixed oxide-based electrodes in the alkaline medium can cause electro-reduction as well as electro-oxidation toward H_2O_2. The extraordinary variety of inter-convertible oxidation states of Co and Ni in spinel $NiCo_2O_4$ is the key factor for its oxidizing and reducing nature. High valence Co^{3+} and Ni^{3+} ions of $NiCo_2O_4$ can be reduced to lower +2 oxidation states, i.e., into Co^{2+} and Ni^{2+} ions. Similarly, lower +2 oxidation states can also be oxidized to higher valencies including Co^{3+}, Co^{4+}, and Ni^{3+} ions. Other factors which decide the electro-reduction and electro-oxidation behavior of the $NiCo_2O_4$ toward H_2O_2 are the pH and the concentration of the H_2O_2 in the medium. At a scan rate of 10 mV s^{-1}, H_2O_2 electro-reduction and electro-oxidation were observed for 0.4 M H_2O_2 in 3.0 M and 0.75 M H_2O_2 in 3.0 M KOH, respectively. Equation 37 represents the overall electro-oxidation of H_2O_2 in an alkaline medium.

$$H_2O_2 + 2OH^- \rightarrow O_2 + 2H_2O + 2e^- \quad (37)$$

The electrons lost during the oxidation of H_2O_2 reduce the trivalent cations (Co^{3+} and Ni^{3+}) ions to their divalent states.

Xue et al. [290] grew ZnO nanowires on Ni foam via a galvanostatic electro-deposition technique. After that, the Ni foam-supported ZnO nanowires and $Co_3O_4/NiCo_2O_4$ double-shelled nanocages were prepared by coprecipitation and annealing processes. The $ZnO/Co_3O_4/NiCo_2O_4$/Ni foam-based electrochemical H_2O_2 sensor exhibited a high sensitivity of 388 μA mM^{-1} cm^{-2}, the low detection limit of 0.163 μM, and a dynamic linear range concentration of 0.2 μM–2.4 mM with a fast response time of 5 s. The fast and high response was attributed to the fast electron transport and short electrical pathway provided by ZnO nanowires. Additionally, $Co_3O_4/NiCo_2O_4$ double-shelled nanocages provided sufficient mesopores and large specific surface area for improved H_2O_2 sensing [290]. Sakthivel et al. [291] compared the electrochemical kinetics of modified $NiCo_2O_4$/GCE, $NiCo_2S_4$/GCE, and $NiCoSe_2$/GCE toward H_2O_2. The modified $NiCoSe_2$/GCE showed better electrochemical

sensing behavior for H_2O_2 than modified $NiCo_2O_4$/GCE and $NiCo_2S_4$/GCE. The greater electrocatalytic efficiency of modified $NiCoSe_2$/GCE was attributed to the large electrochemically active surface area for hydrothermally synthesized $NiCoSe_2$.

4.3 Urea Biosensors

Urea (carbamide or carbonyl diamide) is one of the main end products of protein metabolism in humans and animals. Urea is exclusively formed in the liver, and is transported by the bloodstream to the kidneys for excretion in the human body. The normal level of urea in human blood serum is 2.5–7.5 mM [292–295]. Amount of urea above or below the permissible level in the serum results in chronic renal and hepatic failure, gastrointestinal bleeding, and nephritic syndrome [296]. Similar to other metabolically important biomolecules, the literature reports enzymatic as well as non-enzymatic biosensors for the selective and highly sensitive urea sensors. Enzyme-based urea biosensors explore the use of urease enzyme which facilitates the hydrolysis of urea into ammonium (NH_4^+) and bicarbonate (HCO_3^-) ions (Eq. 38) [297].

$$NH_2CONH_2 + 3H_2O \xrightarrow{\text{Urease}} 2NH_4^+ + HCO_3^- + OH^- \quad (38)$$

However, in this section, some non-enzymatic-modified urea sensor electrodes based on spinel $NiCo_2O_4$ nano-/microstructures are reviewed. Research has proved that urea can be electrochemically oxidized by $NiCo_2O_4$ nano-/microstructures (Eqs. 39–41).

$$6M^{2+} + 18OH^- \rightarrow 6MOOH + 6H_2O + 6e^- \quad (39)$$

$$6MOOH + CO(NH_2)_2 + 2OH^- \rightarrow 6M(OH)_2 + CO_3^{2-} + N_2 \quad (40)$$

The overall reaction can be written as:

$$6M^{2+} + CO(NH_2)_2 + 20OH^- \rightarrow 6M(OH)_2 + 6H_2O + CO_3^{2-} + N_2 + 6e^- \quad (41)$$

Recently, Amin et al. [298] explored the urea sensing behavior of $NiCo_2O_4$ nanoneedle-modified GCE which showed high sensitivity with a linear response concentration range of 0.01–5 mM and low detection limit of 1.0 µM. It was proposed that initially Ni^{2+} ions are oxidized to Ni^{3+} ions to form NiOOH in an alkaline medium which is reduced back to give $Ni(OH)_2$ at the time of urea electro-oxidation [299]. Mesoporous spinel $NiCo_2O_4$ nanostructures prepared via facile chemical deposition method showed higher catalytic activities, lower overpotential, and more tolerance toward urea electro-oxidation as compared to Co_3O_4 [227]. $NiCo_2O_4$/3D graphene/ITO exhibited high sensitivity of 166 µA mM^{-1} cm^{-2}, a linear range of 0.06–0.30 mM, and a low detection limit of 5.0 µM with a very small response time of 1 s through non-enzymatic detection method [300]. Further, a higher oxidation peak for $NiCo_2O_4$/3D graphene in the CV as compared to $NiCo_2O_4$/CNT-modified electrode confirmed the superiority of 3D graphene as a matrix material for electrode fabrication. The higher oxidation current potential was attributed to the highly porous nature and excellent conductivity of the interconnected 3D graphene matrix [301]. Since oxidation of urea is in alkaline medium, higher electrocatalytic oxidation of urea is recorded at higher pH conditions. However, beyond an optimum pH the electro-oxidation decreases due to blockage of the active sites by OH^- ions [302].

4.4 Electrochemical Determination of Some Other Bioanalytes

Some other bioanalytes such as rutin, trypsin, ascorbic acid, dopamine, uric acid, and tryptophan have also been electrochemically analyzed using nano-/micro-structured hybrid $NiCo_2O_4$-modified electrodes. Rutin, a flavonoid substance, is used as anti-bacterial, anti-viral, antiproliferative, antioxidants, antagonists, and anti-inflammatory. It also controls the blood pressure and vascular fragility including hereditary hemorrhagic telangiectasia, haemangiomas, vitamin C deficiency, etc. [303, 304]. Cui et al. [305] reported the fabrication of GCE modified with mesoporous $NiCo_2O_4$-decorated reduced graphene oxide for the electrochemical sensing of rutin using differential pulse voltammetric (DPV) technique. Flake-like $NiCo_2O_4$ sheets anchored on the wrinkled reduced graphene oxide sheets through electrostatic interaction prevented the self-agglomerations. The wide linear range of 0.1–150 µM and a low detection limit of 0.01 µM were observed along with excellent anti-interference capabilities. The strong synergism between reduced graphene sheets

https://doi.org/10.1007/s40820-020-00462-w

Table 2 Electrochemical sensing parameters for various $NiCo_2O_4$-based modified electrodes toward some bioanalytes

Sensor material	Analyte	Sensitivity ($\mu A\ mM^{-1}\ cm^{-2}$)	LDR (mM)	LOD (μM)	Refs.
3D nitrogen-doped holey graphene/$NiCo_2O_4$ nanoflowers	H_2O_2	–	0.001–0.510	0.136	[38]
Co_3O_4–$NiCo_2O_4$ nanosheets	H_2O_2	303.42	0.02–1.1	0.596	[269]
ZnO/Co_3O_4/$NiCo_2O_4$/Ni foam	H_2O_2	388.0	0.0002–2.4	0.163	[290]
$NiCo_2O_4$ nanoneedles	Urea		0.01–5	1.0	[298]
Nickel/cobalt oxide-decorated 3D graphene nanocomposite	Urea	166.0	0.06–0.30	5.0	[300]
Mesoporous $NiCo_2O_4$/rGO	Rutin	–	0.1–150	0.01	[305]
$NiCo_2O_4$ nanosheets/g-C_3N_4 nanocomposite	Trypsin[a]	–	10^{-10}–10^{-4}	10^{-10}	[310]
$NiCo_2O_4$/nano-ZSM-5 nanocomposite	Ascorbic acid	–	1–1200	0.8	[311]
$NiCo_2O_4$/nano-ZSM-5 nanocomposite	Dopamine	–	0.6–900	0.5	[311]
$NiCo_2O_4$/nano-ZSM-5 nanocomposite	Uric acid	–	0.9–1000	0.7	[311]
$NiCo_2O_4$/nano-ZSM-5 nanocomposite	Tryptophan	–	0.9–1000	0.7	[311]

[a]Units in mg mL^{-1}

and mesoporous $NiCo_2O_4$ resulted in increased redox peak current and decreased potential difference. During electrooxidation, rutin is converted into 3′,4′-diquinone with the release of two H^+ ions and two electrons (Eq. 42) [306, 307].

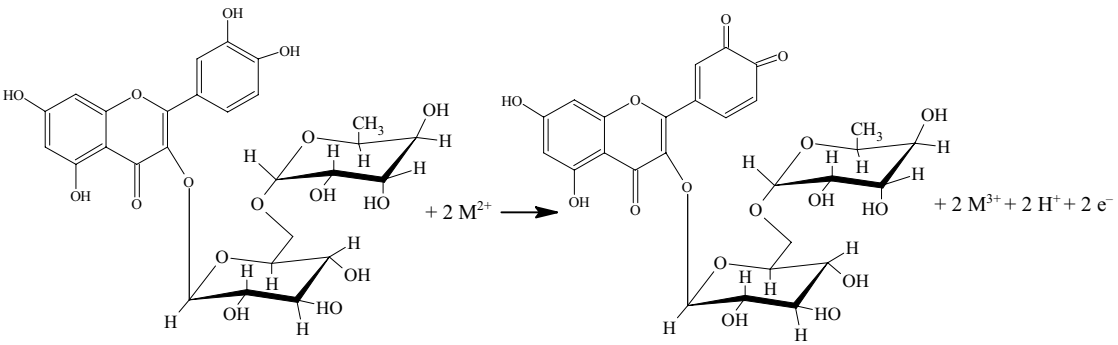

(42)

Trypsin, a serine protease secreted from the pancreas, has also been widely studied recently as it used for identifying and determining the amino acid sequence in protein and peptide, particularly at the C-terminus and as a specific biomarker for diseases like chronic cystic fibrosis, chronic pancreatitis, cancer, and many pathological changes [308, 309]. Lin et al. [310] reported a large and prompt rise in electrochemical signal in the presence of trypsin by $NiCo_2O_4$- poly(amidoamine)/peptide@g-C_3N_4 nanocomposite-modified GCE. 3,4,9,10-perylene tetracarboxylic acid (PTCA) was used to connect the peptides and g-C_3N_4. The modified GCE exhibited increased DPVs peak currents when the trypsin concentration was increased from 10^{-10} to 10^{-4} mg mL^{-1}. Kaur et al. [311] studied the simultaneous electrochemical sensing of ascorbic acid, dopamine, uric acid, and tryptophan using $NiCo_2O_4$/Nano-ZSM-5 nanocomposite-modified GCE. Wide linear ranges were 1–1200, 0.6–900, 0.9–1000, and 0.9–1000 μM, while the corresponding detection limits were 0.8, 0.5, 0.7, and 0.7 μM for ascorbic acid, dopamine, uric acid, and tryptophan, respectively. Simultaneous detection was possible as the anodic oxidative peak currents were observed at different applied potentials, i.e., 0.158, 0.394, 0.561, and 0.820 V, respectively, for ascorbic acid, dopamine, uric acid, and tryptophan in DVP plots at a scan rate of 20 mV s^{-1}.

Detailed comparison from Tables 1 and 2 indicates that the morphology of the $NiCo_2O_4$ nano-/microstructures and the presence of any other component along with $NiCo_2O_4$ significantly affect the biosensing efficiency. Comparative analysis revealed better electrochemical sensing of glucose by one-dimensional nanofibres and nanorods and two-dimensional nanosheets like morphologies of $NiCo_2O_4$ than

other morphologies. Doped and composites/hybrid $NiCo_2O_4$ nano-/microstructures exhibit superior sensing parameters that bare $NiCo_2O_4$. In particular, graphenic nanomaterials due to their excellent conductivity and large surface area significantly elevate the *I–V* characteristics to many folds. These materials also accelerate the rate of heterogeneous electron transfer, i.e., the transfer of electrons from/to electrode to/from bioanalyte molecules [312].

5 Conclusion

Herein, various strategies for the synthesis of spinel $NiCo_2O_4$ nano-/microstructures with versatile morphologies and their subsequent use for the development of biosensors for efficient non-enzymatic sensing and detection of biomolecules such as glucose, H_2O_2 and urea are comprehensively reviewed. As compared to NiO and Co_3O_4, the $NiCo_2O_4$ nanomaterials showed better electrochemical sensing as adjudged by broader redox peaks with larger area coverage in the CV curves. The biosensing efficiency of the $NiCo_2O_4$ nano-/microstructures can be improved by engineering the morphology, specific surface area, porosity, doping and by making composite/hybrids with various carbonaceous materials, conducting polymers, metal oxides, non-metals and metals. These materials not only improve the mechanical, thermal, and chemical stability but also modulate the bandgap energies, electronic and ionic conductivities, dispersion behavior, avoid aggregation of the $NiCo_2O_4$ nanomaterials and provide short electron and ion diffusion pathways. All these factors contribute to better electrocatalytic behavior with excellent sensitivity, selectivity, and long-term stability of the spinel $NiCo_2O_4$ nano-/microstructure-based biosensors. It is hoped that this review will provide basic ideas as well as new insights for future research and progress in this field.

6 Challenges and Future Perspectives

Despite extensive research in this area, many issues that impede the practical application of $NiCo_2O_4$nano-/microstructures need to be addressed for further improvement. Some of these issues have been identified herein.

Structural features of the $NiCo_2O_4$ nanomaterials are controlled by factors like temperature, pH of the reaction solution, precursor concentration, solvent nature and quantity, presence of the growth directing agents and templates, etc. It is, therefore, one of the major challenges to design large-scale and low-cost morphology controlled synthesis of the $NiCo_2O_4$ nanomaterials for next-generation biosensors.

Rational combination of $NiCo_2O_4$ nano-/microstructures with other hybrid materials or conductive substrates to designing $NiCo_2O_4$ composite/hybrids is found to improve the intrinsic characteristics like low electronic conductivity and wide bandgap and hence the biosensing behavior of $NiCo_2O_4$. However, still, more in-depth understanding is required to correlate the synergism between the components of the composite/hybrid materials.

Cost-effectiveness, easy to manufacture, recyclability, sensor disposal, and biocompatibility of $NiCo_2O_4$ nano-/microstructure-based biosensors are other issues that need to be addressed and solved. The high cost of electrochemical work stations restricts the practical applications of these sensors. In this regard, portable and wearable sensing devices will be promising. The toxicity issues of the $NiCo_2O_4$ nano-/microstructures and other components are very rarely discussed in the literature. Future research thus should also focus on studying this important issue.

The biosensing behavior of the $NiCo_2O_4$ nano-/microstructure-based sensors is affected by factors like working temperature, pH of the medium, scan rates, and applied potential. The optimization of these parameters is rarely addressed. Studying the specificity of $NiCo_2O_4$-based sensors from competitive assays requires an appropriate protocol because it is reported that the sensor can detect glucose, H_2O_2, urea, trypsin, etc.

Due to complex structures of the biomolecules, the interface and mechanistic studies at the surface of the nanomaterials are still undefined. The redox transformation of the molecules during electrocatalytic biosensing is also a debatable issue. Therefore, future work should focus on elucidating the interaction mechanism between nanomaterials and biomolecules on the electrode surface, to fabricate a new generation of biosensors.

Acknowledgements The author would like to acknowledge the support of the Principal, Jagdish Chandra DAV College, Dasuya, Distt. Hoshiarpur, Punjab, India (144205).

References

1. C. Shenghai, S. Liping, K. Fanhao, H. Lihua, Z. Hui, Carbon-coated $MnCo_2O_4$ nanowire as bifunctional oxygen catalysts for rechargeable Zn–air batteries. J. Power Sources **430**, 25–31 (2019). https://doi.org/10.1016/j.jpowsour.2019.05.029
2. H. Hou, H. Shao, X. Zhang, G. Liu, S. Hussain, G. Qiao, RGO-loaded flower-like $ZnCo_2O_4$ nanohybrid as counter electrode for dye-sensitized solar cells. Mater. Lett. **225**, 5–8 (2018). https://doi.org/10.1016/j.matlet.2018.04.103
3. R. Shi, Y. Zhang, Z. Wang, Facile synthesis of a $ZnCo_2O_4$ electrocatalyst with three-dimensional architecture for methanol oxidation. J. Alloys Compd. **810**, 151879 (2019). https://doi.org/10.1016/j.jallcom.2019.151879
4. Z. Li, M. Ye, A. Han, H. Du, Preparation, characterization and microwave absorption properties of $NiFe_2O_4$ and its composites with conductive polymer. J. Mater. Sci. Mater. Electron. **27**, 1031–1043 (2016). https://doi.org/10.1007/s10854-015-3848-8
5. L. Li, G. Jiang, J. Ma, $CuMn_2O_4$/graphene nanosheets as excellent anode for lithium-ion battery. Mater. Res. Bull. **104**, 53–59 (2018). https://doi.org/10.1016/j.materresbull.2018.03.051
6. P. Li, W. Sun, Q. Yu, P. Yang, J. Qiao, Z. Wang, D. Rooney, K. Sun, An effective three-dimensional ordered mesoporous $CuCo_2O_4$ as electrocatalyst for Li–O_2 batteries. Solid State Ion. **289**, 17–22 (2016). https://doi.org/10.1016/j.ssi.2016.02.014
7. Y. Jin, L. Wang, Q. Jiang, X. Du, C. Ji, X. He, Morphology controllable synthesis of $CoMn_2O_4$ structures by adjusting the urea concentration: from microflowers to microspheres. Mater. Lett. **168**, 166–170 (2016). https://doi.org/10.1016/j.matlet.2016.01.077
8. F. Du, X. Zuo, Q. Yang, B. Yang, G. Li et al., The stabilization of $NiCo_2O_4$ nanobelts used for catalyzing triiodides in dye-sensitized solar cells by the presence of RGO sheets. Sol. Energy Mater. Sol. Cells **149**, 9–14 (2016). https://doi.org/10.1016/j.solmat.2015.11.025
9. L. Manjakkal, D. Szwagierczak, R. Dahiya, Metal oxides based electrochemical pH sensors: current progress and future perspectives. Prog. Mater. Sci. **109**, 100635 (2020). https://doi.org/10.1016/j.pmatsci.2019.100635
10. X. Han, X. Gui, T.F. Yi, Y. Li, C. Yue, Recent progress of $NiCo_2O_4$-based anodes for high-performance lithium-ion batteries. Curr. Opin. Solid State Mater. Sci. **22**, 109–126 (2018). https://doi.org/10.1016/j.cossms.2018.05.005
11. Y. Li, X. Han, T. Yi, Y. He, X. Li, Review and prospect of $NiCo_2O_4$-based composite materials for supercapacitor electrodes. J. Energy Chem. **31**, 54–78 (2019). https://doi.org/10.1016/j.jechem.2018.05.010
12. Q. Wang, B. Liu, X. Wang, S. Ran, L. Wang, D. Chen, G. Shen, Morphology evolution of urchin-like $NiCo_2O_4$ nanostructures and their applications as psuedocapacitors and photoelectrochemical cells. J. Mater. Chem. **22**, 21647–21653 (2012). https://doi.org/10.1039/c2jm34705a
13. R.R. Owings, G.J. Exarhos, C.F. Windisch, P.H. Holloway, J.G. Wen, Process enhanced polaron conductivity of infrared transparent nickel–cobalt oxide. Thin Solid Films **483**, 175–184 (2005). https://doi.org/10.1016/j.tsf.2005.01.011
14. X. Zhao, L. Mao, Q. Cheng, J. Li, F. Liao, G. Yang, L. Xie, C. Zhao, L. Chen, Two-dimensional spinel structured co-based materials for high performance supercapacitors: a critical review. Chem. Eng. J. **387**, 124081 (2020). https://doi.org/10.1016/j.cej.2020.124081
15. K. Choi, I.K. Moon, J. Oh, An efficient amplification strategy for N-doped $NiCo_2O_4$ with oxygen vacancies and partial Ni/Co-nitrides as a dual-function electrode for both supercapatteries and hydrogen electrocatalysis. J. Mater. Chem. A **7**, 1468–1478 (2019). https://doi.org/10.1039/c8ta07210h
16. Y. Ha, L. Shi, X. Yan, Z. Chen, Y. Li, W. Xu, R. Wu, Multifunctional electrocatalysis on a porous N-doped $NiCo_2O_4$@C nanonetwork. ACS Appl. Mater. Interfaces **11**, 45546–45553 (2019). https://doi.org/10.1021/acsami.9b13580
17. W. Chu, Z. Shi, Y. Hou, D. Ma, X. Bai, Y. Gao, N. Yang, Trifunctional of phosphorus-doped $NiCo_2O_4$ nanowire materials for asymmetric supercapacitor, oxygen evolution reaction, and hydrogen evolution reaction. ACS Appl. Mater. Interfaces **12**, 2763–2772 (2020). https://doi.org/10.1021/acsami.9b13182
18. X. Hu, M. Huang, X. Meng, X. Ju, Fabrication of uniform urchin-like N-doped $NiCo_2O_4$@C hollow nanostructures for high performance supercapacitors. RSC Adv. **9**, 42110–42119 (2019). https://doi.org/10.1039/c9ra07678f
19. J. Zhang, Y. Chen, R. Chu, H. Jiang, Y. Zeng, Y. Zhang, N.M. Huang, H. Guo, Pseudocapacitive P-doped $NiCo_2O_4$ microspheres as stable anode for lithium ion batteries. J. Alloys Compd. **787**, 1051–1062 (2019). https://doi.org/10.1016/j.jallcom.2018.12.275
20. J.H. Lin, Y.T. Yan, T.X. Xu, C.Q. Qu, J. Li, J. Cao, J.C. Feng, J.L. Qi, S doped $NiCo_2O_4$ nanosheet arrays by Ar plasma: an efficient and bifunctional electrode for overall water splitting. J. Colloid Interface Sci. **560**, 34–39 (2020). https://doi.org/10.1016/j.jcis.2019.10.056
21. M. Yang, Y. Li, Y. Yu, X. Liu, Z. Shi, Y. Xing, Self-assembly of three-dimensional zinc-doped $NiCo_2O_4$ as efficient electrocatalysts for oxygen evolution reaction. Chem. A Eur. J. **24**, 13002–13008 (2018). https://doi.org/10.1002/chem.201802325
22. K.L. Yan, X. Shang, Z. Li, B. Dong, X. Li et al., Ternary mixed metal Fe-doped $NiCo_2O_4$ nanowires as efficient

electrocatalysts for oxygen evolution reaction. Appl. Surf. Sci. **416**, 371–378 (2017). https://doi.org/10.1016/j.apsusc.2017.04.204

23. L. Liu, H. Zhang, L. Fang, Y. Mu, Y. Wang, Facile preparation of novel dandelion-like Fe-doped $NiCo_2O_4$ microspheres@nanomeshes for excellent capacitive property in asymmetric supercapacitors. J. Power Sources **327**, 135–144 (2016). https://doi.org/10.1016/j.jpowsour.2016.07.054
24. J. Ma, E. Guo, L. Yin, Porous hierarchical spinel Mn-doped $NiCo_2O_4$ nanosheet architectures as high-performance anodes for lithium-ion batteries and electrochemical reaction mechanism. J. Mater. Sci. Mater. Electron. **30**, 8555–8567 (2019). https://doi.org/10.1007/s10854-019-01176-5
25. W.Y. Xia, N. Li, Q.Y. Li, K.H. Ye, C.W. Xu, Au–$NiCo_2O_4$ supported on three-dimensional hierarchical porous graphene-like material for highly effective oxygen evolution reaction. Sci. Rep. **6**, 23398 (2016). https://doi.org/10.1038/srep23398
26. C. Wei, X. Zheng, R. Li, X. Wang, Z. Xaio, L. Wang, Mesoporous hybrid $NiCo_2O_4/CeO_2$ hierarchical hollow spheres for enhanced supercapacitors. ChemistrySelect **4**, 11149–11155 (2019). https://doi.org/10.1002/slct.201902778
27. C. Wei, R. Zhang, X. Zheng, Q. Ru, Q. Chen, C. Cui, G. Li, D. Zhang, Hierarchical porous $NiCo_2O_4/CeO_2$ hybrid materials for high performance supercapacitors. Inorg. Chem. Front. **5**, 3126–3134 (2018). https://doi.org/10.1039/c8qi01010b
28. S.K. Shinde, M.B. Jalak, G.S. Ghodake, N.C. Maile, H.M. Yadav et al., Flower-like $NiCo_2O_4/NiCo_2S_4$ electrodes on Ni mesh for higher supercapacitor applications. Ceram. Int. **45**, 17192–17203 (2019). https://doi.org/10.1016/j.ceramint.2019.05.274
29. B. Ge, K. Li, Z. Fu, L. Pu, X. Zhang, Z. Liu, K. Huang, The performance of nano urchin-like $NiCo_2O_4$ modified activated carbon as air cathode for microbial fuel cell. J. Power Sources **303**, 325–332 (2016). https://doi.org/10.1016/j.jpowsour.2015.11.003
30. W. Wang, X. Song, C. Gu, D. Liu, J. Liu, J. Huang, A high-capacity $NiCo_2O_4$@reduced graphene oxide nanocomposite Li-ion battery anode. J. Alloys Compd. **741**, 223–230 (2018). https://doi.org/10.1016/j.jallcom.2018.01.097
31. Y.Q. Zhang, M. Li, B. Hua, Y. Wang, Y.F. Sun, J.L. Luo, A strongly cooperative spinel nanohybrid as an efficient bifunctional oxygen electrocatalyst for oxygen reduction reaction and oxygen evolution reaction. Appl. Catal. B Environ. **236**, 413–419 (2018). https://doi.org/10.1016/j.apcatb.2018.05.047
32. L. Hu, L. Wu, M. Liao, X. Fang, High-performance $NiCo_2O_4$ nanofilm photodetectors fabricated by an interfacial self-assembly strategy. Adv. Mater. **23**, 1988–1992 (2011). https://doi.org/10.1002/adma.201004109
33. M. Silambarasan, P.S. Ramesh, D. Geetha, Spinel $NiCo_2O_4$ nanostructures: synthesis, morphological, optical and electrochemical properties, in *Recent Trends in Materials Science and Applications. Springer Proceedings in Physics*, vol. 189, ed. by J. Ebenezar (Springer, Cham, 2017), pp. 219–231. https://doi.org/10.1007/978-3-319-44890-9_21
34. A. Bashir, S. Shukla, R. Bashir, R. Patidar, A. Bruno, D. Gupta, M.S. Satti, Z. Akhter, Low temperature, solution processed spinel $NiCo_2O_4$ nanoparticles as efficient hole transporting material for mesoscopic n-i-p perovskite solar cells. Sol. Energy **196**, 367–378 (2020). https://doi.org/10.1016/j.solener.2019.12.031
35. H. Zhang, Y. Chen, RGO loaded porous $NiCo_2O_4$ nanoplates as alcohol gas sensors. Nanosci. Nanotechnol. Lett. **9**, 374–379 (2017). https://doi.org/10.1166/nnl.2017.2341
36. B. Zhang, F. Qu, X. Zhou, S. Zhang, T. Thomas, M. Yang, Porous coral-like $NiCo_2O_4$ nanospheres with promising xylene gas sensing properties. Sens. Actuators B Chem. **261**, 203–209 (2018). https://doi.org/10.1016/j.snb.2018.01.125
37. N. Joshi, L.F. Da Silva, H. Jadhav, J.C. M'Peko, B.B. Millan Torres, K. Aguir, V.R. Mastelaro, O.N. Oliveira, One-step approach for preparing ozone gas sensors based on hierarchical $NiCo_2O_4$ structures. RSC Adv. **6**, 92655–92662 (2016). https://doi.org/10.1039/c6ra18384k
38. Z. Lu, L. Wu, J. Zhang, W. Dai, G. Mo, J. Ye, Bifunctional and highly sensitive electrochemical non-enzymatic glucose and hydrogen peroxide biosensor based on $NiCo_2O_4$ nanoflowers decorated 3D nitrogen doped holey graphene hydrogel. Mater. Sci. Eng. C **102**, 708–717 (2019). https://doi.org/10.1016/j.msec.2019.04.072
39. L. Liu, Z. Wang, J. Yang, G. Liu, J. Li, L. Guo, S. Chen, Q. Guo, $NiCo_2O_4$ nanoneedle-decorated electrospun carbon nanofiber nanohybrids for sensitive non-enzymatic glucose sensors. Sens. Actuators. B Chem. **258**, 920–928 (2018). https://doi.org/10.1016/j.snb.2017.11.118
40. B. Li, J. Feng, Y. Qian, S. Xiong, Mesoporous quasi-single-crystalline $NiCo_2O_4$ superlattice nanoribbons with optimizable lithium storage properties. J. Mater. Chem. A **3**, 10336–10344 (2015). https://doi.org/10.1039/c5ta01229e
41. Y. Zhu, X. Pu, W. Song, Z. Wu, Z. Zhou et al., High capacity $NiCo_2O_4$ nanorods as electrode materials for supercapacitor. J. Alloys Compd. **617**, 988–993 (2014). https://doi.org/10.1016/j.jallcom.2014.08.064
42. J. Li, S. Xiong, Y. Liu, Z. Ju, Y. Qian, High electrochemical performance of monodisperse $NiCo_2O_4$ mesoporous microspheres as an anode material for Li-ion batteries. ACS Appl. Mater. Interfaces **5**, 981–988 (2013). https://doi.org/10.1021/am3026294
43. R. Batool, A. Rhouati, M.H. Nawaz, A. Hayat, J.L. Marty, A review of the construction of nano-hybrids for electrochemical biosensing of glucose. Biosensors **9**(1), 46 (2019). https://doi.org/10.3390/bios9010046
44. P. Mehrotra, Biosensors and their applications—a review. J. Oral Biol. Craniofac. Res. **6**, 153–159 (2016). https://doi.org/10.1016/j.jobcr.2015.12.002
45. H. Lu, S. Zhang, L. Guo, W. Li, Applications of graphene-based composite hydrogels: a review. RSC Adv. **7**, 51008–51020 (2017). https://doi.org/10.1039/c7ra09634h
46. R. Bhadoria, H.S. Chaudhary, Recent advances of biosensors in biomedical sciences. Int. J. Drug Deliv. **3**, 571 (2011). https://doi.org/10.3389/fbioe.2016.00011

 https://doi.org/10.1007/s40820-020-00462-w

47. J. Peña-Bahamonde, H.N. Nguyen, S.K. Fanourakis, D.F. Rodrigues, Recent advances in graphene-based biosensor technology with applications in life sciences. J. Nanobiotechnol. **16**, 75 (2018). https://doi.org/10.1186/s12951-018-0400-z
48. S. Yin, Z. Jin, T. Miyake, Wearable high-powered biofuel cells using enzyme/carbon nanotube composite fibers on textile cloth. Biosens. Bioelectron. **141**, 111471 (2019). https://doi.org/10.1016/j.bios.2019.111471
49. B.S. Dakshayini, K.R. Reddy, A. Mishra, N.P. Shetti, S.J. Malode, S. Basu, S. Naveen, A.V. Raghu, Role of conducting polymer and metal oxide-based hybrids for applications in ampereometric sensors and biosensors. Microchem. J. **147**, 7–24 (2019). https://doi.org/10.1016/j.microc.2019.02.061
50. N.P. Shetti, S.J. Malode, D. Ilager, K. Raghava Reddy, S.S. Shukla, T.M. Aminabhavi, A novel electrochemical sensor for detection of molinate using ZnO nanoparticles loaded carbon electrode. Electroanalysis **31**, 1040–1049 (2019). https://doi.org/10.1002/elan.201800775
51. G. Wang, X. He, L. Wang, A. Gu, Y. Huang, B. Fang, B. Geng, X. Zhang, Non-enzymatic electrochemical sensing of glucose. Microchim. Acta **180**, 161–186 (2013). https://doi.org/10.1007/s00604-012-0923-1
52. S. Park, H. Boo, T.D. Chung, Electrochemical non-enzymatic glucose sensors. Anal. Chim. Acta **556**, 46–57 (2006). https://doi.org/10.1016/j.aca.2005.05.080
53. X. Hui, X. Xuan, J. Kim, J.Y. Park, A highly flexible and selective dopamine sensor based on Pt–Au nanoparticle-modified laser-induced graphene. Electrochim. Acta **328**, 135066 (2019). https://doi.org/10.1016/j.electacta.2019.135066
54. R. Ahmad, N. Tripathy, M.S. Ahn, K.S. Bhat, T. Mahmoudi et al., Highly efficient non-enzymatic glucose sensor based on CuO modified vertically-grown ZnO nanorods on electrode. Sci. Rep. **7**, 5715 (2017). https://doi.org/10.1038/s41598-017-06064-8
55. R.J. Chung, A.N. Wang, Q.L. Liao, K.Y. Chuang, Non-enzymatic glucose sensor composed of carbon-coated nano-zinc oxide. Nanomaterials **7**(2), 36 (2017). https://doi.org/10.3390/nano7020036
56. N.P. Shetti, S.J. Malode, D.S. Nayak, R.R. Naik, G.T. Kuchinad, K.R. Reddy, S.S. Shukla, T.M. Aminabhavi, Hetero nanostructured iron oxide and bentonite clay composite assembly for the determination of an antiviral drug acyclovir. Microchem. J. **155**, 104727 (2020). https://doi.org/10.1016/j.microc.2020.104727
57. C. Wang, E. Zhou, W. He, X. Deng, J. Huang et al., $NiCo_2O_4$-based supercapacitor nanomaterials. Nanomaterials **7**(2), 41 (2017). https://doi.org/10.3390/nano7020041
58. J.P. Cheng, W.D. Wang, X.C. Wang, F. Liu, Recent research of core–shell structured composites with $NiCo_2O_4$ as scaffolds for electrochemical capacitors. Chem. Eng. J. **393**, 124747 (2020). https://doi.org/10.1016/j.cej.2020.124747
59. H. Osgood, S.V. Devaguptapu, H. Xu, J. Cho, G. Wu, Transition metal (Fe Co, Ni, and Mn) oxides for oxygen reduction and evolution bifunctional catalysts in alkaline media. Nano Today **11**, 601–625 (2016). https://doi.org/10.1016/j.nantod.2016.09.001
60. S.S. Tong, X.J. Wang, Q.C. Li, X.J. Han, Progress on electrocatalysts of hydrogen evolution reaction based on carbon fiber materials. Chin. J. Anal. Chem. **44**, 1447–1457 (2016). https://doi.org/10.1016/S1872-2040(16)60958-1
61. N.P. Shetti, D.S. Nayak, S.J. Malode, R.R. Kakarla, S.S. Shukla, T.M. Aminabhavi, Sensors based on ruthenium-doped TiO_2 nanoparticles loaded into multi-walled carbon nanotubes for the detection of flufenamic acid and mefenamic acid. Anal. Chim. Acta **1051**, 58–72 (2019). https://doi.org/10.1016/j.aca.2018.11.041
62. S.D. Bukkitgar, N.P. Shetti, R.M. Kulkarni, K.R. Reddy, S.S. Shukla, V.S. Saji, T.M. Aminabhavi, Electro-catalytic behavior of Mg-doped ZnO nano-flakes for oxidation of anti-inflammatory drug. J. Electrochem. Soc. **166**, B3072 (2019). https://doi.org/10.1149/2.0131909jes
63. C. Sabu, T.K. Henna, V.R. Raphey, K.P. Nivitha, K. Pramod, Advanced biosensors for glucose and insulin. Biosens. Bioelectron. **141**, 111201 (2019). https://doi.org/10.1016/j.bios.2019.03.034
64. C.V. Reddy, I.N. Reddy, K.R. Reddy, S. Jaesool, K. Yoo, Template-free synthesis of tetragonal Co-doped ZrO_2 nanoparticles for applications in electrochemical energy storage and water treatment. Electrochim. Acta **317**, 416–426 (2019). https://doi.org/10.1016/j.electacta.2019.06.010
65. P.S. Basavarajappa, S.B. Patil, N. Ganganagappa, K.R. Reddy, A.V. Raghu, C.V. Reddy, Recent progress in metal-doped TiO_2, non-metal doped/codoped TiO_2 and TiO_2 nanostructured hybrids for enhanced photocatalysis. Int. J. Hydrogen Energy **45**, 7764–7778 (2020). https://doi.org/10.1016/j.ijhydene.2019.07.241
66. S.B. Patil, P.S. Basavarajappa, N. Ganganagappa, M.S. Jyothi, A.V. Raghu, K.R. Reddy, Recent advances in non-metals-doped TiO_2 nanostructured photocatalysts for visible-light driven hydrogen production, CO_2 reduction and air purification. Int. J. Hydrogen Energy **44**, 13022–13039 (2019). https://doi.org/10.1016/j.ijhydene.2019.03.164
67. C. Chen, Q. Xie, D. Yang, H. Xiao, Y. Fu, Y. Tan, S. Yao, Recent advances in electrochemical glucose biosensors: a review. RSC Adv. **3**, 4473–4491 (2013). https://doi.org/10.1039/c2ra22351a
68. D.W. Hwang, S. Lee, M. Seo, T.D. Chung, Recent advances in electrochemical non-enzymatic glucose sensors—a review. Anal. Chim. Acta **1033**, 1–34 (2018). https://doi.org/10.1016/j.aca.2018.05.051
69. A. Jing, G. Liang, H. Shi, Y. Yuan, Q. Zhan, W. Feng, Three-dimensional holey-graphene architectures for highly sensitive enzymatic electrochemical determination of hydrogen peroxide. J. Nanosci. Nanotechnol. **19**, 7404–7409 (2019). https://doi.org/10.1166/jnn.2019.16613
70. J.C. Chou, C.Y. Wu, Y.H. Liao, C.H. Lai, S.J. Yan, Y.X. Wu, S.H. Lin, Enzymatic urea sensor based on graphene oxide/titanium dioxide films modified by urease-magnetic beads. IEEE Trans. Nanotechnol. **18**, 336–344 (2019). https://doi.org/10.1109/TNANO.2019.2907225

71. E. Zapp, D. Brondani, I.C. Vieira, J. Dupont, C.W. Scheeren, Bioelectroanalytical determination of rutin based on bi-enzymatic sensor containing iridium nanoparticles in ionic liquid phase supported in clay. Electroanalysis **23**, 764–776 (2011). https://doi.org/10.1002/elan.201000619
72. M. Kameya, H. Onaka, Y. Asano, Selective tryptophan determination using tryptophan oxidases involved in bis-indole antibiotic biosynthesis. Anal. Biochem. **438**, 124–132 (2013). https://doi.org/10.1016/j.ab.2013.03.024
73. K.R. Reddy, B.C. Sin, C.H. Yoo, W. Park, K.S. Ryu, J.S. Lee, D. Sohn, Y. Lee, A new one-step synthesis method for coating multi-walled carbon nanotubes with cuprous oxide nanoparticles. Scr. Mater. **58**, 1010–1013 (2008). https://doi.org/10.1016/j.scriptamat.2008.01.047
74. N.L. Reddy, V.N. Rao, M. Vijayakumar, R. Santhosh, S. Anandan et al., A review on frontiers in plasmonic nanophotocatalysts for hydrogen production. Int. J. Hydrogen Energy **44**, 10453–10472 (2019). https://doi.org/10.1016/j.ijhydene.2019.02.120
75. C. Venkata Reddy, I.N. Reddy, B. Akkinepally, K.R. Reddy, J. Shim, Synthesis and photoelectrochemical water oxidation of (Y, Cu) codoped α-Fe_2O_3 nanostructure photoanode. J. Alloys Compd. **814**, 152349 (2020). https://doi.org/10.1016/j.jallcom.2019.152349
76. N.P. Shetti, S.D. Bukkitgar, K.R. Reddy, C.V. Reddy, T.M. Aminabhavi, Nanostructured titanium oxide hybrids-based electrochemical biosensors for healthcare applications. Colloids Surf. B: Biointerfaces **178**, 385–394 (2019). https://doi.org/10.1016/j.colsurfb.2019.03.013
77. S. Kumar, S.D. Bukkitgar, S. Singh, Pratibha, V. Singh et al., Electrochemical sensors and biosensors based on graphene functionalized with metal oxide nanostructures for healthcare applications. ChemistrySelect **4**, 5322–5337 (2019). https://doi.org/10.1002/slct.201803871
78. N.P. Shetti, D.S. Nayak, S.J. Malode, K.R. Reddy, S.S. Shukla, T.M. Aminabhavi, Electrochemical behavior of flufenamic acid at amberlite XAD-4 resin and silver-doped titanium dioxide/amberlite XAD-4 resin modified carbon electrodes. Colloids Surf. B: Biointerfaces **177**, 407–415 (2019). https://doi.org/10.1016/j.colsurfb.2019.02.022
79. K.R. Reddy, V.G. Gomes, M. Hassan, Carbon functionalized TiO_2 nanofibers for high efficiency photocatalysis. Mater. Res. Express **1**, 15012 (2014). https://doi.org/10.1088/2053-1591/1/1/015012
80. D. Kishore Kumar, J. Loskot, J. Kříž, N. Bennett, H.M. Upadhyaya, V. Sadhu, C. Venkata Reddy, K.R. Reddy, Synthesis of SnSe quantum dots by successive ionic layer adsorption and reaction (SILAR) method for efficient solar cells applications. Sol. Energy **199**, 570–574 (2020). https://doi.org/10.1016/j.solener.2020.02.050
81. N.R. Reddy, U. Bhargav, M.M. Kumari, K.K. Cheralathan, M.V. Shankar, K.R. Reddy, T.A. Saleh, T.M. Aminabhavi, Highly efficient solar light-driven photocatalytic hydrogen production over Cu/FCNTs-titania quantum dots-based heterostructures. J. Environ. Manag. **254**, 109747 (2020). https://doi.org/10.1016/j.jenvman.2019.109747
82. C.V. Reddy, I.N. Reddy, V.V.N. Harish, K.R. Reddy, N.P. Shetti, J. Shim, T.M. Aminabhavi, Efficient removal of toxic organic dyes and photoelectrochemical properties of iron-doped zirconia nanoparticles. Chemosphere **239**, 124766 (2020). https://doi.org/10.1016/j.chemosphere.2019.124766
83. V. Navakoteswara Rao, N. Lakshmana Reddy, M. Mamatha Kumari, P. Ravi, M. Sathish et al., Photocatalytic recovery of H_2 from H_2S containing wastewater: surface and interface control of photo-excitons in Cu_2S@TiO_2 core–shell nanostructure. Appl. Catal. B Environ. **254**, 174–185 (2019). https://doi.org/10.1016/j.apcatb.2019.04.090
84. P.S. Basavarajappa, B.N.H. Seethya, N. Ganganagappa, K.B. Eshwaraswamy, R.R. Kakarla, Enhanced photocatalytic activity and biosensing of gadolinium substituted $BiFeO_3$ nanoparticles. ChemistrySelect **3**, 9025–9033 (2018). https://doi.org/10.1002/slct.201801198
85. N.P. Shetti, S.J. Malode, D.S. Nayak, G.B. Bagihalli, S.S. Kalanur et al., Fabrication of ZnO nanoparticles modified sensor for electrochemical oxidation of methdilazine. Appl. Surf. Sci. **496**, 143656 (2019). https://doi.org/10.1016/j.apsusc.2019.143656
86. S. Feng, L. Guanghua, Hydrothermal and solvothermal syntheses, in *Modern Inorganic Synthetic Chemistry*, 2nd edn., ed. by R. Xu, Y. Xu (Elsevier, Amsterdam, 2011), pp. 73–104. https://doi.org/10.1016/B978-0-444-63591-4.00004-5
87. G.W. Morey, Hydrothermal synthesis. J. Am. Ceram. Soc. **36**, 279–285 (1953). https://doi.org/10.1111/j.1151-2916.1953.tb12883.x
88. D. Ohare, *Hydrothermal Synthesis. Encyclopedia of Materials: Science and Technology*, 2nd edn. (Elsevier, Amsterdam, 2001), pp. 3989–3992. https://doi.org/10.1016/B0-08-043152-6/00701-4
89. P. Nayak, M. Sahoo, S.K. Nayak, Urchin-like $NiCo_2O_4$ microsphere by hydrothermal route: structural, electrochemical, optical and magnetic properties. Ceram. Int. **46**(3), 3818–3826 (2020). https://doi.org/10.1016/j.ceramint.2019.10.105
90. S. Debata, S. Patra, S. Banerjee, R. Madhuri, P.K. Sharma, Controlled hydrothermal synthesis of graphene supported $NiCo_2O_4$ coral-like nanostructures: an efficient electrocatalyst for overall water splitting. Appl. Surf. Sci. **449**, 203–212 (2018). https://doi.org/10.1016/j.apsusc.2018.01.302
91. B. Cui, H. Lin, J.B. Li, X. Li, J. Yang, J. Tao, Core–ring structured $NiCo_2O_4$ nanoplatelets: synthesis, characterization, and electrocatalytic applications. Adv. Funct. Mater. **18**, 1440–1447 (2008). https://doi.org/10.1002/adfm.200700982
92. K. Xu, J. Yang, J. Hu, Synthesis of hollow $NiCo_2O_4$ nanospheres with large specific surface area for asymmetric supercapacitors. J. Colloid Interface Sci. **511**, 456–462 (2018). https://doi.org/10.1016/j.jcis.2017.09.113
93. X. Chang, W. Li, Y. Liu, M. He, X. Zheng, X. Lv, Z. Ren, Synthesis and characterization of $NiCo_2O_4$ nanospheres/nitrogen-doped graphene composites with enhanced electrochemical performance. J. Alloys Compd. **784**, 293–300 (2019). https://doi.org/10.1016/j.jallcom.2019.01.036

 https://doi.org/10.1007/s40820-020-00462-w

94. Z.Q. Liu, Q.Z. Xu, J.Y. Wang, N. Li, S.H. Guo et al., Facile hydrothermal synthesis of urchin-like $NiCo_2O_4$ spheres as efficient electrocatalysts for oxygen reduction reaction. Int. J. Hydrogen Energy **38**, 6657–6662 (2013). https://doi.org/10.1016/j.ijhydene.2013.03.092
95. R. Ding, L. Qi, M. Jia, H. Wang, Simple hydrothermal synthesis of mesoporous spinel $NiCo_2O_4$ nanoparticles and their catalytic behavior in CH_3OH electro-oxidation and H_2O_2 electro-reduction. Catal. Sci. Technol. **3**, 3207–3215 (2013). https://doi.org/10.1039/c3cy00590a
96. M. Yu, J. Chen, J. Liu, S. Li, Y. Ma, J. Zhang, J. An, Mesoporous $NiCo_2O_4$ nanoneedles grown on 3D graphene-nickel foam for supercapacitor and methanol electro-oxidation. Electrochim. Acta **151**, 99–108 (2015). https://doi.org/10.1016/j.electacta.2014.10.156
97. Y. Liu, X. Chi, Q. Han, Y. Du, J. Yang, Y. Liu, Vertically self-standing C@ $NiCo_2O_4$ nanoneedle arrays as effective binder-free cathodes for rechargeable Na–O_2 batteries. J. Alloys Compd. **772**, 693–702 (2019). https://doi.org/10.1016/j.jallcom.2018.09.121
98. Y. Zhu, Z. Wu, M. Jing, W. Song, H. Hou, X. Yang, Q. Chen, X. Ji, 3D network-like mesoporous $NiCo_2O_4$ nanostructures as advanced electrode material for supercapacitors. Electrochim. Acta **149**, 144–151 (2014). https://doi.org/10.1016/j.electacta.2014.10.064
99. J. Wang, Y. Zhang, J. Ye, H. Wei, J. Hao, J. Mu, S. Zhao, S. Hussain, Facile synthesis of three-dimensional $NiCo_2O_4$ with different morphology for supercapacitors. RSC Adv. **6**, 70077–70084 (2016). https://doi.org/10.1039/c6ra14242g
100. Q. Zheng, X. Zhang, Y. Shen, Fabrication of free-standing $NiCo_2O_4$ nanoarrays via a facile modified hydrothermal synthesis method and their applications for lithium ion batteries and high-rate alkaline batteries. Mater. Res. Bull. **63**, 211–215 (2015). https://doi.org/10.1016/j.materresbull.2014.12.024
101. W. Jiang, F. Hu, S. Yao, Z. Sun, X. Wu, Hierarchical $NiCo_2O_4$ nanowalls composed of ultrathin nanosheets as electrode materials for supercapacitor and Li ion battery applications. Mater. Res. Bull. **93**, 303–309 (2017). https://doi.org/10.1016/j.materresbull.2017.05.036
102. X. Yang, X. Yu, Q. Yang, D. Zhao, K. Zhang et al., Controllable synthesis and magnetic properties of hydrothermally synthesized $NiCo_2O_4$ nano-spheres. Ceram. Int. **43**, 8585–8589 (2017). https://doi.org/10.1016/j.ceramint.2017.03.121
103. S. Sun, X. Jin, B. Cong, X. Zhou, W. Hong, G. Chen, Construction of porous nanoscale NiO/$NiCo_2O_4$ heterostructure for highly enhanced electrocatalytic oxygen evolution activity. J. Catal. **379**, 1–9 (2019). https://doi.org/10.1016/j.jcat.2019.09.010
104. E. Umeshbabu, G. Rajeshkhanna, G.R. Rao, Urchin and sheaf-like $NiCo_2O_4$ nanostructures: synthesis and electrochemical energy storage application. Int. J. Hydrogen Energy **39**, 15627–15638 (2014). https://doi.org/10.1016/j.ijhydene.2014.07.168
105. W. Zhang, W. Xin, T. Hu, Q. Gong, T. Gao, G. Zhou, One-step synthesis of $NiCo_2O_4$ nanorods and firework-shaped microspheres formed with necklace-like structure for supercapacitor materials. Ceram. Int. **45**, 8406–8413 (2019). https://doi.org/10.1016/j.ceramint.2019.01.149
106. J. Shen, X. Li, N. Li, M. Ye, Facile synthesis of $NiCo_2O_4$-reduced graphene oxide nanocomposites with improved electrochemical properties. Electrochim. Acta **141**, 126–133 (2014). https://doi.org/10.1016/j.electacta.2014.07.063
107. A.K. Mondal, D. Su, S. Chen, X. Xie, G. Wang, Highly porous $NiCo_2O_4$ nanoflakes and nanobelts as anode materials for lithium-ion batteries with excellent rate capability. ACS Appl. Mater. Interfaces. **6**, 14827–14835 (2014). https://doi.org/10.1021/am5036913
108. L. Shen, L. Yu, X.Y. Yu, X. Zhang, X.W.D. Lou, Self-templated formation of uniform $NiCo_2O_4$ hollow spheres with complex interior structures for lithium-Ion batteries and supercapacitors. Angew. Chem. Int. Ed. **54**, 1868–1872 (2015). https://doi.org/10.1002/anie.201409776
109. H. Xin, Z. Xu, Y. Liu, W. Li, Z. Hu, 3D flower-like $NiCo_2O_4$ electrode material prepared by a modified solvothermal method for supercapacitor. J. Alloys Compd. **711**, 670–676 (2017). https://doi.org/10.1016/j.jallcom.2017.03.208
110. J. Tang, A. Paul Alivisatos, Crystal splitting in the growth of Bi_2S_3. Nano Lett. **6**, 2701–2706 (2006). https://doi.org/10.1021/nl0615930
111. G.R. Patzke, Y. Zhou, R. Kontic, F. Conrad, Oxide nanomaterials: synthetic developments, mechanistic studies, and technological innovations. Angew. Chem. Int. Ed. **50**, 826–859 (2011). https://doi.org/10.1002/anie.201000235
112. S.K. Meher, P. Justin, G. Ranga-Rao, Nanoscale morphology dependent pseudocapacitance of NiO: influence of intercalating anions during synthesis. Nanoscale **3**, 683–692 (2011). https://doi.org/10.1039/c0nr00555j
113. Z.Q. Liu, K. Xiao, Q.Z. Xu, N. Li, Y.Z. Su, H.J. Wang, S. Chen, Fabrication of hierarchical flower-like super-structures consisting of porous $NiCo_2O_4$ nanosheets and their electrochemical and magnetic properties. RSC Adv. **3**, 4372–4380 (2013). https://doi.org/10.1039/c3ra23084h
114. A. Jain, B.J. Paul, S. Kim, V.K. Jain, J. Kim, A.K. Rai, Two-dimensional porous nanodisks of $NiCo_2O_4$ as anode material for high-performance rechargeable lithium-ion battery. J. Alloys Compd. **772**, 72–79 (2019). https://doi.org/10.1016/j.jallcom.2018.09.051
115. Q. Wang, X. Wang, J. Xu, X. Ouyang, X. Hou, D. Chen, R. Wang, G. Shen, Flexible coaxial-type fiber supercapacitor based on $NiCo_2O_4$ nanosheets electrodes. Nano Energy **8**, 44–51 (2014). https://doi.org/10.1016/j.nanoen.2014.05.014
116. Y. Chen, B. Qu, L. Hu, Z. Xu, Q. Li, T. Wang, High-performance supercapacitor and lithium-ion battery based on 3D hierarchical NH_4F-induced nickel cobaltate nanosheet-nanowire cluster arrays as self-supported electrodes. Nanoscale **5**, 9812–9820 (2013). https://doi.org/10.1039/c3nr02972g
117. D. Cai, S. Xiao, D. Wang, B. Liu, L. Wang et al., Morphology controlled synthesis of $NiCo_2O_4$ nanosheet array nanostructures on nickel foam and their application for

pseudocapacitors. Electrochim. Acta **142**, 118–124 (2014). https://doi.org/10.1016/j.electacta.2014.06.119

118. B. Cai, W. Mao, Z. Ye, J. Huang, Facile fabrication of all-solid-state SnO_2/$NiCo_2O_4$ biosensor for self-powered glucose detection. Appl. Phys. A Mater. Sci. Process. **122**, 806 (2016). https://doi.org/10.1007/s00339-016-0263-9
119. J. Deng, H. Zhang, Y. Zhang, P. Luo, L. Liu, Y. Wang, Striking hierarchical urchin-like peapoded $NiCo_2O_4$@C as advanced bifunctional electrocatalyst for overall water splitting. J. Power Sources **372**, 46–53 (2017). https://doi.org/10.1016/j.jpowsour.2017.10.062
120. J. Yang, C. Li, Z. Quan, D. Kong, X. Zhang, P. Yang, J. Lin, One-step aqueous solvothermal synthesis of In_2O_3 nanocrystals. Cryst. Growth Des. **8**, 695–699 (2008). https://doi.org/10.1021/cg070340x
121. S.M. Saleh, A.M. Soliman, M.A. Sharaf, V. Kale, B. Gadgil, Influence of solvent in the synthesis of nano-structured ZnO by hydrothermal method and their application in solar-still. J. Environ. Chem. Eng. B (2017). https://doi.org/10.1016/j.jece.2017.02.004
122. F. Fu, J. Li, Y. Yao, X. Qin, Y. Dou, H. Wang, J. Tsui, K.Y. Chan, M. Shao, Hierarchical $NiCo_2O_4$ micro- and nanostructures with tunable morphologies as anode materials for lithium- and sodium-ion batteries. ACS Appl. Mater. Interfaces **9**, 16194–16201 (2017). https://doi.org/10.1021/acsami.7b02175
123. X. Wang, Y. Fang, B. Shi, F. Huang, F. Rong, R. Que, Three-dimensional $NiCo_2O_4$@ $NiCo_2O_4$ core–shell nanocones arrays for high-performance supercapacitors. Chem. Eng. J. **344**, 311–319 (2018). https://doi.org/10.1016/j.cej.2018.03.061
124. Y. Liu, J. Goebl, Y. Yin, Templated synthesis of nanostructured materials. Chem. Soc. Rev. **42**, 2610–2653 (2013). https://doi.org/10.1039/c2cs35369e
125. Q. Ren, G. Wu, W. Xing, J. Han, P. Li et al., Highly ordered mesoporous $NiCo_2O_4$ as a high performance anode material for Li-ion batteries. Front. Chem. **7**, 521 (2019). https://doi.org/10.3389/fchem.2019.00521
126. C. Yuan, J. Li, L. Hou, J. Lin, G. Pang, L. Zhang, L. Lian, X. Zhang, Template-engaged synthesis of uniform mesoporous hollow $NiCo_2O_4$ sub-microspheres towards high-performance electrochemical capacitors. RSC Adv. **3**, 18573–18578 (2013). https://doi.org/10.1039/c3ra42828a
127. W. Stöber, A. Fink, E. Bohn, Controlled growth of monodisperse silica spheres in the micron size range. J. Colloid Interface Sci. **26**, 62–69 (1968). https://doi.org/10.1016/0021-9797(68)90272-5
128. V. Veeramani, R. Madhu, S.M. Chen, M. Sivakumar, Flower-like nickel–cobalt oxide decorated dopamine-derived carbon nanocomposite for high performance supercapacitor applications. ACS Sustain. Chem. Eng. **4**, 5013–5020 (2016). https://doi.org/10.1021/acssuschemeng.6b01391
129. W. Xiong, Y. Gao, X. Wu, X. Hu, D. Lan et al., Composite of macroporous carbon with honeycomb-like structure from mollusc shell and $NiCo_2O_4$ nanowires for high-performance supercapacitor. ACS Appl. Mater. Interfaces **6**, 19416–19423 (2014). https://doi.org/10.1021/am5055228
130. W. Li, F. Yang, Z. Hu, Y. Liu, Template synthesis of C@ $NiCo_2O_4$ hollow microsphere as electrode material for supercapacitor. J. Alloys Compd. **749**, 305–312 (2018). https://doi.org/10.1016/j.jallcom.2018.03.046
131. X. Qi, W. Zheng, G. He, T. Tian, N. Du, L. Wang, $NiCo_2O_4$ hollow microspheres with tunable numbers and thickness of shell for supercapacitors. Chem. Eng. J. **309**, 426–434 (2017). https://doi.org/10.1016/j.cej.2016.10.060
132. C. Li, X.Y. Gao, S.D. Li, Y. Zhao, K. Gao, Novel micron-sized $NiCo_2O_4$ pompon directed by a co-template method as capacitor electrode. Mater. Lett. **244**, 74–77 (2019). https://doi.org/10.1016/j.matlet.2019.02.048
133. Y. Zhu, J. Wang, Z. Wu, M. Jing, H. Hou, X. Jia, X. Ji, An electrochemical exploration of hollow $NiCo_2O_4$ submicrospheres and its capacitive performances. J. Power Sources **287**, 307–315 (2015). https://doi.org/10.1016/j.jpowsour.2015.04.053
134. P. Xu, R. Yu, H. Ren, L. Zong, J. Chen, X. Xing, Hierarchical nanoscale multi-shell Au/CeO_2 hollow spheres. Chem. Sci. **5**, 4221–4226 (2014). https://doi.org/10.1039/c4sc01882f
135. J. Wang, N. Yang, H. Tang, Z. Dong, Q. Jin et al., Accurate control of multishelled Co_3O_4 hollow microspheres as high-performance anode materials in lithium-ion batteries. Angew. Chem. Int. Ed. **52**, 6417–6420 (2013). https://doi.org/10.1002/anie.201301622
136. X. Zeng, J. Yang, L. Shi, L. Li, M. Gao, Synthesis of multi-shelled ZnO hollow microspheres and their improved photocatalytic activity. Nanoscale Res. Lett. **9**, 468 (2014). https://doi.org/10.1186/1556-276X-9-468
137. B. Wang, Y. Cao, Y. Chen, X. Lai, J. Peng, J. Tu, X. Li, Rapid synthesis of rGO conjugated hierarchical $NiCo_2O_4$ hollow mesoporous nanospheres with enhanced glucose sensitivity. Nanotechnology **28**, 025501 (2017). https://doi.org/10.1088/0957-4484/28/2/025501
138. X. Lv, Y. Zhu, H. Jiang, X. Yang, Y. Liu, Y. Su, J. Huang, Y. Yao, C. Li, Hollow mesoporous $NiCo_2O_4$ nanocages as efficient electrocatalysts for oxygen evolution reaction. Dalton Trans. **44**, 4148–4154 (2015). https://doi.org/10.1039/c4dt03803g
139. J. Nai, Y. Tian, X. Guan, L. Guo, Pearson's principle inspired generalized strategy for the fabrication of metal hydroxide and oxide nanocages. J. Am. Chem. Soc. **135**, 16082–16091 (2013). https://doi.org/10.1021/ja402751r
140. W. Huang, Y. Cao, Y. Chen, J. Peng, X. Lai, J. Tu, Fast synthesis of porous $NiCo_2O_4$ hollow nanospheres for a high-sensitivity non-enzymatic glucose sensor. Appl. Surf. Sci. **396**, 804–811 (2017). https://doi.org/10.1016/j.apsusc.2016.11.034
141. X. Hou, S. Xue, M. Liu, X. Shang, Y. Fu, D. He, Hollow irregular octahedra-like $NiCo_2O_4$ cages composed of mesoporous nanosheets as a superior anode material for lithium-ion batteries. Chem. Eng. J. **350**, 29–36 (2018). https://doi.org/10.1016/j.cej.2018.05.164

 https://doi.org/10.1007/s40820-020-00462-w

142. J. Yang, M. Cho, Y. Lee, Synthesis of hierarchical $NiCo_2O_4$ hollow nanorods via sacrificial-template accelerate hydrolysis for electrochemical glucose oxidation. Biosens. Bioelectron. **75**, 15–22 (2016). https://doi.org/10.1016/j.bios.2015.08.008
143. H. Behzad, F.E. Ghodsi, PVP-assisted enhancement in ion storage performance of sol–gel derived nano-structured $NiCo_2O_4$ thin films as battery-type electrode. Mater. Res. Bull. **99**, 336–342 (2018). https://doi.org/10.1016/j.materresbull.2017.11.031
144. M. El Baydi, S.K. Tiwari, R.N. Singh, J.L. Rehspringer, P. Chartier, J.F. Koenig, G. Poillerat, High specific surface area nickel mixed oxide powders $LaNiO_3$ (Perovskite) and $NiCo_2O_4$ (Spinel) via sol–gel type routes for oxygen electrocatalysis in alkaline media. J. Solid State Chem. **116**, 157–169 (1995). https://doi.org/10.1006/jssc.1995.1197
145. B. Hua, W. Zhang, J. Wu, J. Pu, B. Chi, L. Jian, A promising $NiCo_2O_4$ protective coating for metallic interconnects of solid oxide fuel cells. J. Power Sources **195**, 7375–7379 (2010). https://doi.org/10.1016/j.jpowsour.2010.05.031
146. L. Merabet, K. Rida, N. Boukmouche, Sol–gel synthesis, characterization, and supercapacitor applications of MCo_2O_4 (M = Ni, Mn, Cu, Zn) cobaltite spinels. Ceram. Int. **44**, 11265–11273 (2018). https://doi.org/10.1016/j.ceramint.2018.03.171
147. Y.Q. Wu, X.Y. Chen, P.T. Ji, Q.Q. Zhou, Sol–gel approach for controllable synthesis and electrochemical properties of $NiCo_2O_4$ crystals as electrode materials for application in supercapacitors. Electrochim. Acta **56**, 7517–7522 (2011). https://doi.org/10.1016/j.electacta.2011.06.101
148. T.Y. Wei, C.H. Chen, H.C. Chien, S.Y. Lu, C.C. Hu, A cost-effective supercapacitor material of ultrahigh specific capacitances: spinel nickel cobaltite aerogels from an epoxide-driven sol–gel process. Adv. Mater. **22**, 347–351 (2010). https://doi.org/10.1002/adma.200902175
149. M.C. Liu, C. Lu, X.M. Li, L. Bin Kong, Y.C. Luo, L. Kang, X. Li, F.C. Walsh, A sol–gel process for the synthesis of $NiCo_2O_4$ having improved specific capacitance and cycle stability for electrochemical capacitors. J. Electrochem. Soc. **159**, A1262 (2012). https://doi.org/10.1149/2.057208jes
150. Y. Liu, N. Wang, C. Yang, W. Hu, Sol–gel synthesis of nanoporous $NiCo_2O_4$ thin films on ITO glass as high-performance supercapacitor electrodes. Ceram. Int. **42**, 11411–11416 (2016). https://doi.org/10.1016/j.ceramint.2016.04.071
151. J. Bhagwan, G. Nagaraju, B. Ramulu, S.C. Sekhar, J.S. Yu, Rapid synthesis of hexagonal $NiCo_2O_4$ nanostructures for high-performance asymmetric supercapacitors. Electrochim. Acta **299**, 509–517 (2019). https://doi.org/10.1016/j.electacta.2018.12.174
152. J. Liang, Z. Fan, S. Chen, S. Ding, G. Yang, Hierarchical $NiCo_2O_4$ nanosheets@halloysite nanotubes with ultrahigh capacitance and long cycle stability as electrochemical pseudocapacitor materials. Chem. Mater. **26**, 4354–4360 (2014). https://doi.org/10.1021/cm500786a
153. F. Chen, W. Zhang, F. Cheng, Z. Yang, X. Fan, M. Huang, Stepwise co-precipitation to the synthesis of urchin-like $NiCo_2O_4$ hollow nanospheres as high performance anode material. J. Appl. Electrochem. **48**, 1095–1104 (2018). https://doi.org/10.1007/s10800-018-1213-3
154. H.S. Jadhav, R.S. Kalubarme, C.N. Park, J. Kim, C.J. Park, Facile and cost effective synthesis of mesoporous spinel $NiCo_2O_4$ as an anode for high lithium storage capacity. Nanoscale **6**, 10071–10076 (2014). https://doi.org/10.1039/c4nr02183e
155. L. Yu, B. Guan, W. Xiao, X.W. Lou, Formation of yolk-shelled Ni–Co mixed oxide nanoprisms with enhanced electrochemical performance for hybrid supercapacitors and lithium ion batteries. Adv. Energy Mater. **5**, 1500981 (2015). https://doi.org/10.1002/aenm.201500981
156. C. Wang, X. Zhang, D. Zhang, C. Yao, Y. Ma, Facile and low-cost fabrication of nanostructured $NiCo_2O_4$ spinel with high specific capacitance and excellent cycle stability. Electrochim. Acta **63**, 220–227 (2012). https://doi.org/10.1016/j.electacta.2011.12.090
157. H.S. Jadhav, R.S. Kalubarme, J.W. Roh, K.N. Jung, K.H. Shin, C.N. Park, C.J. Park, Facile and cost effective synthesized mesoporous spinel $NiCo_2O_4$ as catalyst for non-aqueous lithium-oxygen batteries. J. Electrochem. Soc. **161**, A2188 (2014). https://doi.org/10.1149/2.077714jes
158. H. Fu, Y. Liu, L. Chen, Y. Shi, W. Kong et al., Designed formation of $NiCo_2O_4$ with different morphologies self-assembled from nanoparticles for asymmetric supercapacitors and electrocatalysts for oxygen evolution reaction. Electrochim. Acta **296**, 719–729 (2019). https://doi.org/10.1016/j.electacta.2018.11.103
159. Y. Wan, J. Chen, J. Zhan, Y. Ma, Facile synthesis of mesoporous $NiCo_2O_4$ fibers with enhanced photocatalytic performance for the degradation of methyl red under visible light irradiation. J. Environ. Chem. Eng. **6**, 6079–6087 (2018). https://doi.org/10.1016/j.jece.2018.09.023
160. K.T. Jeng, C.C. Chien, N.Y. Hsu, S.C. Yen, S. Du Chiou, S.H. Lin, W.M. Huang, Performance of direct methanol fuel cell using carbon nanotube-supported Pt–Ru anode catalyst with controlled composition. J. Power Sources **160**, 97–104 (2006). https://doi.org/10.1016/j.jpowsour.2006.01.057
161. B. Zhang, J. Zhu, H. Liu, P. Shi, W. Wu, F. Wang, Y. Liu, Rapid synthesis of hexagonal mesoporous structured $NiCo_2O_4$ via rotary evaporation for high performance supercapacitors. Ceram. Int. **44**, 8695–8699 (2018). https://doi.org/10.1016/j.ceramint.2018.01.204
162. A. Karatutlu, A. Barhoum, A. Sapelkin, Liquid-phase synthesis of nanoparticles and nanostructured materials, in *Emerging Applications of Nanoparticles and Architecture Nanostructures*, ed. by A. Barhoum, A.S.H. Makhlouf (Elsevier, Amsterdam, 2018), pp. 1–28. https://doi.org/10.1016/B978-0-323-51254-1.00001-4
163. M.T. Crespo, A review of electrodeposition methods for the preparation of alpha-radiation sources. Appl. Radiat. Isot. **70**, 210–215 (2012). https://doi.org/10.1016/j.apradiso.2011.09.010
164. M. Musiani, Electrodeposition of composites: an expanding subject in electrochemical materials science. Electrochim.

Acta **45**, 3397–3402 (2000). https://doi.org/10.1016/S0013-4686(00)00438-2

165. L.K. Wu, J. Xia, H.Z. Cao, Y.P. Tang, G.Y. Hou, G.Q. Zheng, Highly active and durable cauliflower-like $NiCo_2O_4$ film for oxygen evolution with electrodeposited SiO_2 as template. Int. J. Hydrogen Energy **42**, 10813–10825 (2017). https://doi.org/10.1016/j.ijhydene.2017.03.076
166. N. Wang, B. Sun, P. Zhao, M. Yao, W. Hu, S. Komarneni, Electrodeposition preparation of $NiCo_2O_4$ mesoporous film on ultrafine nickel wire for flexible asymmetric supercapacitors. Chem. Eng. J. **345**, 31–38 (2018). https://doi.org/10.1016/j.cej.2018.03.147
167. N. Zhao, H. Fan, M. Zhang, J. Ma, W. Zhang et al., Investigating the large potential window of $NiCo_2O_4$ supercapacitors in neutral aqueous electrolyte. Electrochim. Acta **321**, 134681 (2019). https://doi.org/10.1016/j.electacta.2019.134681
168. C. Yuan, J. Li, L. Hou, X. Zhang, L. Shen, X.W. Lou, Ultrathin mesoporous $NiCo_2O_4$ nanosheets supported on Ni foam as advanced electrodes for supercapacitors. Adv. Funct. Mater. **22**, 4592–4597 (2012). https://doi.org/10.1002/adfm.201200994
169. A. Ramadoss, K.N. Kang, H.J. Ahn, S.I. Kim, S.T. Ryu, J.H. Jang, Realization of high performance flexible wire supercapacitors based on 3-dimensional $NiCo_2O_4$/Ni fibers. J. Mater. Chem. A **4**, 4718–4727 (2016). https://doi.org/10.1039/c5ta10781d
170. J. Xiao, S. Yang, Sequential crystallization of sea urchin-like bimetallic (Ni, Co) carbonate hydroxide and its morphology conserved conversion to porous $NiCo_2O_4$ spinel for pseudocapacitors. RSC Adv. **1**, 588–595 (2011). https://doi.org/10.1039/c1ra00342a
171. B. Ash, R.K. Paramguru, B.K. Mishra, Electrode reactions during electrolytic preparation of nickel hydroxide. Electrochem. Commun. **12**, 48–51 (2010). https://doi.org/10.1016/j.elecom.2009.10.033
172. G. Zhang, T. Wang, X. Yu, H. Zhang, H. Duan, B. Lu, Nanoforest of hierarchical Co_3O_4@ $NiCo_2O_4$ nanowire arrays for high-performance supercapacitors. Nano Energy **2**, 586–594 (2013). https://doi.org/10.1016/j.nanoen.2013.07.008
173. M. Mirzaee, C. Dehghanian, Synthesis of flower-like $NiCo_2O_4$ via chronopotentiometric technique and its application as electrode materials for high-performance supercapacitors. Mater. Today Energy **10**, 68–80 (2018). https://doi.org/10.1016/j.mtener.2018.08.011
174. Y. An, Z. Hu, B. Guo, N. An, Y. Zhang, Z. Li, Y. Yang, H. Wu, Electrodeposition of honeycomb-shaped $NiCo_2O_4$ on carbon cloth as binder-free electrode for asymmetric electrochemical capacitor with high energy density. RSC Adv. **6**, 37562–37573 (2016). https://doi.org/10.1039/c6ra04788b
175. J. Wu, P. Guo, R. Mi, X. Liu, H. Zhang et al., Ultrathin $NiCo_2O_4$ nanosheets grown on three-dimensional interwoven nitrogen-doped carbon nanotubes as binder-free electrodes for high-performance supercapacitors. J. Mater. Chem. A **3**, 15331–15338 (2015). https://doi.org/10.1039/c5ta02719e
176. W.W. Liu, C.X. Lu, K. Liang, B.K. Tay, A high-performance anode material for Li-ion batteries based on a vertically aligned CNTs/$NiCo_2O_4$ core/shell structure. Part. Part. Syst. Charact. **31**, 1151–1157 (2014). https://doi.org/10.1002/ppsc.201400030
177. L. Huang, D. Chen, Y. Ding, Z.L. Wang, Z. Zeng, M. Liu, Hybrid composite $Ni(OH)_2$@ $NiCo_2O_4$ grown on carbon fiber paper for high-performance supercapacitors. ACS Appl. Mater. Interfaces **5**, 11159–11162 (2013). https://doi.org/10.1021/am403367u
178. Y. Zhang, B. Wang, F. Liu, J. Cheng, X.W. Zhang, L. Zhang, Full synergistic contribution of electrodeposited three-dimensional $NiCo_2O_4$@MnO_2 nanosheet networks electrode for asymmetric supercapacitors. Nano Energy **27**, 627–637 (2016). https://doi.org/10.1016/j.nanoen.2016.08.013
179. J. Wang, R. Zhan, Y. Fu, H.Y. Yu, C. Jiang et al., Design and synthesis of hierarchical, freestanding bowl-like $NiCo_2O_4$ as cathode for long-life Li–O_2 batteries. Mater. Today Energy **5**, 214–221 (2017). https://doi.org/10.1016/j.mtener.2017.07.002
180. W. Wang, Z. Li, A. Meng, Q. Li, Network-like holey $NiCo_2O_4$ nanosheet arrays on Ni foam synthesized by electrodeposition for high-performance supercapacitors. J. Solid State Electrochem. **23**, 635–644 (2019). https://doi.org/10.1007/s10008-018-4149-y
181. J. Zhang, R. Chu, Y. Chen, H. Jiang, Y. Zhang, N.M. Huang, H. Guo, Electrodeposited binder-free $NiCo_2O_4$@carbon nanofiber as a high performance anode for lithium ion batteries. Nanotechnology **29**, 125401 (2018). https://doi.org/10.1088/1361-6528/aaa94c
182. P. Dinka, A. Mukasyan, Novel approaches to solution–combustion synthesis of nanomaterials. Int. J Self Propag. High Temp. Synth. **16**, 23–35 (2007). https://doi.org/10.3103/S1061386207010049
183. K.V. Manukyan, Combustion and materials synthesis. Int. J. Self Propag. High Temp. Synth. **26**, 143–144 (2017). https://doi.org/10.3103/S1061386217030025
184. J. Xu, Q. Chen, X. Liu, H. Baoquan, Q. Qian, The combustion synthesis of nanoscale ceria-doped calcia solid solution. Adv. Mater. Res. **610–613**, 547–550 (2012). https://doi.org/10.4028/www.scientific.net/amr.610-613.547
185. R. Alcántara, M. Jaraba, P. Lavela, J.L. Tirado, $NiCo_2O_4$ spinel: first report on a transition metal oxide for the negative electrode of sodium-ion batteries. Chem. Mater. **14**, 2847–2848 (2002). https://doi.org/10.1021/cm025556v
186. S.T. Aruna, A.S. Mukasyan, Combustion synthesis and nanomaterials. Curr. Opin. Solid State Mater. Sci. **12**, 44–50 (2008). https://doi.org/10.1016/j.cossms.2008.12.002
187. A. Varma, A.S. Mukasyan, A.S. Rogachev, K.V. Manukyan, Solution combustion synthesis of nanoscale materials. Chem. Rev. **116**, 14493–14586 (2016). https://doi.org/10.1021/acs.chemrev.6b00279
188. J.C. Toniolo, A.S. Takimi, C.P. Bergmann, Nanostructured cobalt oxides (Co_3O_4 and CoO) and metallic Co powders synthesized by the solution combustion method. Mater. Res. Bull. **45**, 672–676 (2010). https://doi.org/10.1016/j.materresbull.2010.03.001

 https://doi.org/10.1007/s40820-020-00462-w

189. I.T. Papadas, A. Ioakeimidis, G.S. Armatas, S.A. Choulis, Low-temperature combustion synthesis of a spinel $NiCo_2O_4$ hole transport layer for perovskite photovoltaics. Adv. Sci. **5**, 1701029 (2018). https://doi.org/10.1002/advs.201701029
190. T. Huang, B. Liu, P. Yang, Z. Qiu, Z. Hu, Facilely synthesized $NiCo_2O_4$ nanoparticles as electrode material for supercapacitors. Int. J. Electrochem. Sci. **13**, 6144 (2018). https://doi.org/10.20964/2018.06.60
191. A.N. Naveen, S. Selladurai, Novel synthesis of highly porous spinel cobaltite ($NiCo_2O_4$) electrode material for supercapacitor applications. AIP Conf. Proc. **1591**, 246 (2014). https://doi.org/10.1063/1.4872560
192. V. Shanmugavalli, K. Vishista, Low-cost synthesis of cubic spinel structured high efficient $NiCo_2O_4$/polyaniline nanocomposite for supercapacitor application. Mater. Res. Express **6**, 45021 (2019). https://doi.org/10.1088/2053-1591/aae8ee
193. L. Li, S. Peng, Y. Cheah, P. Teh, J. Wang, G. Wee, Y. Ko, C. Wong, M. Srinivasan, Electrospun porous $NiCo_2O_4$ nanotubes as advanced electrodes for electrochemical capacitors. Chem. A: Eur. J. **19**, 5892–5898 (2013). https://doi.org/10.1002/chem.201204153
194. H. Guan, C. Shao, Y. Liu, N. Yu, X. Yang, Fabrication of $NiCo_2O_4$ nanofibers by electrospinning. Solid State Commun. **131**, 107–109 (2004). https://doi.org/10.1016/j.ssc.2004.04.035
195. G. Sun, L. Sun, H. Xie, J. Liu, Electrospinning of nanofibers for energy applications. Nanomaterials **6**(7), E129 (2016). https://doi.org/10.3390/nano6070129
196. Q. Liu, J. Zhu, L. Zhang, Y. Qiu, Recent advances in energy materials by electrospinning. Renew. Sustain. Energy Rev. **81**, 1825–1858 (2018). https://doi.org/10.1016/j.rser.2017.05.281
197. Z. Dong, S.J. Kennedy, Y. Wu, Electrospinning materials for energy-related applications and devices. J. Power Sources **196**, 4886–4904 (2011). https://doi.org/10.1016/j.jpowsour.2011.01.090
198. F. Lai, Y.E. Miao, Y. Huang, T.S. Chung, T. Liu, Flexible hybrid membranes of $NiCo_2O_4$-doped carbon nanofiber@MnO_2 core–sheath nanostructures for high-performance supercapacitors. J. Phys. Chem. C **119**, 13442–13450 (2015). https://doi.org/10.1021/acs.jpcc.5b02739
199. C. Busacca, S.C. Zignani, A. Di Blasi, O. Di Blasi, M. Lo Faro, V. Antonucci, A.S. Aricò, Electrospun $NiMn_2O_4$ and $NiCo_2O_4$ spinel oxides supported on carbon nanofibers as electrocatalysts for the oxygen evolution reaction in an anion exchange membrane-based electrolysis cell. Int. J. Hydrogen Energy **44**, 20987–20996 (2019). https://doi.org/10.1016/j.ijhydene.2019.02.214
200. K. Xu, S. Li, J. Yang, H. Xu, J. Hu, Hierarchical MnO_2 nanosheets on electrospun $NiCo_2O_4$ nanotubes as electrode materials for high rate capability and excellent cycling stability supercapacitors. J. Alloys Compd. **678**, 120–125 (2016). https://doi.org/10.1016/j.jallcom.2016.03.255
201. J. Sun, W. Wang, D. Yu, $NiCo_2O_4$ nanosheet-decorated carbon nanofiber electrodes with high electrochemical performance for flexible supercapacitors. J. Electron. Mater. **48**, 3833–3843 (2019). https://doi.org/10.1007/s11664-019-07135-4
202. D. Lei, X.D. Li, M.K. Seo, M.S. Khil, H.Y. Kim, B.S. Kim, $NiCo_2O_4$ nanostructure-decorated PAN/lignin based carbon nanofiber electrodes with excellent cyclability for flexible hybrid supercapacitors. Polymer (Guildf) **132**, 31–40 (2017). https://doi.org/10.1016/j.polymer.2017.10.051
203. G.M. Tomboc, H. Kim, Derivation of both EDLC and pseudocapacitance characteristics based on synergistic mixture of $NiCo_2O_4$ and hollow carbon nanofiber: an efficient electrode towards high energy density supercapacitor. Electrochim. Acta **318**, 392–404 (2019). https://doi.org/10.1016/j.electacta.2019.06.112
204. A. Mirzaei, G. Neri, Microwave-assisted synthesis of metal oxide nanostructures for gas sensing application: a review. Sens. Actuators B: Chem. **237**, 749–775 (2016). https://doi.org/10.1016/j.snb.2016.06.114
205. L.Y. Meng, B. Wang, M.G. Ma, K.L. Lin, The progress of microwave-assisted hydrothermal method in the synthesis of functional nanomaterials. Mater. Today Chem. **1–2**, 63–83 (2016). https://doi.org/10.1016/j.mtchem.2016.11.003
206. X. Zhang, Y. Zhou, B. Luo, H. Zhu, W. Chu, K. Huang, Microwave-assisted synthesis of $NiCo_2O_4$ double-shelled hollow spheres for high-performance sodium ion batteries. Nano-Micro Lett. **10**, 13 (2018). https://doi.org/10.1007/s40820-017-0164-2
207. A. Shanmugavani, R.K. Selvan, Microwave assisted reflux synthesis of $NiCo_2O_4$/NiO composite: fabrication of high performance asymmetric supercapacitor with Fe_2O_3. Electrochim. Acta **189**, 283–294 (2016). https://doi.org/10.1016/j.electacta.2015.12.043
208. U.T. Nakate, S.N. Kale, Microwave assisted synthesis and characterizations of $NiCo_2O_4$ nanoplates and electrical, magnetic properties. Mater. Today: Proc. **3**(6), 1992–1998 (2016). https://doi.org/10.1016/j.matpr.2016.04.101
209. L. Gu, L. Qian, Y. Lei, Y. Wang, J. Li, H. Yuan, D. Xiao, Microwave-assisted synthesis of nanosphere-like $NiCo_2O_4$ consisting of porous nanosheets and its application in electrocatalytic oxidation of methanol. J. Power Sources **261**, 317–323 (2014). https://doi.org/10.1016/j.jpowsour.2014.03.098
210. Y.Z. Su, Q.Z. Xu, Q.S. Zhong, S.T. Shi, C.J. Zhang, C.W. Xu, $NiCo_2O_4$/C prepared by one-step intermittent microwave heating method for oxygen evolution reaction in splitter. J. Alloys Compd. **617**, 115–119 (2014). https://doi.org/10.1016/j.jallcom.2014.07.195
211. Y. Tao, L. Ruiyi, L. Zaijun, F. Yinjun, A facile and scalable strategy for synthesis of size-tunable $NiCo_2O_4$ with nanocoral-like architecture for high-performance. Electrochim. Acta **134**, 384–392 (2014). https://doi.org/10.1016/j.electacta.2014.03.168
212. Y. Zhu, X. Ji, R. Yin, Z. Hu, X. Qiu, Z. Wu, Y. Liu, Nanorod-assembled $NiCo_2O_4$ hollow microspheres assisted by an ionic liquid as advanced electrode materials for supercapacitors. RSC Adv. **7**, 11123–11128 (2017). https://doi.org/10.1039/c7ra00067g

213. N.S. Chaubal, V.Y. Joshi, Nonionic polymeric surfactant template for mesoporous $NiCo_2O_4$ Formation. J. Porous Mater. **18**, 177–183 (2011). https://doi.org/10.1007/s10934-010-9368-2

214. T.V. Gavrilović, D.J. Jovanović, M.D. Dramićanin, Chapter 2—synthesis of multifunctional inorganic materials: from micrometer to nanometer dimensions. Nanomater. Green Energy **1**, 55–81 (2018). https://doi.org/10.1016/B978-0-12-813731-4.00002-3

215. M. Kundu, G. Karunakaran, E. Kolesnikov, V.E. Sergeevna, S. Kumari, M.V. Gorshenkov, D. Kuznetsov, Hollow $NiCo_2O_4$ nano-spheres obtained by ultrasonic spray pyrolysis method with superior electrochemical performance for lithium-ion batteries and supercapacitors. J. Ind. Eng. Chem. **59**, 90–98 (2018). https://doi.org/10.1016/j.jiec.2017.10.010

216. Y. Ma, Z. Yu, M. Liu, C. Song, X. Huang, M. Moliere, G. Song, H. Liao, Deposition of binder-free oxygen-vacancies $NiCo_2O_4$ based films with hollow microspheres via solution precursor thermal spray for supercapacitors. Ceram. Int. **45**, 10722–10732 (2019). https://doi.org/10.1016/j.ceramint.2019.02.145

217. T. Li, X. Li, Z. Wang, H. Guo, Y. Li, A novel $NiCo_2O_4$ anode morphology for lithium-ion batteries. J. Mater. Chem. A **3**, 11970–11975 (2015). https://doi.org/10.1039/c5ta01928a

218. J. Leng, Z. Wang, X. Li, H. Guo, T. Li, H. Liang, Self-templated formation of hierarchical $NiCo_2O_4$ yolk–shell microspheres with enhanced electrochemical properties. Electrochim. Acta **244**, 154–161 (2017). https://doi.org/10.1016/j.electacta.2017.05.109

219. D.P. Lapham, J.L. Lapham, The porosity of $NiCo_2O_4$ films and powders by three common preparation techniques. Microporous Mesoporous Mater. **223**, 35–45 (2016). https://doi.org/10.1016/j.micromeso.2015.10.025

220. R.J. Deokate, R.S. Kalubarme, C.J. Park, C.D. Lokhande, Simple synthesis of $NiCo_2O_4$ thin films using spray pyrolysis for electrochemical supercapacitor application: a novel approach. Electrochim. Acta **224**, 378–385 (2017). https://doi.org/10.1016/j.electacta.2016.12.034

221. G.D. Park, J.K. Lee, Y.C. Kang, Three-dimensional macroporous CNTs microspheres highly loaded with $NiCo_2O_4$ hollow nanospheres showing excellent lithium-ion storage performances. Carbon **128**, 191–200 (2018). https://doi.org/10.1016/j.carbon.2017.11.088

222. R.A. Soomro, Z.H. Ibupoto, Sirajuddin, M.I. Abro, M. Willander, Electrochemical sensing of glucose based on novel hedgehog-like NiO nanostructures. Sens. Actuators B: Chem. **209**, 966–974 (2015). https://doi.org/10.1016/j.snb.2014.12.050

223. E. Zhang, Y. Xie, S. Ci, J. Jia, Z. Wen, Porous Co_3O_4 hollow nanododecahedra for nonenzymatic glucose biosensor and biofuel cell. Biosens. Bioelectron. **81**, 46–53 (2016). https://doi.org/10.1016/j.bios.2016.02.027

224. K.K. Naik, S. Kumar, C.S. Rout, Electrodeposited spinel $NiCo_2O_4$ nanosheet arrays for glucose sensing application. RSC Adv. **5**, 74585–74591 (2015). https://doi.org/10.1039/c5ra13833g

225. M. Hussain, Z.H. Ibupoto, M.A. Abbasi, X. Liu, O. Nur, M. Willander, Synthesis of three dimensional nickel cobalt oxide nanoneedles on nickel foam, their characterization and glucose sensing application. Sensors **14**, 5415–5425 (2014). https://doi.org/10.3390/s140305415

226. R. Elakkiya, G. Maduraiveeran, A three-dimensional nickel–cobalt oxide nanomaterial as an enzyme-mimetic electrocatalyst for the glucose and lactic acid oxidation reaction. New J. Chem. **43**, 14756–14762 (2019). https://doi.org/10.1039/c9nj01291e

227. R. Ding, L. Qi, M. Jia, H. Wang, Facile synthesis of mesoporous spinel $NiCo_2O_4$ nanostructures as highly efficient electrocatalysts for urea electro-oxidation. Nanoscale **6**, 1369–1376 (2014). https://doi.org/10.1039/c3nr05359h

228. Y. Feng, D. Xiang, Y. Qiu, L. Li, Y. Li, K. Wu, L. Zhu, MOF-derived spinel $NiCo_2O_4$ hollow nanocages for the construction of non-enzymatic electrochemical glucose sensor. Electroanalysis **32**(3), 571–580 (2020). https://doi.org/10.1002/elan.201900558

229. S. Wang, S. Zhang, M. Liu, H. Song, J. Gao, Y. Qian, MoS_2 as connector inspired high electrocatalytic performance of $NiCo_2O_4$ nanoplates towards glucose. Sens. Actuators B: Chem. **254**, 1101–1109 (2018). https://doi.org/10.1016/j.snb.2017.08.011

230. H. Zhao, J. Xu, Q. Sheng, J. Zheng, W. Cao, T. Yue, $NiCo_2O_4$ nanorods decorated MoS_2 nanosheets synthesized from deep eutectic solvents and their application for electrochemical sensing of glucose in red wine and honey. J. Electrochem. Soc. **166**, H404 (2019). https://doi.org/10.1149/2.0141910jes

231. A.P. Abbott, G. Capper, D.L. Davies, R.K. Rasheed, V. Tambyrajah, Novel solvent properties of choline chloride/urea mixtures. Chem. Commun. **9**, 70–71 (2003). https://doi.org/10.1039/b210714g

232. M. Avalos, R. Babiano, P. Cintas, J.L. Jiménez, J.C. Palacios, Greener media in chemical synthesis and processing. Angew. Chem. Int. Ed. **45**, 3904–3908 (2006). https://doi.org/10.1002/anie.200504285

233. A.P. Abbott, K. El Ttaib, G. Frisch, K.J. McKenzie, K.S. Ryder, Electrodeposition of copper composites from deep eutectic solvents based on choline chloride. Phys. Chem. Chem. Phys. **11**, 4269–4277 (2009). https://doi.org/10.1039/b817881j

234. F.H. Aidoudi, P.J. Byrne, P.K. Allan, S.J. Teat, P. Lightfoot, R.E. Morris, Ionic liquids and deep eutectic mixtures as new solvents for the synthesis of vanadium fluorides and oxyfluorides. Dalton Trans. **40**, 4324–4331 (2011). https://doi.org/10.1039/c0dt01765e

235. L. Wei, Z.Y. Zhou, S.P. Chen, C.D. Xu, D. Su, M.E. Schuster, S.G. Sun, Electrochemically shape-controlled synthesis in deep eutectic solvents: triambic icosahedral platinum nanocrystals with high-index facets and their enhanced catalytic activity. Chem. Commun. **49**, 11152–11154 (2013). https://doi.org/10.1039/c3cc46473c

236. L. Wei, Y.J. Fan, N. Tian, Z.Y. Zhou, X.Q. Zhao, B.W. Mao, S.G. Sun, Electrochemically shape-controlled synthesis in deep eutectic solvents—a new route to prepare Pt

 https://doi.org/10.1007/s40820-020-00462-w

nanocrystals enclosed by high-index facets with high catalytic activity. J. Phys. Chem. C **116**, 2040–2044 (2012). https://doi.org/10.1021/jp209743h

237. S. Cui, J. Zhang, Y. Ding, S. Gu, P. Hu, Z. Hu, Rectangular flake-like mesoporous $NiCo_2O_4$ as enzyme mimic for glucose biosensing and biofuel cell. Sci. China Mater. **60**, 766–776 (2017). https://doi.org/10.1007/s40843-017-9072-9
238. F.C. Sun, J.T. Zhang, H. Ren, S.T. Wang, Y. Zhou, J. Zhang, "Dry" $NiCo_2O_4$ nanorods for electrochemical non-enzymatic glucose sensing. Chin. J. Chem. Phys. **31**, 799 (2018). https://doi.org/10.1063/1674-0068/31/cjcp1804061
239. Q. Guo, W. Zeng, Y. Li, Highly sensitive non-enzymatic glucose sensor based on porous $NiCo_2O_4$ nanowires grown on nickel foam. Mater. Lett. **256**, 126603 (2019). https://doi.org/10.1016/j.matlet.2019.126603
240. P. Arul, S.A. John, Organic solvent free in situ growth of flower like Co-ZIF microstructures on nickel foam for glucose sensing and supercapacitor applications. Electrochim. Acta **306**, 254–263 (2019). https://doi.org/10.1016/j.electacta.2019.03.117
241. X. Luo, M. Huang, D. He, M. Wang, Y. Zhang, P. Jiang, Porous $NiCo_2O_4$ nanoarray-integrated binder-free 3D open electrode offers a highly efficient sensing platform for enzyme-free glucose detection. Analyst **143**, 2546–2554 (2018). https://doi.org/10.1039/c8an00668g
242. D. Zhang, J. Tong, B. Xia, Q. Xue, Ultrahigh performance humidity sensor based on layer-by-layer self-assembly of graphene oxide/polyelectrolyte nanocomposite film. Sens. Actuators B: Chem. **203**, 263–270 (2014). https://doi.org/10.1016/j.snb.2014.06.116
243. D. Zhang, J. Tong, B. Xia, Humidity-sensing properties of chemically reduced graphene oxide/polymer nanocomposite film sensor based on layer-by-layer nano self-assembly. Sens. Actuators B: Chem. **197**, 66–72 (2014). https://doi.org/10.1016/j.snb.2014.02.078
244. T.H. Ko, S. Radhakrishnan, M.K. Seo, M.S. Khil, H.Y. Kim, B.S. Kim, A green and scalable dry synthesis of $NiCo_2O_4$/graphene nanohybrids for high-performance supercapacitor and enzymeless glucose biosensor applications. J. Alloys Compd. **696**, 193–200 (2017). https://doi.org/10.1016/j.jallcom.2016.11.234
245. M. Wu, S. Meng, Q. Wang, W. Si, W. Huang, X. Dong, Nickel–cobalt oxide decorated three-dimensional graphene as an enzyme mimic for glucose and calcium detection. ACS Appl. Mater. Interfaces **7**, 21089–21094 (2015). https://doi.org/10.1021/acsami.5b06299
246. G. Ma, M. Yang, C. Li, H. Tan, L. Deng, S. Xie, F. Xu, L. Wang, Y. Song, Preparation of spinel nickel–cobalt oxide nanowrinkles/reduced graphene oxide hybrid for nonenzymatic glucose detection at physiological level. Electrochim. Acta **220**, 545–553 (2016). https://doi.org/10.1016/j.electacta.2016.10.163
247. Y. Ni, J. Xu, H. Liu, S. Shao, Fabrication of RGO-$NiCo_2O_4$ nanorods composite from deep eutectic solvents for nonenzymatic amperometric sensing of glucose. Talanta **185**, 335–343 (2018). https://doi.org/10.1016/j.talanta.2018.03.097
248. F. Meng, J. Li, S.K. Cushing, M. Zhi, N. Wu, Solar hydrogen generation by nanoscale p–n junction of p-type molybdenum disulfide/n-type nitrogen-doped reduced graphene oxide. J. Am. Chem. Soc. **135**, 10286–10289 (2013). https://doi.org/10.1021/ja404851s
249. Y. Liu, K. Yan, O.K. Okoth, J. Zhang, A label-free photoelectrochemical aptasensor based on nitrogen-doped graphene quantum dots for chloramphenicol determination. Biosens. Bioelectron. **74**, 1016–1021 (2015). https://doi.org/10.1016/j.bios.2015.07.067
250. L. Feng, N. Xie, J. Zhong, Carbon nanofibers and their composites: a review of synthesizing, properties and applications. Materials **7**, 3919–3945 (2014). https://doi.org/10.3390/ma7053919
251. W. Lu, T. He, B. Xu, X. He, H. Adidharma, M. Radosz, K. Gasem, M. Fan, Progress in catalytic synthesis of advanced carbon nanofibers. J. Mater. Chem. A **5**, 13863–13881 (2017). https://doi.org/10.1039/c7ta02007d
252. D.W. Kim, C.H. Kim, C.M. Yang, S. Ahn, Y.H. Kim et al., Deriving structural perfection in the structure of polyacrylonitrile based electrospun carbon nanofiber. Carbon **147**, 612–615 (2019). https://doi.org/10.1016/j.carbon.2019.02.066
253. M. Naebe, T. Lin, X. Wang, Carbon nanotubes reinforced electrospun polymer nanoibres, in *Nanofibres*, ed. by A. Kumar (Intech, Croatia, 2010), pp. 309–328. https://doi.org/10.5772/8160
254. T. Fujita, Hierarchical nanoporous metals as a path toward the ultimate three-dimensional functionality. Sci. Technol. Adv. Mater. **18**, 724–740 (2017). https://doi.org/10.1080/14686996.2017.1377047
255. T. Fujita, L.H. Qian, K. Inoke, J. Erlebacher, M.W. Chen, Three-dimensional morphology of nanoporous gold. Appl. Phys. Lett. **92**, 251902 (2008). https://doi.org/10.1063/1.2948902
256. X.Y. Lang, H.Y. Fu, C. Hou, G.F. Han, P. Yang, Y.B. Liu, Q. Jiang, Nanoporous gold supported cobalt oxide microelectrodes as high-performance electrochemical biosensors. Nat. Commun. **4**, 2169 (2013). https://doi.org/10.1038/ncomms3169
257. W. Li, H. Qi, B. Wang, Q. Wang, S. Wei, X. Zhang, Y. Wang, L. Zhang, X. Cui, Ultrathin $NiCo_2O_4$ nanowalls supported on a 3D nanoporous gold coated needle for non-enzymatic amperometric sensing of glucose. Microchim. Acta **185**, 124 (2018). https://doi.org/10.1007/s00604-017-2663-8
258. K.K. Naik, A. Gangan, B. Chakraborty, C.S. Rout, Superior non-enzymatic glucose sensing properties of Ag–/Au–$NiCo_2O_4$ nanosheets with insight from electronic structure simulations. Analyst **143**, 571–579 (2018). https://doi.org/10.1039/c7an01354j
259. K.K. Naik, A. Gangan, B. Chakraborty, S.K. Nayak, C.S. Rout, Enhanced nonenzymatic glucose-sensing properties of electrodeposited $NiCo_2O_4$–Pd nanosheets: experimental and DFT investigations. ACS Appl. Mater. Interfaces **9**, 23894–23903 (2017). https://doi.org/10.1021/acsami.7b02217

260. G. Cakmak, Z. Kǧükyavuz, S. Kǧükyavuz, Conductive copolymers of polyaniline, polypyrrole and poly(dimethylsiloxane). Synth. Met. **151**, 10–18 (2005). https://doi.org/10.1016/j.synthmet.2005.02.019
261. A.S. Hammad, H. Noby, M.F. Elkady, A.H. El-Shazly, In-situ polymerization of polyaniline/polypyrrole copolymer using different techniques, in *IOP Conference Series: Materials Science and Engineering,* vol. 290 (2018), p. 012001. https://doi.org/10.1088/1757-899X/290/1/012001
262. J.M. Jeong, B.G. Choi, S.C. Lee, K.G. Lee, S.J. Chang et al., Hierarchical hollow spheres of Fe_2O_3@polyaniline for lithium ion battery anodes. Adv. Mater. **25**, 6250–6255 (2013). https://doi.org/10.1002/adma.201302710
263. Z. Yu, H. Li, X. Zhang, N. Liu, W. Tan, X. Zhang, L. Zhang, Facile synthesis of $NiCo_2O_4$@Polyaniline core–shell nanocomposite for sensitive determination of glucose. Biosens. Bioelectron. **75**, 161–165 (2016). https://doi.org/10.1016/j.bios.2015.08.024
264. X. Duan, K. Liu, Y. Xu, M. Yuan, T. Gao, J. Wang, Non-enzymatic electrochemical glucose biosensor constructed by $NiCo_2O_4$@Ppy nanowires on nickel foam substrate. Sens. Actuators B: Chem. **292**, 121–128 (2019). https://doi.org/10.1016/j.snb.2019.04.107
265. A.B. Vennela, D. Mangalaraj, N. Muthukumarasamy, S. Agilan, K.V. Hemalatha, Structural and optical properties of Co_3O_4 nanoparticles prepared by sol–gel technique for photocatalytic application. Int. J. Electrochem. Sci. **14**, 3535–3552 (2019). https://doi.org/10.20964/2019.04.40
266. O. Mounkachi, E. Salmani, M. Lakhal, H. Ez-Zahraouy, M. Hamedoun, M. Benaissa, A. Kara, A. Ennaoui, A. Benyoussef, Band-gap engineering of SnO_2. Sol. Energy Mater. Sol. Cells **148**, 34–38 (2016). https://doi.org/10.1016/j.solmat.2015.09.062
267. E. Cockayne, L. Li, First-principles DFT + U studies of the atomic, electronic, and magnetic structure of α-MnO_2 (cryptomelane). Chem. Phys. Lett. **544**, 53–58 (2012). https://doi.org/10.1016/j.cplett.2012.06.061
268. M.C. Liu, L. Bin Kong, C. Lu, X.M. Li, Y.C. Luo, L. Kang, A sol–gel process for fabrication of NiO/$NiCo_2O_4$/Co_3O_4 composite with improved electrochemical behavior for electrochemical capacitors. ACS Appl. Mater. Interfaces **4**, 4631–4636 (2012). https://doi.org/10.1021/am301010u
269. D. Chen, D. Pang, S. Zhang, H. Song, W. Zhu, J. Zhu, Synergistic coupling of $NiCo_2O_4$ nanorods onto porous Co_3O_4 nanosheet surface for tri-functional glucose, hydrogen-peroxide sensors and supercapacitor. Electrochim. Acta **330**, 135326 (2020). https://doi.org/10.1016/j.electacta.2019.135326
270. B. Xue, K. Li, L. Feng, J. Lu, L. Zhang, Graphene wrapped porous Co_3O_4/$NiCo_2O_4$ double-shelled nanocages with enhanced electrocatalytic performance for glucose sensor. Electrochim. Acta **239**, 36–44 (2017). https://doi.org/10.1016/j.electacta.2017.04.005
271. D. Chen, S. Wang, M. Liu, J. Gao, H. Song, S. Zhang, Bionics-inspired strong coupling of streptococcus-like $NiCo_2O_4$ to needle-like MnO_2 for enhanced electrocatalytic determination of glucose. J. Electrochem. Soc. **166**, B1653 (2019). https://doi.org/10.1149/2.1291915jes
272. Y. Su, B. Luo, J.Z. Zhang, Controllable cobalt oxide/Au hierarchically nanostructured electrode for nonenzymatic glucose sensing. Anal. Chem. **88**, 1617–1624 (2016). https://doi.org/10.1021/acs.analchem.5b03396
273. Z. Qin, Q. Cheng, Y. Lu, J. Li, Facile synthesis of hierarchically mesoporous $NiCo_2O_4$ nanowires for sensitive nonenzymatic glucose detection. Appl. Phys. A Mater. Sci. Process. **123**, 492 (2017). https://doi.org/10.1007/s00339-017-1108-x
274. W. Huang, T. Lin, Y. Cao, X. Lai, J. Peng, J. Tu, Hierarchical $NiCo_2O_4$ hollow sphere as a peroxidase mimetic for colorimetric detection of H_2O_2 and glucose. Sensors **17**, 217 (2017). https://doi.org/10.3390/s17010217
275. L. Su, W. Dong, C. Wu, Y. Gong, Y. Zhang, L. Li, G. Mao, S. Feng, The peroxidase and oxidase-like activity of $NiCo_2O_4$ mesoporous spheres: mechanistic understanding and colorimetric biosensing. Anal. Chim. Acta **951**, 124–132 (2017). https://doi.org/10.1016/j.aca.2016.11.035
276. M. Saraf, K. Natarajan, S.M. Mobin, Multifunctional porous $NiCo_2O_4$ nanorods: sensitive enzymeless glucose detection and supercapacitor properties with impedance spectroscopic investigations. New J. Chem. **41**, 9299–9313 (2017). https://doi.org/10.1039/c7nj01519d
277. H. Yin, T. Zhan, D. Qin, X. He, Q. Nie, J. Gong, Self-assembly of dandelion-like $NiCo_2O_4$ hierarchical microspheres for non-enzymatic glucose sensor. Inorg. Nano Met. Chem. **47**, 1560–1567 (2017). https://doi.org/10.1080/24701556.2017.1357610
278. W. Chen, S. Cai, Q.Q. Ren, W. Wen, Y. Di Zhao, Recent advances in electrochemical sensing for hydrogen peroxide: a review. Analyst **137**, 49–58 (2012). https://doi.org/10.1039/c1an15738h
279. K. Dhara, D.R. Mahapatra, Recent advances in electrochemical nonenzymatic hydrogen peroxide sensors based on nanomaterials: a review. J. Mater. Sci. **54**, 12319–12357 (2019). https://doi.org/10.1007/s10853-019-03750-y
280. R. Zhang, W. Chen, Recent advances in graphene-based nanomaterials for fabricating electrochemical hydrogen peroxide sensors. Biosens. Bioelectron. **89**, 249–268 (2017). https://doi.org/10.1016/j.bios.2016.01.080
281. P. Kannan, T. Maiyalagan, A. Pandikumar, L. Guo, P. Veerakumar, P. Rameshkumar, Highly sensitive enzyme-free amperometric sensing of hydrogen peroxide in real samples based on Co_3O_4 nanocolumn structures. Anal. Methods **11**, 2292–2302 (2019). https://doi.org/10.1039/c9ay00230h
282. R. Ding, L. Qi, M. Jia, H. Wang, Porous $NiCo_2O_4$ nanostructures as bi-functional electrocatalysts for CH_3OH oxidation reaction and H_2O_2 reduction reaction. Electrochim. Acta **113**, 290–301 (2013). https://doi.org/10.1016/j.electacta.2013.09.053
283. Y. Wang, K. Cheng, D. Cao, F. Yang, P. Yan, W. Zhang, G. Wang, Preparation of $NiCo_2O_4$ nanosheet arrays and its high catalytic performance for H_2O_2 electroreduction. Fuel Cells **15**, 298–305 (2015). https://doi.org/10.1002/fuce.201300299

 https://doi.org/10.1007/s40820-020-00462-w

284. L. Ning, X. Guan, J. Ma, M. Wang, X. Fan, G. Zhang, F. Zhang, W. Peng, Y. Li, A highly sensitive nonenzymatic H_2O_2 sensor based on platinum, $ZnFe_2O_4$ functionalized reduced graphene oxide. J. Alloys Compd. **738**, 317–322 (2018). https://doi.org/10.1016/j.jallcom.2017.12.161
285. X. Xiong, C. You, X. Cao, L. Pang, R. Kong, X. Sun, Ni_2P nanosheets array as a novel electrochemical catalyst electrode for non-enzymatic H_2O_2 sensing. Electrochim. Acta **253**, 517–521 (2017). https://doi.org/10.1016/j.electacta.2017.09.104
286. F. Xie, X. Cao, F. Qu, A.M. Asiri, X. Sun, Cobalt nitride nanowire array as an efficient electrochemical sensor for glucose and H_2O_2 detection. Sens. Actuators B: Chem. **255**, 1254–1261 (2018). https://doi.org/10.1016/j.snb.2017.08.098
287. Y. Li, M. Zhang, X. Zhang, G. Xie, Z. Su, G. Wei, Nanoporous carbon nanofibers decorated with platinum nanoparticles for non-enzymatic electrochemical sensing of H_2O_2. Nanomaterials **5**, 1891–1905 (2015). https://doi.org/10.3390/nano5041891
288. L. Tian, K. Xia, W. Hu, X. Zhong, Y. Chen et al., A wide linear range and stable H_2O_2 electrochemical sensor based on Ag decorated hierarchical Sn_3O_4. Electrochim. Acta **231**, 190–199 (2017). https://doi.org/10.1016/j.electacta.2017.02.052
289. X. Xiao, F. Yang, K. Cheng, X. Wang, J. Yin, K. Ye, G. Wang, D. Cao, $NiCo_2O_4$ nanostructures with various morphologies as the high-performance electrocatalysts for H_2O_2 electroreduction and electrooxidation. J. Electroanal. Chem. **729**, 103–108 (2014). https://doi.org/10.1016/j.jelechem.2014.07.010
290. B. Xue, K. Li, S. Gu, L. Zhang, J. Lu, Ni foam-supported ZnO nanowires and $Co_3O_4/NiCo_2O_4$ double-shelled nanocages for efficient hydrogen peroxide detection. Sens. Actuators B: Chem. **262**, 828–836 (2018). https://doi.org/10.1016/j.snb.2018.02.091
291. M. Sakthivel, R. Sukanya, S.M. Chen, K. Pandi, K.C. Ho, Synthesis and characterization of bimetallic nickel–cobalt chalcogenides ($NiCoSe_2$, $NiCo_2S_4$, and $NiCo_2O_4$) for non-enzymatic hydrogen peroxide sensor and energy storage: electrochemical properties dependence on the metal-to-chalcogen composition. Renew. Energy **138**, 139–151 (2019). https://doi.org/10.1016/j.renene.2019.01.079
292. R.L. King, G.G. Botte, Hydrogen production via urea electrolysis using a gel electrolyte. J. Power Sources **196** (5), 2773–2778 (2011). https://doi.org/10.1016/j.jpowsour.2010.11.006
293. W.M. Omymen, J.R. Rogan, B.Z. Jugović, M.M. Gvozdenović, B.N. Grgur, Photo-assisted electrochemical oxidation of the urea onto TiO_2-nanotubes modified by hematite. J. Saudi Chem. Soc. **21**(8), 990–997 (2017). https://doi.org/10.1016/j.jscs.2017.05.010
294. J. Kim, W.J.K. Choi, J. Choi, M.R. Hoffmann, H. Park, Electrolysis of urea and urine for solar hydrogen. Catal. Today **199**, 2–7 (2013). https://doi.org/10.1016/j.cattod.2012.02.009
295. B.K. Boggs, R.L. King, G.G. Botte, Urea electrolysis: direct hydrogen production from urine. Chem. Commun. **32**, 4859–4861 (2009). https://doi.org/10.1039/b905974a
296. A.A. Ibrahim, R. Ahmad, A. Umar, M.S. Al-Assiri, A.E. Al-Salami, R. Kumar, S.G. Ansari, S. Baskoutas, Two-dimensional ytterbium oxide nanodisks based biosensor for selective detection of urea. Biosens. Bioelectron. **98**, 254–260 (2017). https://doi.org/10.1016/j.bios.2017.06.015
297. G. Dhawan, G. Sumana, B.D. Malhotra, Recent developments in urea biosensors. Biochem. Eng. J. **44**, 42–52 (2009). https://doi.org/10.1016/j.bej.2008.07.004
298. S. Amin, A. Tahira, A. Solangi, V. Beni, J.R. Morante et al., A practical non-enzymatic urea sensor based on $NiCo_2O_4$ nanoneedles. RSC Adv. **9**, 14443–14451 (2019). https://doi.org/10.1039/c9ra00909d
299. N. Senthilkumar, G. Gnana kumar, A. Manthiram, 3D hierarchical core–shell nanostructured arrays on carbon fibers as catalysts for direct urea fuel cells. Adv. Energy Mater. **8**(6), 1702207 (2018). https://doi.org/10.1002/aenm.201702207
300. N.S. Nguyen, G. Das, H.H. Yoon, Nickel/cobalt oxide-decorated 3D graphene nanocomposite electrode for enhanced electrochemical detection of urea. Biosens. Bioelectron. **77**, 372–377 (2016). https://doi.org/10.1016/j.bios.2015.09.046
301. H.J. Choi, S.M. Jung, J.M. Seo, D.W. Chang, L. Dai, J.B. Baek, Graphene for energy conversion and storage in fuel cells and supercapacitors. Nano Energy **1**, 534–551 (2012). https://doi.org/10.1016/j.nanoen.2012.05.001
302. V. Vedharathinam, G.G. Botte, Understanding the electrocatalytic oxidation mechanism of urea on nickel electrodes in alkaline medium. Electrochim. Acta **81**, 292–300 (2012). https://doi.org/10.1016/j.electacta.2012.07.007
303. H.N. Siti, J. Jalil, A.Y. Asmadi, Y. Kamisah, Roles of rutin in cardiac remodeling. J. Funct. Foods **64**, 103606 (2020). https://doi.org/10.1016/j.jff.2019.103606
304. M.L. Yola, C. Göde, N. Atar, Determination of rutin by $CoFe_2O_4$ nanoparticles ionic liquid nanocomposite as a voltammetric sensor. J. Mol. Liq. **246**, 350–353 (2017). https://doi.org/10.1016/j.molliq.2017.09.072
305. S. Cui, L. Li, Y. Ding, J. Zhang, H. Yang, Y. Wang, Mesoporous $NiCo_2O_4$-decorated reduced graphene oxide as a novel platform for electrochemical determination of rutin. Talanta **164**, 291–299 (2017). https://doi.org/10.1016/j.talanta.2016.10.109
306. K.H.G. Freitas, O. Fatibello-Filho, I.L. de Mattos, Square-wave voltammetric determination of rutin in pharmaceutical formulations using a carbon composite electrode modified with copper (II) phosphate immobilized in polyester resin. Braz J. Pharm. Sci. **48**, 2175–9790 (2012). https://doi.org/10.1590/S1984-82502012000400007
307. J. Kang, X. Lu, H. Zeng, H. Liu, B. Lu, Investigation on the electrochemistry of rutin and its analytical application. Anal. Lett. **35**, 677–686 (2002). https://doi.org/10.1081/AL-120003169
308. P. Miao, T. Liu, X. Li, L. Ning, J. Yin, K. Han, Highly sensitive, label-free colorimetric assay of trypsin using silver

nanoparticles. Biosens. Bioelectron. **49**, 20–24 (2013). https://doi.org/10.1016/j.bios.2013.04.038

309. X. Lin, Z. Zhu, C. Zhao, S. Li, Q. Liu, A. Liu, L. Lin, X. Lin, Robust oxidase mimicking activity of protamine-stabilized platinum nanoparticles units and applied for colorimetric sensor of trypsin and inhibitor. Sens. Actuators B: Chem. **284**, 346–353 (2019). https://doi.org/10.1016/j.snb.2018.12.109
310. Y. Lin, R. Shen, N. Liu, H. Yi, H. Dai, J. Lin, A highly sensitive peptide-based biosensor using $NiCo_2O_4$ nanosheets and g-C_3N_4 nanocomposite to construct amplified strategy for trypsin detection. Anal. Chim. Acta **1035**, 175–183 (2018). https://doi.org/10.1016/j.aca.2018.06.040
311. B. Kaur, B. Satpati, R. Srivastava, Synthesis of $NiCo_2O_4$/Nano-ZSM-5 nanocomposite material with enhanced electrochemical properties for the simultaneous determination of ascorbic acid, dopamine, uric acid and tryptophan. New J. Chem. **39**, 1115–1124 (2015). https://doi.org/10.1039/c4nj01360c
312. T. Tite, E.A. Chiticaru, J.S. Burns, M. Ioniţă, Impact of nano-morphology, lattice defects and conductivity on the performance of graphene based electrochemical biosensors. J. Nanobiotechnol. **17**, 101 (2019). https://doi.org/10.1186/s12951-019-0535-6

 https://doi.org/10.1007/s40820-020-00462-w